The Role of the *S. cerevisiae* Sco2p and Its Homologues in Antioxidant Defense Mechanisms

DISSERTATION

zur Erlangung des akademischen Grades
Doctor rerum naturalium
(Dr. rer. nat.)
vorgelegt
der Fakultät Biologie
der Technische Universität Dresden
von

M. Sc. Aslihan Ekim Kocabey
aus Ankara, Türkei

Eingereicht am 31.01.2018
Verteidigt am 04.06.2018

Gutachter: Prof. Dr. Gerhard Rödel; Prof. Dr. Dirk Lindemann

"Everything is theoretically impossible,
until it is done."

Robert A. Heinlein

Erklärung entsprechend §5.5 der Promotionsordnung

Hiermit versichere ich, dass ich die vorliegende Arbeit ohne unzulässige Hilfe Dritter und ohne Benutzung anderer als der angegebenen Hilfsmittel angefertigt habe; die aus fremden Quellen direkt oder indirekt übernommenen Gedanken sind als solche kenntlich gemacht. Die Arbeit wurde bisher weder im Inland noch im Ausland in gleicher oder ähnlicher Form einer anderen Prüfungsbehörde vorgelegt.

Die Dissertation wurde im Zeitraum vom 01.02.2015 bis 31.01.2018 verfasst und von Prof. Dr. Gerhard Rödel, Institute für Genetik, Fachrichtung Biologie betreut.

Meine Person betreffend erkläre ich hiermit, dass keine früheren erfolglosen Promotionsverfahren stattgefunden haben.

Ich erkenne die Promotionsordnung der Fakultät Biologie, Technische Universität Dresden an.

Conferences participation:

- EMBO Workshop, "Thiol Oxidation in toxicity and signaling", Sant Feliu de Guixols, Spain, 17-21.09.2017, **poster presentation & flash talk**

- 28th International Conference on Yeast Genetics and Molecular Biology (ICYGMB), Prag, Czech Republic, 27.08-01.09.2017, **poster presentation**

- Gordon Research Conference "Oxidative Stress & Disease", Lucca, Italy, 19-24.03.2017, **poster presentation**

Acknowledgments

Throughout my PhD, I encountered tough times that I faced with a lot of unknowns and obstacles. I went through with all difficulties with the continuous help of others and here I would like to take this chance to thank all my supporters again.

Firstly, I am very grateful to Prof. Dr. Gerhard Rödel for believing in me and accepting me into his group. During my PhD, I have always felt myself lucky to work on this exciting project in an amazing lab environment. I am also very thankful for his encouraging and helpful advices.

I am thankful to all members of the AG Rödel group for the great working atmosphere they generated and immeasurable guidance. I am particularly grateful to Uta Gey for giving generously her time and advice over these three years.

I would like to thank my TAC members, Prof. Dr. Dirk Lindemann and Dr. Simon Alberti for their valuable advices. I would like to also thank Prof. Dr. Michael Schroeder and Dr. Sebastian Salentin for all their help and motivation in bioinformatic analyses.

I would like to express my gratitude to the Dresden International Graduate School of Biomedicine and Bioengineering (DIGS-BB) for all financial and helpful support during my PhD.

I am indebted to my family particularly to my mother, father and brother for their endless support and sincere motivation. I believe that without them, I could not take this substantial step in my life.

I owe a huge thank to my husband for his constant encouragement, support and patience. I am extremely lucky to go through all this scientific journey together with him.

Abstract

The Sco proteins, present in all kind of organisms, are regarded as one of the key players in the cytochrome *c* oxidase assembly. However, experimental and structural data, such as the presence of a thioredoxin-like fold, suggest that Sco proteins may also play a role in redox homeostasis.

Our current studies in *S. cerevisiae* have strongly suggested an antioxidant role to Sco2 protein (ySco2p). While the single deletion of *SCO2* does not result in a distinctive phenotype, the concomitant deletion of superoxide dismutase 1 (*SOD1*) leads to an increased sensitivity to oxidative stress generating agents (paraquat, menadione, plumbagin) compared to the respective single mutants.

Since *S. cerevisiae* is a good model to functionally characterize genes from more complex organisms, identification of such a phenotype has paved the way to test whether the Sco2 homologues from other organisms are able to substitute for the function of ySco2p. The Sco homologues from *Homo sapiens, Schizosaccharomyces pombe, Arabidopsis thaliana, Drosophila melanogaster* and *Kluyveromyces lactis* were integrated into the genome of the double deletion mutant. The functional complementation was tested by both growth and biochemical ROS assays. All homologues except for *K. lactis* K07152 and *A. thaliana HCC1* were able to complement the phenotype, indicating their role in antioxidant defense. Interestingly, pathogenic human *Sco2* point mutations failed to restore this function.

The observation of non-functional homologues despite of the high sequence similarity to ySco2p strengthened our hypothesis on the importance of conserved aminoacid(s) for the defensive role. For this purpose, selected homologues were aligned and the conservation was judged not only based on identity but also similarity (e.g. charge, hydrophobicity). Interestingly, alignment results have pointed out an aminoacid site (located 15 aminoacids downstream of CxxxC motif) that a positively charged lysine is found only in the nonfunctional homologues. Subsequent mutagenesis analyses verified the functional importance of this aminoacid site (gain and loss of functions) and revealed the detrimental effect of positive charge on antioxidant function. In order to explain the observed functional change, further effort will be put into the calculations of the electrostatic potential and identifications of protein-protein interactions.

Contents

List of figures

List of tables

Abbreviations

Å	Angstrom
aa	Aminoacid(s)
ADP	Adenosine diphosphate
AEBSF	4-(2-Aminoethyl) benzene sulfonyl fluoride hydrochloride
APS	Ammonium per sulfate
A. thaliana	*Arabidopsis thaliana*
ATP	Adenosine triphosphate
BHT	Butylated hydroxytoluene
bp	Base pairs
cDNA	Complementary DNA
COX	Cytochrome c oxidase
Cu	Copper
ddH_2O	Double distilled water
DIG	Digoxigenin
DMSO	Dimethyl sulfoxide
DNA	Deoxyribonucleic acid
dNTP	Desoxyribonucleosidtriphosphate
DTT	Dithiothreitol
D. melanogaster	*Drosophila melanogaster*
EDTA	Ethylenediaminetetraacetic acid
ETC	Electron transport chain
ExT	Extension time
$FADH_2$	Flavin adenine dinucleotide
xg	Gravity (measurement of centrifugal force)
gDNA	Genomic DNA
GSH	Glutathione
GPx	Glutathione peroxidase
Grx	Glutaredoxin
GR	Grx-reductase
H_2O_2	Hydrogen peroxide
$OH^{\cdot}$	Hydroxyl radical
HA tag	Hemagglutinin antigen-protein-tag
HCl	Hydrochloric acid
HR	Homologous recombination
HRP	Horseradish peroxidase
H. sapiens	*Homo sapiens*
IMM	Inner mitochondrial membrane
IMS	Intermembrane space
Kb	Kilo base pairs
kDa	Kilo Dalton
K. lactis	*Kluyveromyces lactis*
LiAc	Lithium acetate
MDA	Malondialdehyde
$MgCl_2$	Magnesium chloride
MM	Minimal medium
Mn	Manganese
mt	Mitochondrial

MTS	Mitochondrial targeting sequence
NADH	Nicotinamide adenine dinucleotide
NADPH	Nicotinamide adenine dinucleotide phosphate
O_2^-	Superoxide anion
OD	Optical density
o/n	Overnight
OXPHOS	Oxidative phosphorylation
PAGE	Polyacrylamide gel electrophoresis
PCR	Polymerase chain reaction
PDB	Protein data bank
PEG	Polyethylene glycol
PGK1	Phosphoglycerate kinase 1
PI	Proteinase inhibitors mix
PPI	Protein-protein interactions
Prx	Thioredoxin peroxidase
PVDF	Polyvinylidene fluoride
PQ	Paraquat
RNA	Ribonucleic acid
ROS	Reactive oxygen species
RT	Room temperature
RT-PCR	Reverse transcriptase PCR
S. cerevisiae	*Saccharomyces cerevisiae*
SCO1	Synthesis of cytochrome c oxidase 1
SCO2	Synthesis of cytochrome c oxidase 2
SD	Standard deviation
SDS	Sodium dodecyl sulfate
SOD	Superoxide dismutase
S. pombe	*Schizosaccharomyces pombe*
TAE	Tris-acetic acid-EDTA
T_{an}	Annealing temperature
TBS-T	Tris-buffered-saline-tween 20
TEMED	Tetramethylethylenediamine
TM	Transmembrane domain
Tris	Tris(hydroxymethyl)aminomethane
Trx	Thioredoxin
TrxR	Trx-reductase
URA	Uracil
UTR	Untranslated region
WT	Wild type
YPD	Yeast extract-peptone-dextrose
Zn	Zinc

1 Introduction

Redox biology and reactive species are in the focus of research since the 1950s [1]. Reactive molecules had been considered for a long time as toxic to biological components. This view changed by the discovery of their regulatory and defensive role in endothelial smooth muscle [2] and leucocytes [3], respectively. Additionally, research data in the last years emphasized their role as signal molecules [4-6].

Thus, it is now evident that these species play a dual role in living organisms and in healthy cells; their production and elimination are finely balanced [7]. If this balance is disturbed, oxidative damage induced by elevated reactive molecules can impair physiological functions and result in several disorders (such as cardiovascular, neurological diseases, atherosclerosis, cancer [8]) and aging [9, 10].

The term "reactive species" is commonly used to define two distinct by-products; reactive oxygen species (ROS) and reactive nitrogen species (RNS) [11]. In this thesis the focus is on ROS and ROS-linked outcomes.

1.1 ROS production

In living organisms, ROS can be generated at distinct sites including mitochondria, endoplasmic reticulum (ER), peroxisomes, plasma and nuclear membranes [12, 13].

It is clearly indicated that in eukaryotic cells under physiological conditions, the majority of ROS (more than 90%) is produced in mitochondria through the reaction of leaking electrons from the electron transport chain (ETC, particularly complex I & III) with molecular oxygen. The superoxide anion ($O_2^{\cdot-}$) that is initially formed, is further enzymatically or spontaneously converted into hydrogen peroxide (H_2O_2). The H_2O_2 can be reduced either to water or the highly reactive hydroxyl radical ($OH^{\cdot}$, via Fenton and Haber–Weiss reactions) that cannot be detoxified enzymatically (figure 1) [14, 15].

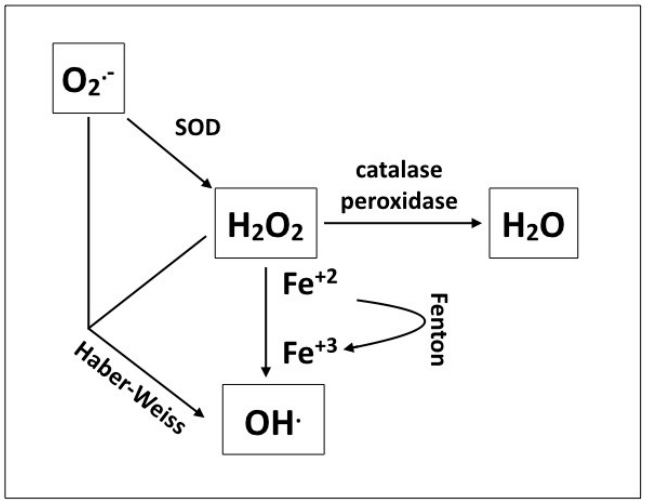

Figure 1. Inter-conversion of ROS in living organisms by either cellular defense mechanisms (SOD, catalase, peroxidase) or spontaneous reactions (Haber- Weiss and Fenton).

The electron leakage from ETC is strongly dependent on the physiological state of cells. Aerobic organisms that rely on ETC, developed complex antioxidant defensive systems to sustain ROS at a non-toxic level [13].

1.2 Oxidative stress

Alterations in environmental conditions including nutrient deficiency [16], dramatic temperature changes [17] and xenobiotic exposure [18, 19] can disrupt the redox balance and lead to stress in organisms. This stress is mostly linked to ROS, that either lowers the antioxidant levels or/and stimulates further ROS production [15, 20, 21]. As the accumulation of ROS can cause severe irreversible damages to essential biomolecules including nucleic acids, lipids and proteins, multiple defense mechanisms have been evolved in living organisms including our model organism, the yeast *Saccharomyces* (*S.*) *cerevisiae* (figure 2).

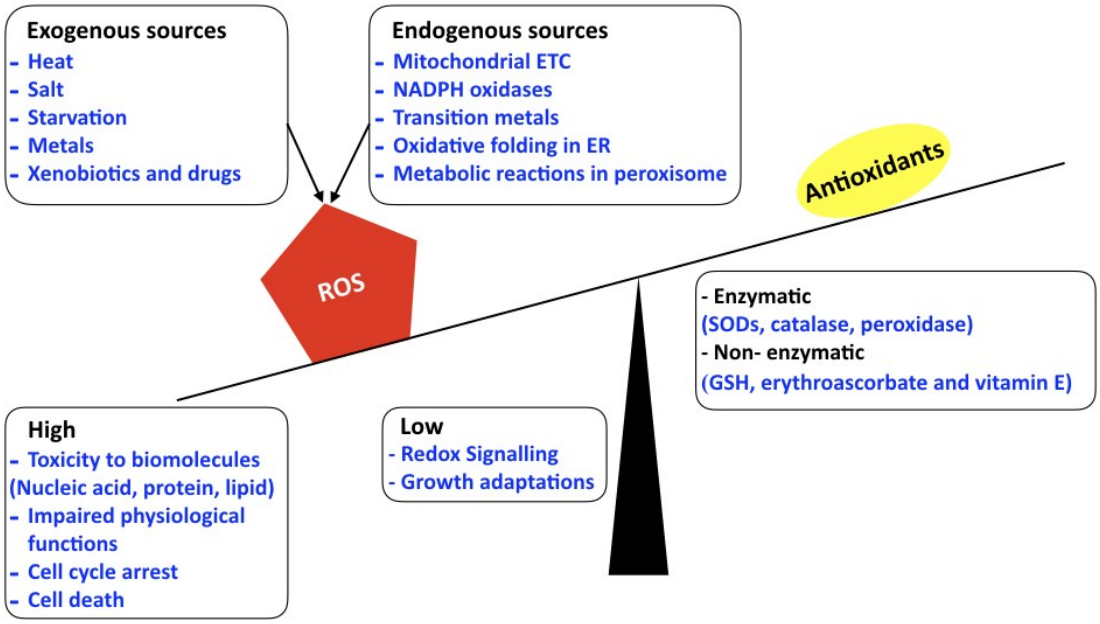

Figure 2. Oxidative stress is a consequence of the imbalance between ROS production and antioxidant systems.
Increased ROS produced from endogenous and exogenous sources can disrupt the balance in favor of oxidative stress. It causes severe damages to cells and outcompetes the beneficial roles of ROS such as signaling and adaptations.

In further parts of this section, activation of antioxidant response and key players of this defense system in *S. cerevisiae* are addressed in detail.

1.3 Antioxidant response

The antioxidant response toward ROS is composed of two steps: early (adaptive) and late. Under normal growth conditions, yeast cells have a limited amount of antioxidant and this is insufficient for the protection of cells at stress conditions. Thus, at the initial phase of stress while an early protection with the existing antioxidants is carried out, also transcription factors essential for the synthesis of additional antioxidants are induced [22, 23]. Thereby, the late response is triggered, and these newly synthesized antioxidants lead to higher protection against ROS and hence recovery of redox homeostasis [21].

There are four main transcription factors in *S. cerevisiae* essential for the cellular response toward stress: Yap1p, Skn7p, Msn2p, and Msn4p. Among them, Yap1p and Skn7p are particularly responsible for the oxidative stress response. The activation of antioxidant genes such as γ-glutamylcysteine synthase (*GSH1*), glutathione synthase (*GSH2*), glutathione peroxidase (*GPX2*) and thioredoxin peroxidase (*TSA1*) via

Yap1p has been shown [7]. Additionally, it was demonstrated that Yap1p acts in concert with Skn7p to up-regulate other antioxidant genes including thioredoxin (*TRX2*), thioredoxin reductase (*TRR1*), cytochrome *c* peroxidase (*CCP1*), catalase T (*CTT1*), superoxide dismutase 1 (*SOD1*), superoxide dismutase 2 (*SOD2*), thioredoxin reductase 2 (*TRR2*), thiol specific antioxidant and alkyl hydroperoxide reductase (*AHP1*) in response to H_2O_2 [7, 24, 25]. These up-regulated antioxidant genes play overlapping but also distinct defensive roles in connected detoxification pathways.

There are two superoxide dismutases (Sod1p, Sod2p) that fulfill the conversion of highly reactive $O_2^{\cdot-}$ to H_2O_2. Even though they carry out the same reaction, they have different intracellular localizations (Sod1p (Cu/Zn): cytosol & mitochondrial (mt) intermembrane space (IMS); Sod2p (Mn): mt matrix) and distinct catalytic metal(s) in their active sites (Cu/Zn or Mn) that influence their specificity toward distinct stressors [26-29].

The H_2O_2 converted by SOD enzymes is decomposed into water and oxygen via heme containing catalase A (Cta1p, peroxisomal) and catalase T (Ctt1p, cytosol).

Peroxidases, that are localized to different cellular compartments (nucleus, cytoplasm and mitochondria), catalyze the reduction of hydroperoxides with the aid of redox-sensitive cysteines [30]. They are divided into two groups regarding the electron donor: glutathione (GPx) & thioredoxin peroxidases (Prx). While GPx utilize glutathione (GSH) as a reductant substrate, Prx use thioredoxin (Trx). Besides their protective role aganist reactive species, they can sense H_2O_2 (Gpx3p [31] , Tsa1p [32]) and activate Yap1p for subsequent expression of antioxidants.

Glutaredoxins (Grx) and Trx are redundant thiol-oxidoreductase enzymes that reduce disulfide bonds to thiols via redox- active thiolated cysteines. Even though these two enzymes share many similarities (such as a “Trx fold” [33]) and act coordinately in cellular functions including protein repair, DNA synthesis and sulphur metabolism, there are remarkable differences between the systems. Different from Trx, Grx uses GSH as an electron donor. Additionally, despite both systems use the electrons of NADPH for recycling the oxidized form of the enzymes, specific reductase enzymes regenerate the reduced form of enzymes: Grx-reductase (GR) and Trx-reductase (TrxR) (figure 3) [34].

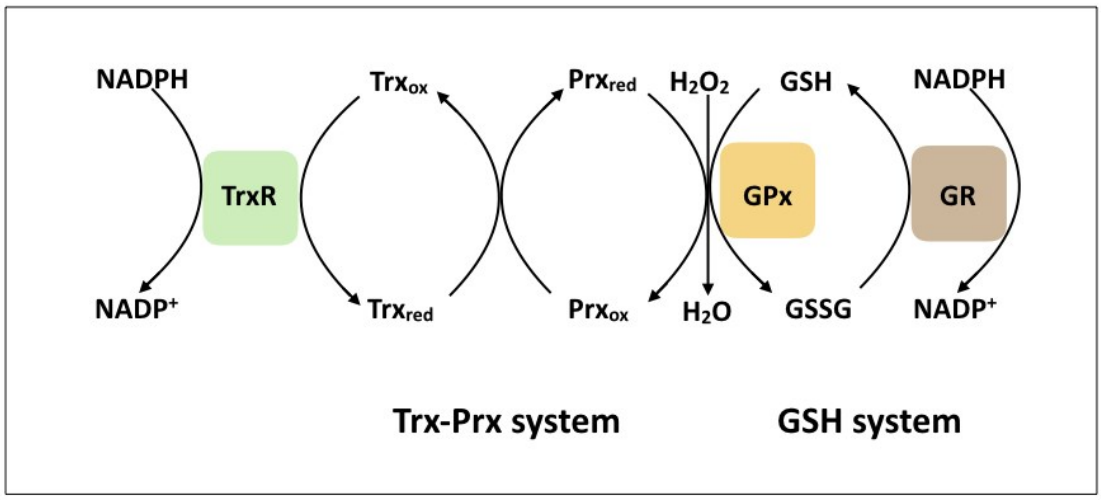

Figure 3. Mechanism of the Trx-Prx and GSH systems in detoxification of H_2O_2.
H_2O_2 is converted to water via two different peroxidases, glutathione (GPx) and thioredoxin peroxidases (Prx). Their oxidized forms are reduced by glutathione (GSH) and thioredoxin (Trx), respectively. Grx-reductase (GR) and Trx-reductase (TrxR) regenerate the reduced form of enzymes by utilizing the electrons of NADPH. The suffixes "ox" and "red" stand for oxidized and reduced forms of the enzymes, respectively (adapted from [35]).

In addition to the enzymatic defense at multiple cellular sites (figure 4), small molecules such as GSH, erythroascorbate, ubiquinone and vitamin E also play protective roles against reactive species in *S. cerevisiae* [36]. Besides their high reducing power, they can induce the synthesis [37] and activity of antioxidant enzymes [38] to increase the radical scavenging capacity of cells.

The cooperation between the players of distinct antioxidant pathways indicates an interconnection between these pathways and also reveals the complexity of the antioxidant defense mechanisms. To gain a deeper understanding into the interacting antioxidant networks, it is crucial to focus on the investigation of new players.

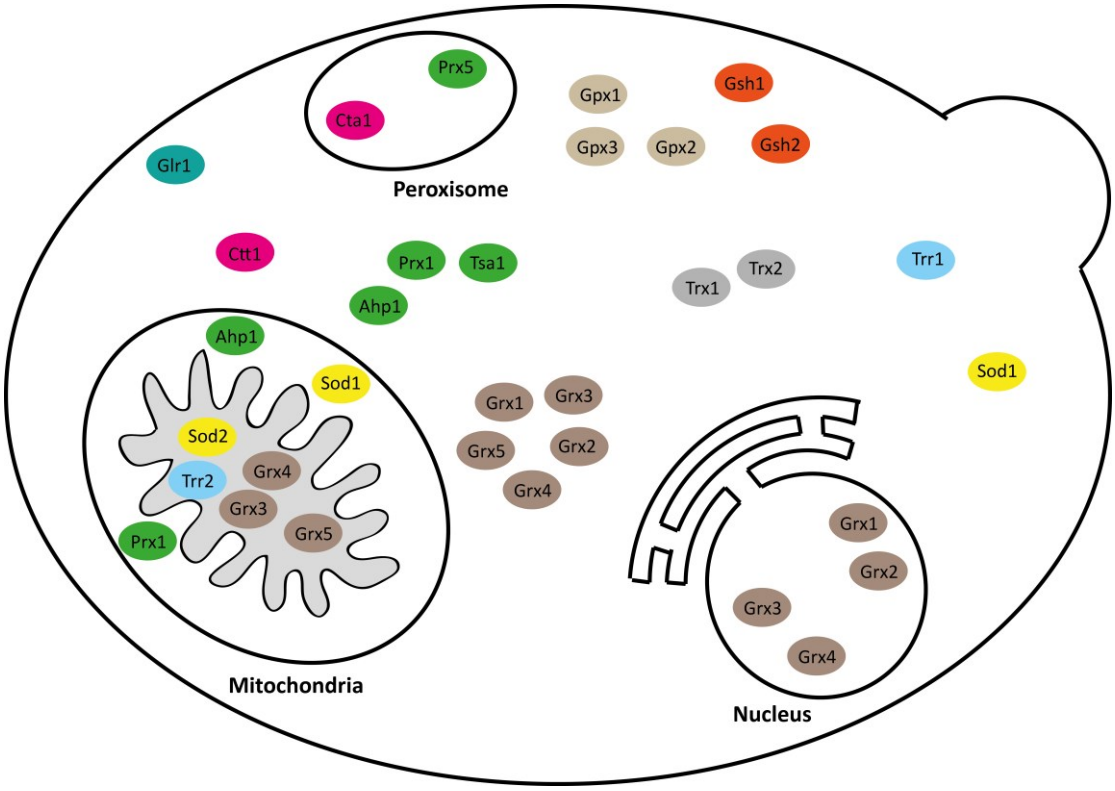

Figure 4. Subcellular localizations of main antioxidant enzymes in yeast.
Antioxidant enzymes are localized into different cellular compartments to detoxify the generated reactive oxygen species at the site effectively. (Glutaredoxin:dark brown, glutathione peroxidase: light brown, glutathione synthase:red, glutathione reductase: green-cyan, thioredoxin:gray, thioredoxin reductase: blue, superoxide dismutase: yellow, peroxiredoxin: green, catalase: pink)

1.4 The thioredoxin fold: From structure to function

The thioredoxin (Trx) fold is a structural protein motif that is composed of four central β-sheets surrounded by three α-helices [33]. Trx-fold proteins are present in all organisms and perform divergent functions such as protein folding [39], ROS [40] and xenobiotics [41] detoxification. These proteins are grouped into superfamilies based on their biological functions (table 1, [42]). The Sco (synthesis of cytochrome *c* oxidase) protein family is one of these Trx-fold proteins.

Table 1. Biological functions of Trx-fold superfamilies (adapted from [42]).

Superfamily	Function
Thioredoxin (Trx)	Reduction of disulfide bonds in proteins
Glutathione peroxidases (Gpx)	Reduction of hydroperoxides
Peroxiredoxins (AhpC-TSA, Redoxin, Prx)	Reduction of hydroperoxides
Sco (SCO1-SenC)	Copper (Cu) ion binding, Cu homeostasis, thiol-disulfide oxidoreductase activity
Dsb (DSBA)	Formation of disulfide bonds in proteins
ArsC	Reduction of arsenate
Glutaredoxin (Grx)	Reduction of disulfide bonds in proteins, deglutathionylation of proteins
Glutathione transferase (GST, GST_N)	Addition of glutathione to small molecules; reduction of hydroperoxides

1.5 Sco proteins

Sco proteins exist in all type of organisms. These proteins were firstly identified in *S. cerevisiae* as a vital gene product for the biogenesis of the cytochrome *c* oxidase (COX) [43].

COX is the terminal enzyme complex of the respiratory chain that catalyzes the reduction of water to oxygen via the transfer of electrons from cytochrome *c* to molecular oxygen. It is a multimeric protein that has a catalytic core comprised of three mt-encoded subunits (Cox 1-3). Eukaryotic COX has four redox-active metal centers (heme *a*, heme a_3, Cu_A and Cu_B) and belongs to the superfamily of heme-Cu containing oxidases. The two Cu centers Cu_A and Cu_B are located in the highly conserved Cox2 and Cox1, respectively [44-46].

The number of SCO genes varies among organisms: While some prokaryotes have up to seven [47], many eukaryotes carry two *SCO* genes resulting from a genome duplication process [48]. Overexpression studies in *S. cerevisiae* first proposed a Cu delivery role to Cox2 for Sco proteins. The phenotype of a *cox17* (a Cu chaperone) deletion mutant was rescued by the overexpression of Sco1/2p [49]. Investigation of the Cu binding ability (mostly via a conserved histidine and cysteines of CxxxC motif, figure 9) [47, 50] of both prokaryotic and eukaryotic Sco proteins strengthened the proposed Cu-associated role. Moreover, subsequent experiments in eukaryotes provided deeper knowledge on the possible stages in which Sco proteins could

participate for the delivery of Cu to Cu_A site [51]. Although the exact mechanism behind the Sco proteins-mediated Cox2 maturation is yet to be clarified, so far the most detailed explanation was provided by human studies.

The obtained results suggested a cooperative role for human Sco1 (hSco1) & Sco2 (hSco2) in the synthesis, maturation and inclusion of Cox2 into the COX holoenzyme. In the proposed model, both hSco2 and hSco1 were metallated via Cox17 in their reduced and oxidized state, respectively. The interaction of Cu-loaded Sco2 with newly synthesized Cox2 stimulates both the insertion of hSco1 to the hSco2– Cox2 complex and metallation of hSco1. The Sco proteins transfer the Cu to Cox2 sequentially and form the Cu_A site. Besides the Cu delivery, hSco2 perform a thiol-disulphide oxidoreductase activity and oxidize the cysteines of hSco1 during Cox2 maturation [52].
Although the sequential transfer of Cu to Cu_A site had been shown before in bacteria [53], it was the first time that a thiol-disulphide oxidoreductase activity was suggested for an eukaryotic Sco [52]. These studies shed a light on the divergent roles of Sco proteins.

On the other hand, genome analysis of several prokaryotes, which do not harbor a COX, revealed the existence of SCO genes and hint at distinct function(s) independent of COX biogenesis [47]. These findings are consistent with experimental results that demonstrated the broad roles of Sco proteins in the regulation of gene expression [54], defense against oxidative stress and disulfide reductase activity [55-57] in prokaryotes.

1.5.1. Structural similarity of Sco proteins to antioxidant enzymes

The structural homology between Sco proteins and antioxidant enzymes (peroxiredoxins and thiol-disulfide oxidoreductases) was first revealed by PSI-BLAST searches [58]. The subsequent structural characterizations of both eukaryotic and prokaryotic Sco proteins confirmed the PSI-BLAST results and revealed a highly conserved Trx-fold in these structures [53, 59-63]. However, in comparison with other Trx-fold members, eukaryotic Sco proteins have a special structural motif, the so-called “Sco fold”. It is a β-hairpin forming a solvent-exposed loop that connects helix α3 to strand β6 in the Trx-fold. (figure 5) [50].

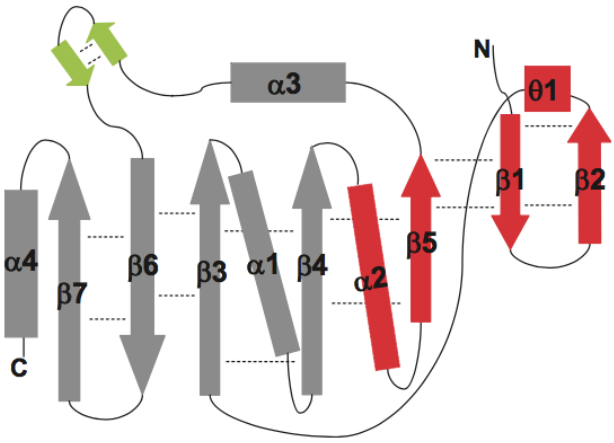

Figure 5. Topology diagram of the protein fold of Sco proteins.
The well-conserved secondary structure elements of the Trx-fold and additional elements found in Sco proteins are shown in gray and red, respectively. The Sco protein-specific structural motif, the so-called "Sco fold", is shown in green [50].

The results obtained so far not only identified the diverse roles of Sco proteins but also revealed the functional and structural conservation among distant organisms. Regarding the conservation, additional functions (such as oxidative stress defense) observed in prokaryotes could be also proposed for eukaryotic Sco proteins.

However, the complexity of biological systems particularly in higher eukaryotic organisms could complicate the identification of interconnected functions (*e.g.* respiration-ROS generation). Therefore, I decided to choose the simple and facultative aerobic organism *S.cerevisiae* for investigation of whether a defensive role aganist ROS is conserved in eukaryotic Sco proteins.

1.5.2. Current knowledge about Sco proteins of *S. cerevisiae*

S. cerevisiae has two *SCO* genes: *SCO1* (*ySCO1*) and *SCO2* (*ySCO2*) that have overlapping but also distinct functions (as is the case for human homologues). Previous studies showed the contribution of both Sco proteins to respiratory function [64]. While the single deletion mutant of *SCO1* (Δ*sco1*) has an obvious respiratory deficiency phenotype, the single deletion mutant of *SCO2* (Δ*sco*2) does not. On the other hand, the double deletion mutant of *SCO2* with another COX assembly factor *COA6* (Δ*sco2*Δ*coa6*) cannot grow on a non-fermentable carbon source [65].

It has been shown that *sco* mutants (Δ*sco1*, Δ*sco1*Δ*sco2*) have lower levels of Cox2p

[64]. This could be caused by improper metallation of CuA site by Sco proteins that leads to destabilized Cox2p. Both Sco proteins physically interact via the C-terminal domain of this subunit [64], but Sco2 is not able to rescue the phenotype of Δ*sco1* [66]. The effort put into identification of functionally interchangeable parts between these homologues revealed a unique 13 aminoacids (aa) part of Sco1p (immediately adjacent to the transmembrane (TM) region) that is crucial for the respiration-associated function [64].

In addition to a respiratory role, redox function has been postulated for yeast Sco proteins due to the presence of the Trx-fold. Stress experiments performed with H_2O_2 (in both Δ*sco1* and Δ*sco2*) strengthened the proposed redox role for *ySCO1* by the observation of an increased sensitivity of Δ*sco1* [62, 63, 67]. However, further studies identified that the H_2O_2 sensitivity is caused by the accumulation of the pro-oxidant COX subunit (Cox1 intermediate), not due to perturbations in redox homeostasis [68].

1.6 Background studies

For ySco2p, there has been no phenotypic evidence for a putative role in the redox homeostasis so far, as the deletion mutant does not exhibit an obvious phenotype. This might be due to a compensation of the possible function by other cellular proteins. To overcome this, a series of double deletion mutants were generated and tested under stress conditions (Gehlhar, 2013; Kost, 2015).

To induce oxidative stress, redox cyclers such as paraquat (PQ) and menadione were used. It is well known that these chemicals exert their cytotoxicity by accepting an electron from a reductant (including NADH ubiquinone oxidoreductase) and forming semiquinone radicals. As these radicals immediately react with O_2 under aerobic conditions, ROS such as $O_2^{\cdot -}$ generation is induced [69-71].

While the single deletion mutants of *ySCO1* and *ySCO2* do not have a distinctive stress-sensitive phenotype under stress conditions, double deletion mutants with concomitant deletion of Sod1p (Δ*sco1*Δ*sod1* and Δ*sco2*Δ*sod1*) exhibit a phenotype (figure 6). Further double deletion mutants were generated by concomitantly deleting other mt antioxidant enzymes (such as Trr2p and Trx3p), but none of these double mutants showed a pronounced phenotype (Gehlhar, 2013; Kost, 2015).

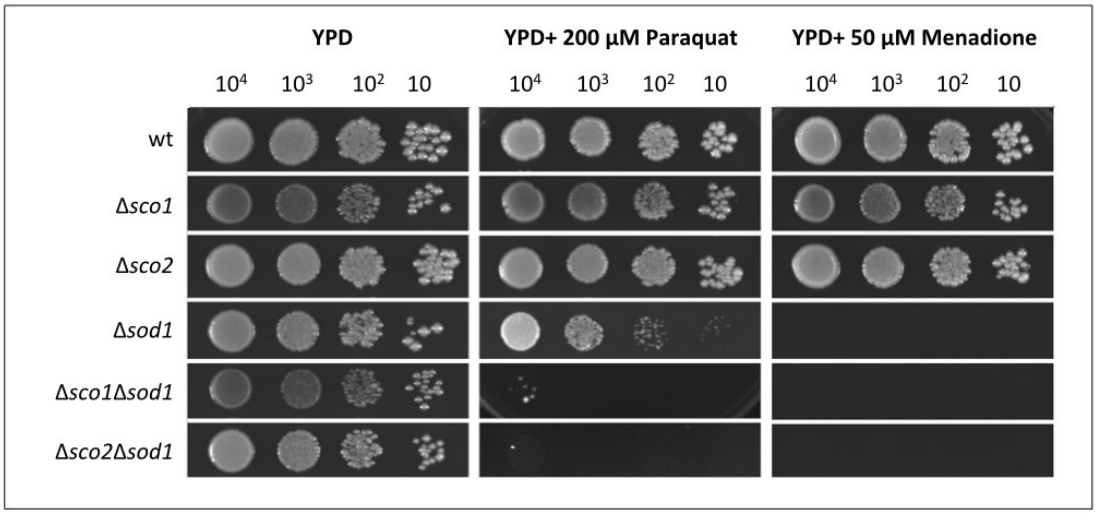

Figure 6. Growth assay of wt and mutant *S. cerevisiae* strains in the presence of different stressors (Kost, 2015).
Yeast cells were dropped in a serial dilution on YPD plates with or without stressors. The plates were incubated for two (YPD) or three (YPD+ stress inducing reagents) days at 30 °C.

The observation of a stress-sensitive phenotype for *SCO* deletion mutants does not only suggest an antioxidant role for these proteins, but also paves the way for cross-species complementation studies in yeast.

1.7 Using yeast as a model

1.7.1 Cross-species complementation studies

Yeast is an excellent eukaryotic experimental platform for the study of biological systems in higher organisms including human. Regarding its easy manipulation, compact genome size and genetic tractability [72], various genome-wide methods have been developed for complementation analyses over the last decades. The studies, particularly in *S. cerevisiae* (referred as yeast in this section), have helped researchers to define cellular pathways and reveal a detailed list of essential genes for various biological functions [73].

Complementation by candidate homologues can be analysed via the ability to rescue the phenotype caused by either deletion or suppression of the vital yeast gene. On the other hand, for non-essential genes firstly a phenotype is triggered (by external stressors (such as drug) or synthetic lethality), and then complementation can be tested in the same way as done for vital genes [73].
The functional complementation assays in the yeast system can be extended to

mutational analyses. For this purpose, either homologous mutations are generated in the yeast orthologues (parallel mutations) or the mutant gene is directly expressed in the host yeast strain [72-74]. The studies based on parallel mutations could be misleading, as the non-synonymous substitutions might cause different functional effects in distinct species [75]. Therefore, the latter approach is favorable in case of a functional complementation between the species.

1.7.2 Yeast model for human mitochondrial studies

Even though humans have more complex mitochondria compared to yeast, there is a high conservation of mt systems between these distant species. Additionally, the facultative aerobic nature of yeast make them a powerful model organism for both studying the mt function and the molecular mechanisms behind the human mt disorders [76].

With the aid of genome-wide functional screens in yeast, several mt proteins were identified and characterized [77]. Subsequent complementation studies contributed to the investigation of functional human homologues and verification of the damaging effects of human mutations [78] in mt enzymes particularly in the oxidative phosphorylation (OXPHOS) system [76, 79].

1.8 Aim of the study

Identification of a stress-sensitive phenotype for *SCO* deletion mutants of *S. cerevisiae* does not only propose a defensive role for Sco proteins against oxidative stress but also leads up to cross-species complementation studies in yeast.

The main objective of this thesis was to reveal the ability of Sco2 homologues from different organisms to functionally complement the putative antioxidant role of ySco2p.

During the scope of this study, the homologues of *ySCO2* should be selected from various organisms with different complexity to judge the functional conservation across distant species. Moreover, the recombinant strains should be generated via homologous recombination in the yeast *SCO2* locus to exclude artifacts of plasmid transformations (such as stability and copy number variation). To investigate the functional conservation between *ySCO2* and the selected homologues, a genetic complementation assay should be done first. Then, the level of oxidative stress should be quantified by direct and indirect assays to strengthen the claim on the possible

antioxidant role of *ySCO2* and the identified functional homologues.

In case of successful cross-species complementation, protein sequence alignment should be done to reveal whether there is any conserved aa or motifs that could be crucial for the function. If alignment results indicate the presence of conserved site(s), further mutagenesis analyses should be done to verify the functional importance of such aa residue(s). As the structural similarity of Sco proteins to antioxidant enzymes is well known, available structural data should be taken into consideration while interpreting the experimental data.

2 Materials & Methods

2.1 Materials

2.1.1 Chemicals and Reagents

Name	Supplier
Acetic Acid	Thermo Fischer Scientific
AEBSF	AppliChem Panreac
Agar	Formedium
Amersham hyperfilm EC	GE Healthcare
Ammonium Acetate	Fluka
Ammonium persulfate (APS)	Merck
Ammonium Sulphate	AppliChem Panreac
Butylated hydroxytoluene (BHT)	Sigma Aldrich
Bromophenol Blue	Serva
Chloroform	AppliChem
Coomassie® brilliant blue G-250	Merck
Complete Supplement Mixture	Formedium
dNTP mix	New England Biolabs
DTT	AppliChem
EDTA	AppliChem
Ethanol	VWR
Glycerol	VWR
HCl	VWR
Herring Sperm DNA	Invitrogen
Immobilon-P PVDF membrane	Millipore
Isopropanol	VWR
Lithium Acetate	Carl Roth
Mannitol	Roth
Maleic Acid	AppliChem
Menadione	Sigma Aldrich
Methanol	VWR
Non-fat dried Milk Powder	AppliChem

Nylon membrane	Amersham Pharmacia Biotech
Paraquat (PQ)	Sigma Aldrich
Peptone	Formedium
Phosphoric Acid	VWR
Phusion Polymerase	New England Biolabs
PI Mix	Roche
Plumbagin	Sigma Aldrich
Polyethylene glycol 3350	Sigma Aldrich
Red Safe Nucleic Acid Staining Solution	iNtRON Biotechnology
SDS Ultra Pure	AppliChem
Sodium lauroyl sarcosinate	Sigma Aldrich
TEMED	AppliChem
Tris	Carl Roth
Trisodium citrate	Roth
Trisodium sulfate	Roth
Tween-20	AppliChem Panreac
Yeast Extract	Formedium
Yeast Nitrogen Base	Formedium
2-mercaptoethanol	Carl Roth
30 % acrylamide/bisacrylamide	AppliChem

2.1.2 Equipment

Name	Supplier
Analytical balance TE214S	Sartorius
Block thermostat BT 100	Kleinfeld Labortechnik
Centrifuge SIGMA 3-18 K	Sigma
Chemi Imager Ready	Alpha Innotech
Eppendorf Thermocycler	Eppendorf
Eppendorf Thermomixer Comfort	Eppendorf
Fluorescence Microscope BZ-8100E	Keyence
Geldocumentation Alpha Imager	Alpha Innotech
Geldocumentation Smart3	VWR
Hoefer Slab Gel Dryer	Amersham BioScience
Incubator	Binder
Infinite M200 Plate Reader	Tecan
Mixer Mill M200	Retsch
PerfectBlue Gelsystem mini (SDS-PAGE)	PeqLab
PerfectBlue Horizontal Minigelsystems	PeqLab
PerfectBlue Semi Dry Blotter (Western Blot)	PeqLab
pH-Meter 766 Calimatic	Knick
Shaking incubator (Multitron Standard)	Infors
Shaking incubator (Series 25 Incubator Shaker)	New Brunswick Scientific
Table top centrifuge SIGMA 1-15 K	Sigma
Ultrospec 3000 UV/visible Spectrophotometer	Pharmacia Biotech

2.1.3 Kits

Name	**Supplier**
Amplex® Red Hydrogen Peroxide/Peroxidase Assay Kit	Invitrogen
Amersham™ ECL™ Western Blotting Analysis System	GE Healthcare
Bioxytech® LPO-586	Hölzel Diagnostika
GeneJET RNA Purification Kit	Thermo Fisher Scientific
NucleoSpin® Extract II	Machery-Nagel
RevertAid First Strand cDNA Synthesis Kit *Turbo DNA-Free™ Kit*	Thermo Fisher Scientific Life Technologies
PCR DIG Probe Synthesis Kit	Roche

2.1.4 Antibodies

Both primary and secondary antibodies were prepared in TBS-T with 5% (w/v) non-fat milk powder.

Name	**Target**	**Format**	**Dilution**	**Supplier**
HA	HA tag from human influenza hemagglutinin	mouse, monoclonal	1:1000	Roche
Pgk1	Phosphoglycerate kinase (*S. cerevisiae*)	mouse, monoclonal	1:5000	Invitrogen
Cox2	Cytochrome c oxidase (*S. cerevisiae*)	mouse, monoclonal	1:1000	Invitrogen
Sco2	Synthesis of cytochrome c oxidase 2	rabbit, polyclonal	1:1000	Aviva Systems
Sco2	Synthesis of cytochrome c oxidase 2	rabbit, polyclonal	1:1000	Thermo Fischer Scientific
DIG-AP	Digoxigenin	Sheep, polyclonal	1:20000	Roche
Rabbit-HRP	Anti-rabbit IgG antibody linked to horseradish peroxidase	donkey	1:10000	GE Healthcare
Mouse-HRP	Anti-mouse IgG antibody linked to horseradish peroxidase	sheet	1:10000	GE Healthcare

2.1.5 Plasmid

Name	**Marker**	**Source**
pUC19HA (3HA-URA)	*KlURA3*	W. Zachariae, MPI-B Martinsried

2.1.6 Primers

Table 2. List of overhang PCR primers (Primer annealing regions are in bold)

No	Name	Sequence (5´-3´)
#1	ySCO2 HA 55 for	ACAGGATCTTTTATAATATCACCATAGAAAGGGG AATTTGGGAAGCGAGAGTAAA**ATGTTGAATAGT TCAAGAAA**
#2	ySCO2 rev	**ATTGAAGATAAAAGAGTACC**
#3	ySCO2 HA tag for	CTCTTTTATCTTCAAT **TCCGGTTCTGCTGCTAG**
#4	ySCO2 HA 55 rev	ACGCCCTTAAGCCCAATTAATAATTTGAACTGAC AAGCATAATCATTTGACTTTC**CCTCGAGGCCAG AAGAC**
#5	K07152 HA 55 for	ACAGGATCTTTTATAATATCACCATAGAAAGGGG AATTTGGGAAGCGAGAGTAAA**ATGTTACGCAGC ATTGTTC**
#6	K07152 rev	**AAACAAGAAGGAATACCATTTGTC**
#7	K07152 HA tag for	CAAATGGTATTCCTTCTTGTTT**TCCGGTTCTGCT GCTAG**
#8	SpSCO1 HA 55 for	ACAGGATCTTTTATAATATCACCATAGAAAGGGG AATTTGGGAAGCGAGAGTAAA**ATGTTTCGAAGG GGTTTAGTT**
#9	SpSCO1 rev	**TTTCTGTTTCTTTCGGGACAA**
#10	SpSCO1 HA tag for	CCGAAAGAAACAGAAA **TCCGGTTCTGCTGCTAG**
#11	HCC1 HA 55 for	ACAGGATCTTTTATAATATCACCATAGAAAGGGG AATTTGGGAAGCGAGAGTAAA**ATGGCGTCTGCT CTATGTAG**
#12	HCC1 rev	**CTTCCGGTACTGACGGATC**
#13	HCC1 HA tag for	GATCCGTCAGTACCGGAAG**TCCGGTTCTGCTGC TAG**
#14	HCC2 HA 55 for	ACAGGATCTTTTATAATATCACCATAGAAAGGGG AATTTGGGAAGCGAGAGTAAA**ATGCTTCCTTGT CGCCGT**
#15	HCC2 rev	**CTGTGAAACAGAAGCAACTTC**
#16	HCC2 HA tag for	TGCTTCTGTTTCACAG **TCCGGTTCTGCTGCTAG**
#17	hSCO1 HA 55 for	ACAGGATCTTTTATAATATCACCATAGAAAGGGG AATTTGGGAAGCGAGAGTAAA**ATGGCGATGCT GGTCCTAG**
#18	hSCO1 rev	**GCTCTTTTTTCTGTATGGCC**
#19	hSCO1 HA tag for	CCATACAGAAAAAAGAGC**TCCGGTTCTGCTGCT AG**
#20	hSCO2 HA 55 for	ACAGGATCTTTTATAATATCACCATAGAAAGGGG AATTTGGGAAGCGAGAGTAAA**ATGCTGCTGCTG ACTCG**
#21	hSCO2 rev	**AGACAGGACACTGCGGAA**
#22	hSCO2 HA tag for	CCGCAGTGTCCTGTCT **TCCGGTTCTGCTGCTAG**

#23	SCOX HA 55 for	ACAGGATCTTTTATAATATCACCATAGAAAGGGG AATTTGGGAAGCGAGAGTAAA**ATGTCCCGCTCC CTGC**
#24	SCOX rev	**GCTGAACCATCCCTTTTTG**
#25	SCOX HA tag for	CAAAAAGGGATGGTTCAGC**TCCGGTTCTGCTGC TAG**
#26	K07152 w/stop codon rev	**TTAAAACAAGAAGGAATACCATTTG**
#27	K07152 w/stop codon for	TATTCCTTCTTGTTTTAA**TCTAGCTAAAAAGTGA ACGATC**
#28	ySCO2 w/o TM domain for	ACAGGATCTTTTATAATATCACCATAGAAAGGGG AATTTGGGAAGCGAGAGTAAA**CCAGAAGAGCTT GACAGATTAACG**

Table 3. List of sequencing primers

No	Name	Sequence (5´-3´)
#29	seq SCO2 for	GTATGAATTTCGAGAAGTCC
#30	seq SCO2 rev	CGTAATCTGGAACGTCATATG
#31	seq SCO2 rev w/o HA tag	CAATAGAGGAAAAAACGTATC

Table 4. List of overlap primers (final step)

No	Name	Sequence (5´-3´)
#32	ov SCO2 for	ACAGGATCTTTTATAATATCACCATAG
#33	ov SCO2 rev	ACGCCCTTAAGCCCAATT

Table 5. List of site-directed mutagenesis primers

No	Name	Sequence (5´-3´)
#34	hSCO2 C133S for	CACTCACAGCCCTGACATC
#35	hSCO2 C133S rev	GATGTCAGGGCTGTGAGTG
#36	hSCO2 E140K for	CCAGACAAGCTGGAGAAGCT
#37	hSCO2 E140K rev	AGCTTCTCCAGCTTGTCTGG
#38	hSCO2 L151P for	CAGCCGGAAGCAGAGC
#39	hSCO2 L151P rev	GCTCTGCTTCCGGCTG
#40	hSCO2 R171W for	CGAGTGGGACGACGTTG
#41	hSCO2 R171W rev	CAACGTCGTCCCACTCG
#42	hSCO2 S225F for	GACCACTTCATTGCCATCTAC
#43	hSCO2 S225F rev	GTAGATGGCAATGAAGTGGTC
#44	hSCO1 M294V for	CCACACACGTGAGGCC
#45	hSCO1 M294V rev	GGCCTCACGTGTGTGG
#46	ySCO2 D173K for	TCTGAATTAAAGGATAAAGACCA
#47	ySCO2 D173K rev	TGGTCTTTATCCTTTAATTCAGA
#48	K07152 K186E for	ACTGAGTTAGAGAAGCGTGAC

#49	K07152 K186E rev	GTCACGCTTCTCTAACTCAGT
#50	hSCO2 E152K for	GCAGCTGAAAGCAGAGC
#51	hSCO2 E152K rev	GCTCTGCTTTCAGCTGC
#52	HCC1 K225E for	GACAAAATAGAGGAAAATTCGG
#53	HCC1 K225E rev	CCGAATTTTCCTCTATTTTGTC
#54	hSCO1 D188K for	GGATGAAATAAAAAGCATTACAAC
#55	hSCO1 D188K rev	GTTGTAATGCTTTTTATTTCATCC
#56	ySCO2 D173A for	TCTGAATTAGCGGATAAAGACC
#57	ySCO2 D173A rev	TGGTCTTTATCCGCTAATTCAGA
#58	K07152 K186A for	ACTGAGTTAGCAAAGCGTGAC
#59	K07152 K186A rev	GTCACGCTTTGCTAACTCAGT
#60	hSCO2 E152A for	GCAGCTGGCAGCAGAG
#61	hSCO2 E152A rev	CTCTGCTGCCAGCTGC
#62	HCC1 K225A for	GACAAAATAGCGGAAAATTCG
#63	HCC1 K225A rev	CGAATTTTCCGCTATTTTGTC
#64	hSCO1 D188A for	GGATGAAATAGCAAGCATTACAAC
#65	hSCO1 D188A rev	GTTGTAATGCTTGCTATTTCATCC
#66	ySCO2 C154S for	CAGTCATAGCCCCGACATT
#67	ySCO2 C154S rev	AATGTCGGGGCTATGACTG
#68	ySCO2 C158S for	AGTCATTGCCCCGACATTTCTCCAGAA
#69	ySCO2 C158S rev	TTCTGGAGAAATGTCGGGGCAATGACT

Table 6. List of screening primers

No	Name	Sequence (5′-3′)
#70	ySCO2 chk for	GATTCGTGAACAAATTCAGGCGTA
#71	SCO2 chk rev	ATTCCCGCATGTTTACGC
#72	hSCO2 chk for	CATCTACCTGCTCAACCCT
#73	HCC2 chk for	CTCT CACAAGAGCTTCTTA
#74	hSCO1 chk for	TAGCTGCTTCAATTGCCAC
#75	HCC1 chk for	GTTGACTCGTTGACAGACG
#76	SpSCO1 chk for	GCTCGTGCAATCGGTTCT
#77	K07152 chk for	CATGTATCTGCTTATGTTCCAA
#78	SCOX chk for	GTGAACATAGCCAAGTGGAA

Table 7. List of genomic DNA(gDNA) contamination check primers

No	Name	Sequence (5′-3′)
#79	RPL17A for	ATGGCTAGATACGGTGCTAC
#80	RPL17A rev	TTAAGCAGCAATACGCTTTTG
#81	hSCO1 gDNA chk for	GGATGAAATAGCAAGCATTACAAC
#82	hSCO1 gDNA chk rev	GCTCTTTTTTCTGTATGGCC
#83	hSCO2 gDNA chk for	AGAGACAGGTGGGCAGGG
#84	hSCO2 gDNA chk rev	GCCTGGGCAACCTGTTTG

Table 8. List of Southern blotting primers

No	Name	Sequence (5´-3´)
#85	URA3 southern for	GAAAACACACGTTGATATCTTGGATG
#86	URA3 southern rev	CCTCTGCCAACAATGATGATATC

2.1.7 *S. cerevisiae* strains

Strain	**Genotype**	**Source**
BY 4741	*MAT*a, *his3Δ1*, *leu2Δ0*, *met15Δ0*, *ura3Δ0, [rho+]*	Euroscarf acc. no. Y00000
YBR024w (Δ*sco2*)	BY4741; *MAT*a; *his3Δ1*; *leu2Δ0*; *met15Δ0*; *ura3Δ0*; YBR024w::kanMX4	Euroscarf acc. no. Y03161
YJR104c (Δ*sod1*)	BY4741; *MAT*a; *his3Δ1*; *leu2Δ0*; *met15Δ0*; *ura3Δ0*; YJR104c::kanMX4	Euroscarf acc. no. Y06913
Δ*sco2*Δ*sod1*	BY4741; *MAT*a; *his3Δ1*; *leu2Δ0*; *lys2Δ0*; *met15Δ0*; *ura3Δ0*; YBR024w::kanMX4; YJR104c::kanMX4	Gehlhar 2013

2.1.8 Media

Two different media were used for cultivation of yeast cells: either a nutritionally rich yeast extract-peptone-dextrose (YPD) medium or a selective minimal medium (MM) supplemented with aa. All prepared cultures were autoclaved before usage. Heat sensitive substances including stressors (menadione, PQ, plumbagin) and aa supplements were added after cooling the media to 55 °C. Prior to addition, these substances were filter sterilized to maintain aseptic conditions.

YPD (*S. cerevisiae*)

Yeast Extract	10 g/l
Peptone	20 g/l
Glucose	20 g/l
Agar*	15 g/l

Minimal Media (*S. cerevisiae*)

Ammonium sulfate	5 g/l
Yeast nitrogen base	1.9 g/l
Glucose	20 g/l
Complete supplement mixture	600 mg/l
Agar*	25 g/l
Supplementary aa	
Arginine	20 mg/l
Histidine	60 mg/l
Leucine	80 mg/l
Lysine	30 mg/l
Methionine	20 mg/l
Threonine	200 mg/l
Tryptophan	80 mg/l

*Agar is only added in preparation of solid media plates.

2.2 Methods

2.2.1 Cultivation of *S. cerevisiae* cells

2.2.1.1 Culture conditions

For all experiments except screening, cells were revived from glycerol stocks. Briefly, with an inoculating loop the surface of frozen stock was scraped, and cells were streaked on fresh YPD plates. Plates were incubated at 30 °C for three days and preferably single colonies were picked to inoculate liquid cultures for further experiments.

2.2.1.2 Preparation of glycerol stocks

For long-term storage of cells, glycerol stocks were prepared from overnight (o/n) cultures by mixing with 50 % (v/v) glycerol solution in a 1:1 ratio. The samples were kept at -80°C.

2.2.2 Molecular biology methods

2.2.2.1 *S. cerevisiae* genomic DNA (gDNA) isolation

Yeast strains were grown in YPD media for approximately 16 h. For gDNA isolation, 2 ml of cell cultures were taken, and cells were harvested by centrifugation (3,500 xg/ 3 min/ room temperature (RT)). The cell pellet was washed with 1 ml ddH_2O and then resuspended in 500 µl of lysis buffer. The same volumes of glass beads were added, and cells were disrupted using the Mixer mill 200 (30 cycles/s for 2 min). Subsequently, 275 µl of ammonium acetate (7M, pH 7) was added to the supernatant, and incubated at 65 °C for 5 min. Samples were cooled on ice for 5 min. Then, 500 µl of chloroform was added, shaked vigorously and centrifuged (13,000 xg/ 2 min/ RT). The upper clear phase was taken, mixed with 1 ml of isopropanol and incubated for 5 min at RT to precipitate DNA. Samples were centrifuged (13,000 xg/ 5 min/ RT) and the DNA pellet was washed with 1 ml of 70 % ethanol and air-dried. The obtained pellet was resuspended in 100 µl ddH_2O and kept at -20 °C until use.

Lysis Buffer:	100 mM	Tris-HCl pH 8.0
	50 mM	EDTA
	1 % (w/v)	SDS

2.2.2.2 RNA isolation

2.2.2.2a Cultured mammalian cells (HEK293). Cells ($5x10^6$) were harvested and RNA was isolated with the GeneJet RNA purification kit and contaminating DNA was removed with Turbo DNA-free Kit according to the manufacturer's instructions.

2.2.2.2b Drosophila (D.) melanogaster. Twenty mg of flies were collected, and samples were frozen in liquid nitrogen immediately. Then, the frozen flies were ground in a reaction tube with a small pestle and total RNA was isolated with the GeneJet RNA purification kit according to the manufacturer's instructions. Subsequently, DNAase I treatment was done to remove any contaminating DNA.

2.2.2.3 RNA purity and concentration determination

RNA concentration and purity were determined by Nanodrop spectrophotometer measurement. For measurements, 1.5 µl of isolated RNA samples were taken and the ratio of absorbance at 260 and 280 ($A_{260/280}$) was used to determine purity (a ratio of ~2 is regarded as pure).

2.2.2.4 Reverse transcription

Reverse transcription was performed with the RevertAid first strand cDNA synthesis kit according to the manufacturer's instructions. The RNA samples (treated with DNAase I) were reverse transcribed in 20 µl reactions using Oligo (dT)18 primer and cDNA samples were stored at -20 °C.

2.2.2.5 Polymerase chain reaction (PCR)

2.2.2.5a Standard PCR

Phusion polymerase

For all PCR reactions except screening, the Phusion high-fidelity DNA polymerase was used to minimize the possible mutation rate. The PCR reaction was performed with different sets of forward and reverse primers (0.5 µM each), using 5 µl Phusion HF buffer, 0.5 µl Phusion polymerase and 0.5 µl dNTP (200 µM each) per 25 µl reaction. The annealing temperature (T_{an}) was calculated for each primer sets using the website of the producer and extension time (ExT) was adjusted according to the length of the amplicon (~30 s/kb).

The following PCR programme was used on thermocycler: 1x [98 °C/ 5 min], 30x [98 °C/ 10 s; T_{an}/ 30 s; 72 °C/ ExT], 1x [72 °C/ 5 min].

Taq polymerase

For all screening reactions, Taq polymerase (prepared in-house) was used. For PCR amplification, gDNA (~1 µg) was mixed with primers of interest (0.4 µM each), 2.5 µl 10x GoldTaq buffer, 0.75 µl $MgCl_2$ (50 mM), 0.5 µl dNTP (200 µM each) and 0.5 µl Taq polymerase (0.026 U/ µl) per 25 µl reaction. Annealing temperature and extension time were adjusted according to the primer's T_{an} and amplicon size (~1 min/kb).

The following PCR programme was used on thermocycler: 1x [94 °C/ 5 min], 30x [94 °C/ 10 s; T_{an}/ 30 s; 72 °C/ ExT], 1x [72 °C/ 5 min].

10x GoldTaq Buffer:	0.75 M	Tris-HCl pH 8.8
	0.2 M	Ammonium sulfate
	10 % (v/v)	Tween- 20

Table 9. Primers used for screening of positive clones (for primer details refer to table 6).

Recombinant strain	Primers for check PCR
ySCO2	#70, #71
hSCO2	#72, #71
HCC2	#73, #71
hSCO1	#74, #71
HCC1	#75, #71
SpSCO1	#76, #71
K07152	#77, #71
SCOX	#78, #71

2.2.2.5b Overhang PCR

The homology arms (55 bp), both at the 5'- and 3'-side of the sequence of interest, were included via overhang PCR. Regarding the high binding fidelity of the 3' end of primers for a specific sequence, overhang sequences (corresponding to homology arms) were added to the 5' end of both forward and reverse primers. At the first cycle of the PCR, primers anneal to the template via complementary sites and create a product with the overhang regions. Following cycles then amplify this new strand of DNA and generate the desired product. These PCR reactions were performed with the Phusion polymerase.

2.2.2.5c Overlap extension PCR

To generate recombinant DNA products, overlap PCR was used. All integration cassettes (including gene of interest, triple HA tag (3HA) and selectable marker (*URA3*)) were generated by this PCR method. The amplicons generated by standard PCR were hybridized through overlapping region (≥18 bp) and the final product is amplified via PCR. The integration cassettes and primers used for their generation are listed in table 10.

The first five cycles are critical for hybridization of overlap fragments and synthesizing full-length amplicon that serve as a template for following PCR cycles. Therefore, for the first five cycles lower annealing temperature (T_{an}-5) was used with extended time (1 min).

The programme was as follows: 1x [98 °C/ 5 min], 5x [98 °C/ 10 s; T_{an}-5/ 1 min; 72°C/ ExT s], 25x [98°C/ 10 s; T_{an}/ 1 min; 72°C/ ExT s], 1x [72°C/ 5 min].

Table 10. Integration cassettes and primers used for their generation.
To generate the integration cassettes, two rounds of PCR were carried out. The primer sets used in the first round (standard PCR) were separated by semicolon and in the second round, primer set in the third column was utilized for overlap PCR (for primer details refer to table 2 & 4).

Integration cassette	Primers for standard PCR	Primers for overlap PCR
ySCO2-3HA-*URA3*	#1, #2; #3, #4	#32, #33
K07152-3HA-*URA3*	#5, #6; #7, #4	#32, #33
SpSCO1-3HA-*URA3*	#8, #9; #10, #4	#32, #33
HCC1-3HA-*URA3*	#11, #12; #13, #4	#32, #33
HCC2-3HA-*URA3*	#14, #15; #16, #4	#32, #33
hSCO1-3HA-*URA3*	#17, #18; #19, #4	#32, #33
hSCO2-3HA-*URA3*	#20, #21; #22, 4	#32, #33
SCOX-3HA-*URA3*	#23, #24; #25, #4	#32, #33
K07152-URA3	#5, #26; #27, #4	#32, #33

2.2.2.5d Site-directed mutagenesis by overlap extension PCR

All mutant genes were generated via this PCR and all mutations generated were for single aa changes. The mutation sites were included into amplified products via mutagenic primers, whereby these sites were positioned to the center of the primers to allow binding. The mutated fragments were joined through the complementary region of mutagenic primers by overlap PCR (figure 7, table 11).

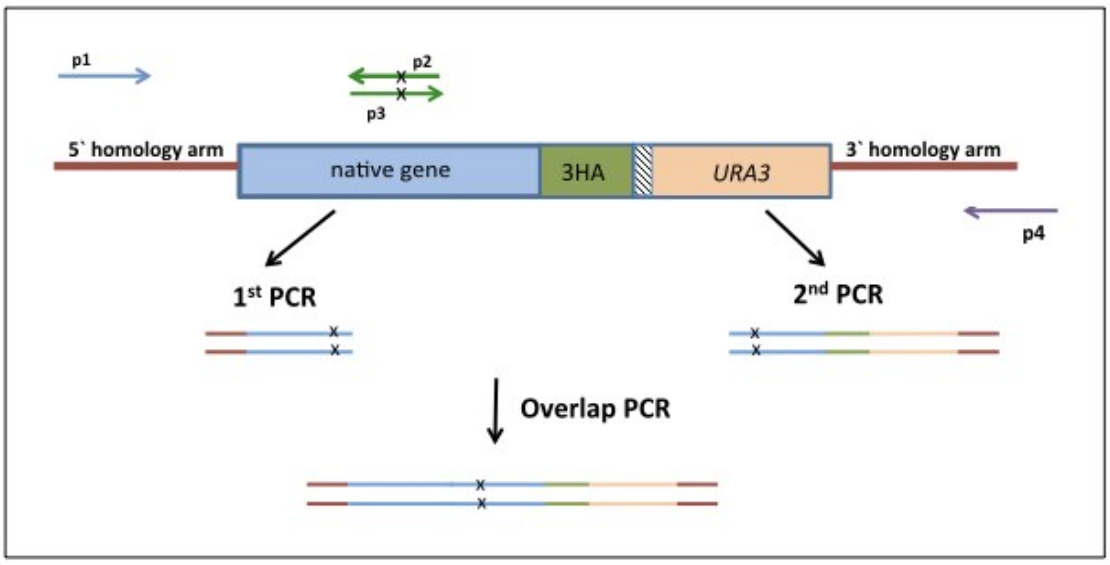

Figure 7. Site-directed mutagenesis by overlap-extension PCR.
All mutations are generated in the gene locus of either ySCO2 or its homologues. The gene-specific primers (p2&p3) harboring the desired mutations in overlap region (marked as x) are designed. In the first round, mutant amplicons are produced after two PCR reactions carried out with primer pairs p1/p2 (1^{st}) and p3/p4 (2^{nd}). In the second round, these mutant amplicons hybridize through overlapping region and the final product is amplified via PCR. The final amplicon includes the mutant gene fused to HA tag (stop codon highlighted in white striped box) with *URA3* cassette.

Table 11. Mutant strains and primers used for their generation.
To generate these mutant fragments, two rounds of PCR were carried out. The primer sets used in the first round (standard PCR) were separated by semicolon and in the second round, primer set in the third column was utilized for overlap PCR (for primer details refer to table 4 & 5).

Mutant strain	Primers for standard PCR	Primers for overlap PCR
hSCO2 (C133S)	#32, #35; #33, #34	#32, #33
hSCO2 (E140K)	#32, #37; #33, 36	#32, #33
hSCO2 (L151P)	#32, #39; #33, #38	#32, #33
hSCO2 (R171W)	#32, #41; #33, #40	#32, #33
hSCO2 (S225F)	#32, #43; #33, #42	#32, #33
K07152 (K186E)	#32, #49; #33, #48	#32, #33
HCC1 (K225E)	#32, #53; #33, 52	#32, #33
ySCO2 (D173K)	#32, #47; #33, #46	#32, #33
hSCO2 (E152K)	#32, #51; #33, #50	#32, #33
hSCO2 (E152A)	#32, #61; #33, #60	#32, #33
ySCO2 (D173A)	#32, #57; #33, #56	#32, #33
K07152 (K186A)	#32, #59; #33, #58	#32, #33
ySCO2 (w/o MTS and TM)	#28, #33	N/A
ySCO2 (C154S)	#32, #67; #66, #33	#32, #33
ySCO2 (C158S)	#32, #69; #68, #33	#32, #33

2.2.2.6 DNA agarose gel electrophoresis

Standard agarose gel electrophoresis was used for the analysis of DNA fragments. To

resolve the expected fragments, 1 % agarose gels were prepared. For DNA staining and visualization under UV, RedSafe solution was included into all gels. All samples were loaded into wells after mixing with 6x loading buffer. Electrophoresis was run in TAE buffer at 90V. Gels were visualized via the Chemi Imager Ready.

6x Loading Buffer:	29.6 % (v/v)	Glycerol
	0.1 M	EDTA pH 8.0
	0.002 % (v/v)	Bromophenol blue

TAE Buffer:	40 mM	Tris
	20 mM	Acetic acid
	1 mM	EDTA pH 8.0

2.2.2.7 DNA gel extraction and clean-up

For purification and extraction of DNA samples, NucleoSpin extract II kit was used according to manufacturer`s instructions. At final step, DNA was eluted in 30 µl of "NE" buffer and Nanodrop spectrophotometer was utilized to determine the concentration and purity of DNA (the ratio of $A_{260/280}$ ~1.8 is regarded as pure).

2.2.2.8 DNA sequencing

The commercial supplier Eurofins Genomic, Germany, performed all DNA sequencing. The DNA concentration for purified PCR fragments was 5-10 ng/ µl (15 µl final volume) and specific primers (final concentration 1.18 µM) were used.

2.2.2.9 Southern Blotting

To verify the single-site integration of the complementation cassettes, Southern blot analysis was performed.

2.2.2.9a DNA preparation

4 µg genomic DNA was digested with 40 U of high-fidelity restriction enzymes (*EcoR*I-HF & *Spe*I-HF) at 37 °C for 2.5 h. The digested DNA was run o/n on a 1% agarose gel to separate the fragments. The wt sample and DIG-labeled *URA3* specific probe were run in parallel as controls. After the run, the gel was incubated in solution I for 10 min to depurinate the DNA. Then, it was washed in the Solution II for 30 min (separation of the dsDNA) and then in Solution III for 30 min (neutralization) with

mild shaking.

Solution I: 0.25 M HCl

Solution II: 1 M NaCl
0.5 M NaOH

Solution III: 1 M NaCl
0.5 M NaOH

2.2.2.9b Blotting

DNA was transferred to a nylon membrane by capillary blotting. Three filter papers and the membrane were equilibrated in 2xSSC buffer (pH 7) and the system was set up as follows: the gel was put onto Saran wrap and the equilibrated membrane was placed onto the gel carefully to avoid any air bubbles. The corners of the gel were covered with parafilm to prevent a liquid flux and filter papers were placed onto the membrane. Finally, a stack of paper towels was put onto top and weighed down with a bottle and transfer was done for 3 h.

2x SSC solution: 0.3 M NaCl
0.03 M Trisodium sulfate

2.2.2.9c Preparation of a DIG-labelled probe

For detection of all samples by a single probe, a probe specific for *URA3* was designed and synthesized according to the manufacturer's instructions (using primers #85, #86; PCR DIG Probe Synthesis Kit). Since the labeling causes a size shift, the synthesis was checked on 1% agarose gel by running the unlabeled probe as a control in parallel.

2.2.2.9d Hybridization of the DIG-labelled probe to DNA

After drying the membrane, it was exposed to UV for 3 min to crosslink the transferred DNA to the membrane. Next, membrane was placed into a hybridization tube filled with 50 ml prehybridization solution and incubated for 2 hours at 65 °C. The DIG-labeled *URA3* probe (7ng/µl) was boiled at 95°C for 10 min and then immediately cooled on ice for 10 min. The probe (~10 ng/ml) was mixed with the freshly prepared prehybridization solution and added onto the membrane followed by

o/n incubation at 65 °C. The next day, the membrane was washed twice with 40 ml pre-heated washing solution I for 10 min at 65 °C and then again twice with 40 ml pre-heated washing solution II. The last washing was done with washing solution III for 5 min at RT.

1x Blocking Solution:	1 % (w/v)	Blocking reagent
	10 mM	Maleic acid
	15 mM	NaCl
20x SSC Solution:	3 M	NaCl
	0.3 M	Trisodium sulfate
Prehybridization Solution:	5x SSC	
	0.1 % (w/v)	Sodium lauroyl sarcosinate
	0.1 % (w/v)	SDS
	0.1 % (v/v)	Blocking solution
10x Maleic acid buffer:	1 M	Maleic acid
	1.5 M	NaCl
	NaOH to pH 7.5	
Washing Solution I:	0.3 M	NaCl
	0.03 M	Trisodium citrate
	0.1 % (w/v)	SDS
Washing Solution II:	0.75 M	NaCl
	0.075 M	Trisodium citrate
	0.1 % (w/v)	SDS
Washing Solution III:	1x Maleic acid buffer	

2.2.2.9e Detection of the hybridized DIG-labelled *URA3* probe

The membrane was blocked in blocking solution for 3 h and then incubated in antibody solution (anti-DIG-Fab, 1:20000) for 1 h at RT. Afterwards, it was washed

twice with washing solution III for 15 min each and equilibrated in detection solution for 5 min. For detection, 2 ml of detection solution was mixed with 20 µl CPD Star (Roche) and spread onto membrane. After 5 min incubation in dark, the membrane was air-dried and exposed to film for varying times.

Detection Buffer: 100 mM Tris/HCl pH 9.5

2.2.2.10 Yeast transformation

Yeast cells were transformed as described [80]. Yeast strains were cultured o/n in YPD media and in the morning, a fresh culture (10 ml) was set up with an OD_{600} of 0.5. Cells were grown till they reach an OD_{600} ~2 (approximately 4,5 h) and harvested by centrifugation (3,500 xg/ 3 min/ RT). They were washed firstly with ddH_2O and then with 100 mM lithium acetate (LiAc). After washings, the following components were added onto the cell pellet: 240 µl 50 % PEG 3350 (w/v)), 36 µl 1 M LiAc, 10 µl single stranded DNA (from Herring sperm, 10 mg/µl), PCR product (~300 ng) and ddH_2O to a final volume of 360 µl. Since the single stranded DNA is used as a carrier for transforming DNA, it was denatured by heating to 95 °C for 5 min and immediately chilled on ice prior to addition. The cell pellet was completely dissolved by vortexing and heat-shocked at 45 °C for 40 min. Then, cells were pelleted by centrifugation (3,000 xg/ 20 s/ RT) and resuspended in 100 µl of dH_2O. They were spread onto solid minimal media plates without uracil for selection of transformants. After three days, single colonies were picked and streaked onto fresh minimal media plates to eliminate any contaminating non-transformed cells.

2.2.2.11 Yeast growth assay

The sensitivity of yeast strains toward oxidative stress was tested on solid YPD media plates and all plates were prepared freshly one day before the experiment. Yeast strains were inoculated in 5 ml YPD as a pre-culture. After 24 hours, it was used to set up the main culture (1:100). The main culture was grown o/n and OD_{600} of samples was measured. It was assumed that the OD_{600} of 1 is equivalent to 1×10^7 cells/ml. Before spotting onto solid media, yeast cultures were sequentially diluted from 1.25×10^6 to 1.25×10^3 cells/ml. From each dilution, 8 µl was taken and spotted onto the respective plates. While control plates (without stressor) were incubated at 30 °C for two days, stress plates were incubated for three days. Experiments were

performed at least three times for each included strains.

2.2.3 Protein methods

To check the expression and localization of homologues, Western Blot analysis was performed.

2.2.3.1 Isolation of crude mitochondria from yeast

For isolation of mitochondria, yeast strains were inoculated in 5 ml of YPD as a pre-culture. After 24 h, it was used to set up the main cultures (1:100). The cultures were grown o/n and the next day, cells were collected by centrifugation (3,500 xg/ 3 min/ RT). The cell pellet was washed once in 1 ml dH_2O and then resuspended in 500 µl of ice-cold MTE buffer. Then, glass beads (the same volume as cell pellet) were added and cells were disrupted using the Mixer mill 200 (30 cycles/s for 5 min). Samples were kept on ice until the glass beads sediment and the supernatant was transferred to a new tube. The beads were washed with fresh 400 µl of MTE buffer and both supernatants were combined. To remove remaining cell debris, samples were centrifuged (3,500 xg/ 5 min/ 4 °C). Then, the supernatant was transferred to a new tube and centrifuged (12,000 xg/ 15 min/ 4 °C) for fractionation. After centrifugation, the collected supernatant was kept as the "cytoplasmic" fraction and the pellet resuspended in 50 µl of MTE buffer was used as the "mitochondrial" fraction.
Protein concentration was determined with the NanoDrop spectrophotometer (A_{260}) for further protein analyses.

MTE buffer:	650 mM	Mannitol
	20 mM	Tris/HCl pH 7.6
	1 mM	EDTA
	1x	PI mix (added freshly)
	1 mM	AEBSF (added freshly)

2.2.3.2 SDS-PAGE

To separate proteins, 15 % SDS-PAGE gels were used. Samples were mixed with 6x Laemmli buffer and incubated at 95 °C for 5 min. Subsequently, all samples as well as a protein ladder (PageRuler plus prestained) were loaded to the wells and the gels were run in 1x running buffer. The electrophoretic separation was performed at 80 V in the stacking gel and at 120 V in the separating gel for about 2-2.5 h.

6x Laemmli buffer:	300 mM	Tris/HCl pH 6.8
	10 % (w/v)	SDS
	1 % (w/v)	Bromophenol blue
	10 % (w/v)	Glycerol
	100 mM	DTT (added freshly)

1x Running buffer:	25 mM	Tris
	192 mM	Glycine
	0.1 % (w/v)	SDS

2.2.3.3 Protein transfer

Due to the higher transfer efficiency, wet blotting was used to transfer proteins from the SDS-PAGE gels to a PVDF membrane. Firstly, protein gel and filter papers (same size as a gel) were equilibrated in 1x transfer buffer for 10 min with gentle shaking. Then, a "transfer sandwich" was prepared in this order: filter paper-gel-membrane-filter paper. The assembled sandwich was placed into a tank between the electrodes and fully filled with transfer buffer. The transfer was performed at a constant voltage (100 V) for 30 min. To dissipate the heat, the transfer was conducted with an ice pack and run at 4 °C.

1x Transfer buffer:	25 mM	Tris
	192 mM	Glycine
	0.01 % (w/v)	SDS
	10 % (v/v)	Methanol

2.2.3.4 Colloidal Coomassie gel staining

After the transfer, proteins in the gels were stained with colloidal Coomassie staining procedure [81]. Briefly, gels were fixed in fixer solution for 30 min and then stained in colloidal Coomassie staining solution o/n.

1x Fixer solution:	10 % (v/v)	Acetic acid
	40 % (v/v)	Ethanol

Staining solution:	8 % (w/v)	Ammonium sulfate
	0.96 % (v/v)	Phosphoric acid
	0.08 % (w/v)	Coomassie Blue G-250
	20 % (v/v)	Methanol

2.2.3.5 Protein detection

The air-dried membranes were reactivated in methanol and washed in 1x TBS-T shortly. Blocking was done for 1 h in TBS-T within 5 % (w/v) non-fat milk powder. Subsequently, blocked membranes were incubated with the primary antibody o/n at 4 °C. The next day, membranes were washed three times for 10 min in TBS-T and then incubated with secondary antibody (coupled to HRP) for 30 min. After incubation, membranes were washed three times for 10 min with TBS-T again.

Amersham ECL prime Western blotting detection reagent was used as a substrate for HRP-catalyzed chemiluminescent detections. The chemiluminescence was documented by exposure of a film to the membrane for varying times (depending on the strength of signal).

1x TBS-T:	20 mM	Tris/HCl pH 7.6
	137 mM	NaCl
	0.001 % (v/v)	Tween-20

2.2.3.6 Stripping the membrane and reprobing

For probing multiple targets on the same membrane, the previously bound antibodies were removed from the membrane. Briefly, the membrane was incubated in stripping buffer for 30 min at 55 °C with mild shaking. Then, the membrane was washed twice in TBS-T for 15 min and blocked again in 5 % (w/v) non-fat dried milk powder in TBS-T for 1 h at room temperature for further immunological detections.

Striping buffer:	62.5 mM	Tris/HCl pH 6.7
	2 % (w/v)	SDS
	100 mM	2-mercaptoethanol (added freshly)

2.2.4 Biochemical methods

For all analysis in this section, yeast strains of interest were inoculated in 5 ml of YPD as a pre-culture, grown for 16 h and used to set up the main cultures (1:100 in

fresh YPD). PQ (100 µM) was freshly prepared in water and added to cultures after 4 h. After 24 hours treatment, OD_{600} of samples was measured.

2.2.4.1 Methylene Blue staining

To assess the viability of cells in untreated and PQ-treated cultures, samples were stained with methylene blue. Since the cell density was lower in PQ-treated cultures of Δ*sod1* and Δ*sco2*Δ*sod1*, they were 3 and 10 times concentrated, respectively prior to staining. Then, 10 µl of cell suspension (in YPD) was mixed with 90 µl of methylene blue solution and incubated for 10 min at RT. Cells treated with 60 % (v/v) ethanol for 30 min was included as a control and viability was examined by microscope. While viable cells were colorless, dead cells were blue.

Methylene blue solution: 0.2 mg/ml Methylene blue
150 mM Phosphate buffer pH 7.2

2.2.4.2 Quantification of ROS

2.2.4.2a Amplex Red staining

The release of hydrogen peroxide from cells was measured with an Amplex red hydrogen peroxide/peroxidase assay kit. Cell suspension was incubated for 30 min in the presence of 10 µM Amplex Red and 5 U/ml of horseradish peroxidase. Then, cells were pelleted by centrifugation (3,000 xg/ 20 s/ RT) and supernatant was kept for fluorescence measurements (ex: 525±10, em: 585±10) with the plate reader. The settings were as follows: 25 reads (from bottom of the plate), gain 120, four reads per well. A sample without cells was used as a blank and the amount of hydrogen peroxide was calculated from standard curve with known concentrations.

2.2.4.2b Lipid peroxidation assay

The Bioxytech LPO-586 kit was used to measure the lipid peroxide levels in *S. cerevisiae* strains. Harvested cells were resuspended in 500 µl of lysis buffer and disrupted in the presence of glass beads (the same volume as cell pellet) using the Mixer mill 200 (30 cycles/s for 2 min). Subsequently, samples were centrifuged (3,500 xg/ 5 min/ 4 °C) and the supernatant were collected into a new tube. 1.5 µl was taken to measure the protein concentration (A_{260}, NanoDrop) and 100 µl was used to quantify lipid peroxidation levels according to the manufacturer's instructions. Hydrochloric acid was utilized in all experiments to specifically measure the end

product, malondialdehyde (MDA) amount in samples. All samples were run in duplicates and absorbance at 586 nm was read out with a plate reader. A separate blank was prepared for each sample according to the manufacturer's instructions and the lipid peroxidation levels were normalized to the protein concentrations in the final supernatants.

Lysis buffer: 1x PBS pH 7.4
5 mM BHT

2.2.5 Bioinformatics

The Protein Data Bank (PDB) was used to retrieve protein structures and SWISS-MODEL was utilized to generate template-based model structures. Top-ranked templates (based on sequence identity) identified by Protein Model Portal were chosen and used by SWISS-MODEL to build the respective models.

Clustal Omega was utilized for multiple sequence alignment and building the phylogenetic tree based on these alignment results (via neighbor joining method).

Salt bridges at mutation sites were estimated by the PLIP software [82] using default parameters. Briefly, the distances between atoms of positively and negatively charged aa were calculated on either characterized or model structures. As long as the distance does not exceed 5.5 Å, the interaction was classified as salt bridge.

The protein figures included in this thesis were generated by PyMOL [83]. Several scripts provided by the programme were run for different purposes such as identifying mutation sites, superimposing structures and finding the surface exposed aa. Moreover, the APBS plugin supported by PyMOL [84] was used together with PDB2PQR [85] to calculate the electrostatic potential surfaces.

2.2.6 Statistical Analysis

The significance of differences between untreated (- PQ) and treated samples (+ PQ) was evaluated by using two-tailed t-test. Analyses were done with GraphPad Prism 5 software (GraphPad Software, San Diego, California).

Table 12: Bioinformatics online databases, tools and analysis software

Name	**Web Address**	**Description/ Purpose of Usage**	**References**
SGD	https://www.yeastgenome.org	The *Saccharomyces* Genome Database Advanced search and analysis tool	
NCBI	https://www.ncbi.nlm.nih.gov	A comprehensive resource of sequence information Availability of various online tools	
NEB Tm Calculator	http://tmcalculator.neb.com/#!/	Server for calculation of suitable annealing temperature regarding to different conditions	
Clustal Omega	https://www.ebi.ac.uk/Tools/msa/clustalo/	Server for multiple sequence alignment of proteins	
SWISS-MODEL	https://swissmodel.expasy.org	Automated protein structure modeling server	[86]
Protein Model Portal	http://www.proteinmodelportal.org	Comparative protein structure modeling and analysis	[87]
PLIP	http://plip.biotec.tu-dresden.de/plip-web/plip/index	Automated interaction profiler	[82]
MitoFates	http://mitf.cbrc.jp/MitoFates/cgi-bin/top.cgi	Software for prediction of mt targeting sequences	[88]
ApE	http://biologylabs.utah.edu/jorgensen/wayned/ape/	Software for analysis of sequences	Wayne Davis
TAIR	https://www.arabidopsis.org	The *Arabidopsis thaliana* database	

		Advanced search and analysis tool	
PomBase	https://www.pombase.org	The *Schizosaccharomyces pombe* database Advanced search and analysis tool	
KEGG	http://www.genome.jp/kegg/genes.html	The *Kluyveromyces lactis* database Advanced search and analysis tool	
EMBOSS Needle	http://www.ebi.ac.uk/Tools/psa/emboss_needle/	Server for pairwise sequence alignment	
ExPASy	http://web.expasy.org/compute_pi/	Server for calculating the isoelectronic point and molecular weight of proteins	
UniProt	http://www.uniprot.org	Database of protein sequence and functional information	
TMPred	https://www.ch.embnet.org/software/TMPRED_form.html	Server for prediction of transmembrane regions	

3 Results

3.1 Selection of homologues by bioinformatic analysis

The homologues of *ySCO2* were selected from eukaryotic organisms with different genetic complexity*: Homo sapiens (hSCO1&2)*, *Schizosaccharomyces pombe (SpSCO1)*, *Arabidopsis thaliana (HCC1&2)*, *Drosophila melanogaster (SCOX)* and *Kluyveromyces lactis (K07152)*. The number of *SCO* genes in the chosen organisms vary [50]. The related information (*e.g.* sequences) about homologues were retrieved from the databases mentioned in section 2. The similarity of the respective homologues to ySco2p was assessed by the pairwise alignment tool using Emboss Needle (figure 8a) and the phylogenetic tree was constructed based on the alignment of the aa sequences by CLUSTAL Omega (figure 8b). While the highest degree of conservation is observed among yeast species (SpSco1 and K07152), aa identity between ySco2p and its homologues from higher organisms (Hcc1, Hcc2, hSco1, hSco2, Scox) is in the order of 30 %.

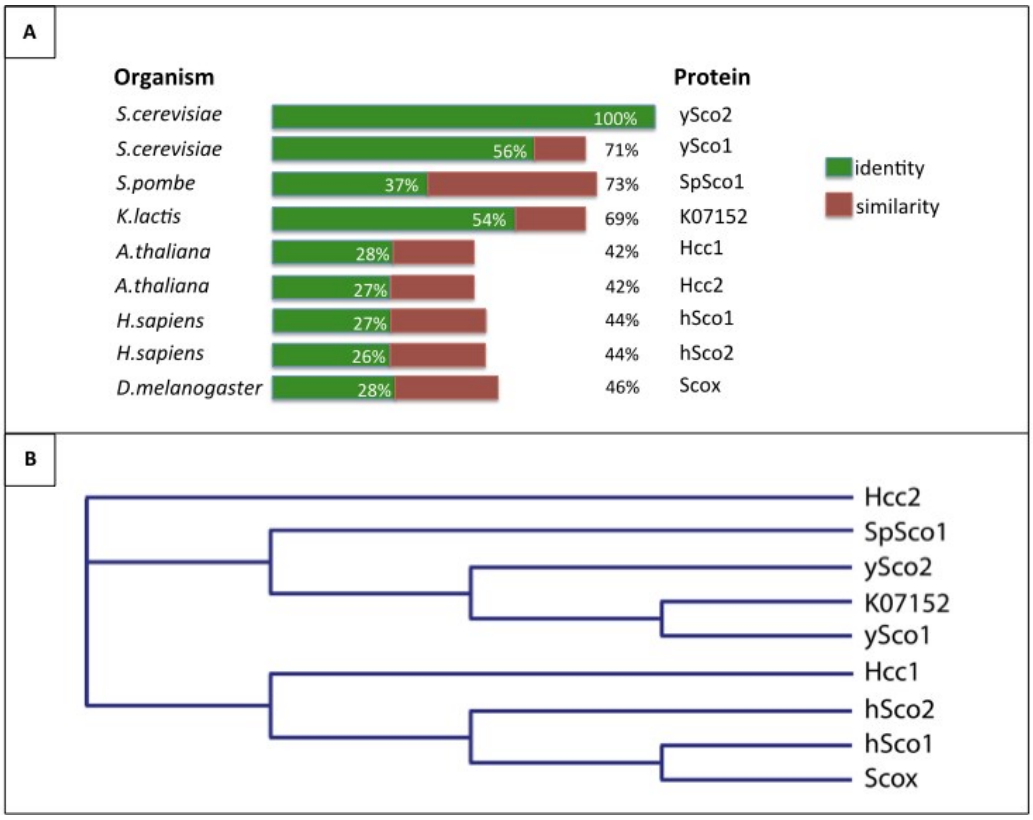

Figure 8. Comparison of protein sequences via bioinformatics tools.
A. The protein sequences of homologues are compared to ySco2p (pairwise alignment) and the percentage of identity & similarity is calculated by Emboss Needle.
B. The phylogenetic tree of Sco homologues is constructed based on the alignment of aa sequences by Clustal Omega.

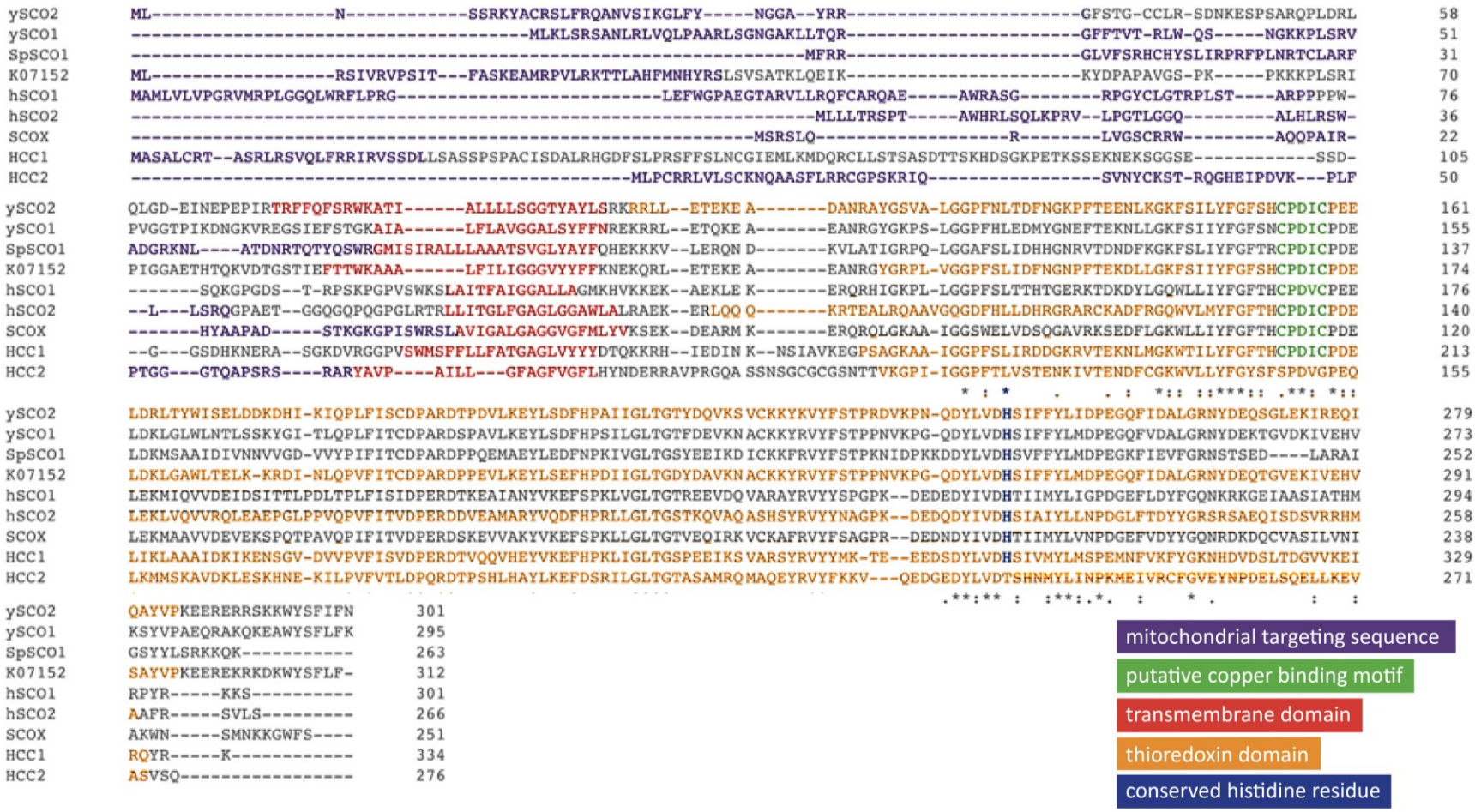

Figure 9. Multiple sequence alignment of Sco2 homologues from different organisms.
Within the aligned aa sequences, the asterisks indicate identical residues. Single and double dots show the highly and moderately conserved residues, respectively. The dashes are corresponding to the gaps that were included for the optimization of the alignment. The characteristic sequences and conserved residues are highlighted. Predicted mt targeting sequences (MTS) and transmembrane (TM) domain are shown in purple and red, respectively. Highly conserved putative Cu binding motif is depicted in green while (predicted) thioredoxin domain is in orange. Conserved histidine residue proposed to be crucial for Cu coordination is highlighted in blue.

Alignment results (figure 9) clearly show that C-terminal part of proteins is more conserved among homologues compared to N-terminal part, particularly the sequences in close proximity to putative Cu binding motif and Cu coordinating histidine. Different prediction programmes and databases were utilized for the analysis of primary protein sequences of homologues. The prediction tool, MitoFates used for estimation of MTS (all selected homologues) and TM domain was predicted with TMpred for SpSco1 and K07152 (for others this information was retrieved from either literature or online database, UniProt). The information regarding the Trx domain was obtained from UniProt.

Taken together, these data show that while the N-terminal part of proteins contains the MTS and TM domain (single helix), the Cu binding motif (CxxxC) and Trx domain are located at the C-terminal part. The CxxxC motif, which is highly conserved across Sco family proteins [47, 50], is also present in all analysed homologues except Hcc2. The Trx domain encompasses almost the entire C-terminal portion of proteins. Existing structural data have already showed the participation of conserved histidine (highlighted in blue, figure 8) of hSco1 [60], hSco2 [61] and ySco1 [62] into the Cu coordination. Even though this information is missing for other selected homologues (due to lack of structural data), conservation of this residue together with CxxxC motif could be a strong evidence for the Cu binding ability of these homologues (except Hcc2).

3.2 Generation of recombinant strains

After selection of the homologues, integration cassettes with the gene of interest were designed (see section 2.2.2.5). Since exons of higher organisms are poorly spliced in *S. cerevisiae* [74], the respective cDNAs of these homologues were used and generated cassettes were transformed into the host strain Δ*sco2*Δ*sod1* (figure 10). Owing to the highly efficient homologous recombination machinery of *S. cerevisiae* [89], a PCR-mediated gene targeting approach was applied by including homology arms to both 5`- and 3`ends. Due to the unavailability of antibodies for the majority of the homologues, 3HA tag was fused to all genes for further immunological detection.

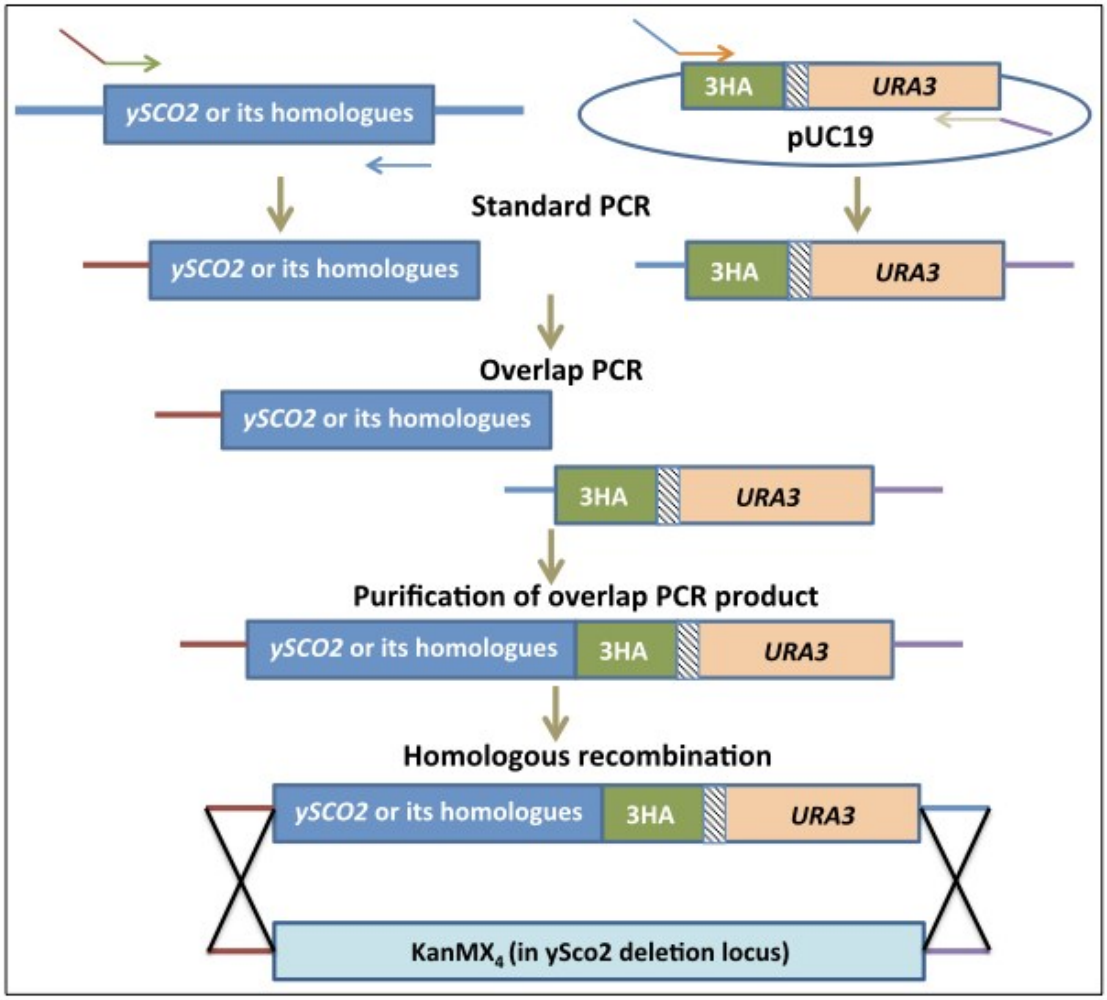

Figure 10. A scheme of the strategy for the construction of the integration cassettes and homologous recombination.
Standard PCR was carried out for amplification of cDNA fragments (of *SCO2* homologues from the corresponding organisms) and of a selectable marker cassette (*URA3,* including triple HA tag (3HA)) flanked by homology arms. By overlap extension PCR, the fragments were joined and amplified. The final product (*SCO2* homologue fused to HA tag (stop codon highlighted in white striped box) with *URA3* cassette) was purified and integrated into the targeted genomic locus via homologous recombination.

The recombinant strains and integration cassettes used for their generation are listed in table 13.

Table 13. Integration cassettes used for generation of recombinant strains.

Strain	Integration cassette
ySCO2	*ySCO2*-3HA-*URA3*
SpSCO1	*SpSCO1*-3HA-*URA3*
K07152	*K07152*-3HA-*URA3*
K07152 (w/o HA tag)	*K07152-URA3*
hSCO1	*hSCO1*-3HA-*URA3*
hSCO2	*hSCO2*-3HA-*URA3*
HCC1	*HCC1*-3HA-*URA3*
HCC2	*HCC2*-3HA-*URA3*
SCOX	*SCOX*-3HA-*URA3*

3.3 Confirmation of site-specific integration by check PCR

Although the frequency of targeted recombination is high in *S. cerevisiae*, some transformants could also emerge from untargeted recombination events [89]. To eliminate these transformants, site-specific integration was verified by PCR analysis. For such a check PCR, specific primers were designed: While the forward primers bind to the complementing gene within the integration cassette, the reverse primers bind downstream of the 3`homology arm (figure 11). Only in positive clones the expected PCR products were amplified (data not shown). Those positive clones were selected and the sequence of the integrated genes (homologues) was verified by sequencing. These sequence-verified clones were included in further functional analyses.

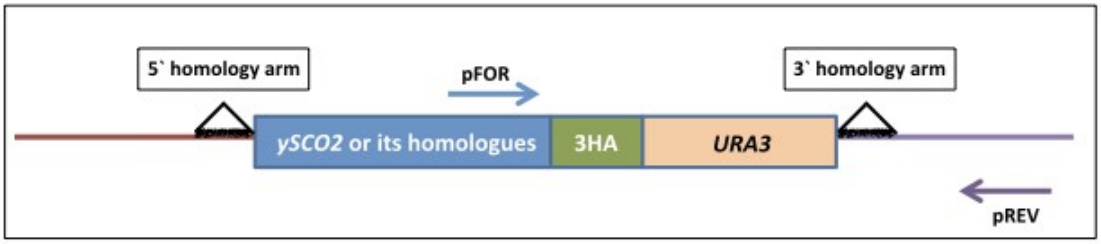

Figure 11. A scheme of the PCR strategy for verification of the site-specific integration.
The binding sites of the screening primers pFOR and pREV were designed to amplify the regions within the integrated cassette and downstream of the integration site. In case of a targeted recombination, amplicons of the expected size were produced.

3.4 Verification of single site integration by Southern Blotting

To verify the single site integration of the cassette into the target locus, the samples from the positive clones of chosen strains (ySCO2, hSCO1 & 2, SpSCO1, HCC2) were subjected to Southern Blot hybridization (figure 12). Extracted genomic DNA

was digested with two different restriction endonucleases (*EcoR*I-HF and *Spe*I-HF) individually and the wt strain was included as a control. Digested fragments were detected with the *URA3* specific probe (DIG-labeled). Single bands observed for all samples except HCC2 (figure 12a) confirmed the single site integration. When the sequence of *HCC2* was checked later, a recognition site for *EcoR*I (but not for *Spe*I) was found, which explains the detection of two bands.

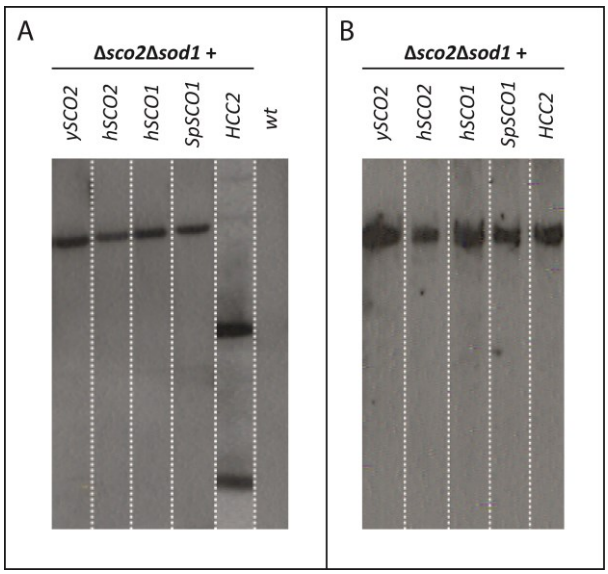

Figure 12. Southern blot of the complementation strains with the integration cassette.
Genomic DNA of selected strains (ySCO2, hSCO1&2, SpSCO1, HCC2) was digested with (A) *EcoR*I-HF and (B) *Spe*I-HF. The wt strain was included as a control and blots were probed with a *URA3* specific DIG-labelled probe.

3.5 Analysis of the functional homology between selected homologues and *ySCO2*

As previously mentioned, the aa sequence identity of the selected homologues to ySco2p ranges from 56 % to 26 %, but the conservation is higher when only the C-terminal part of the proteins are taken into account. The Trx-like fold, which might be crucial for a possible antioxidant function, is located at the Trx domain/ C-terminal part, possibly hinting at a functional conservation even across distant species [60-62].

3.5.1 Complementation assay in solid media

The functional homology between *ySCO2* and its homologues was tested under oxidative stress conditions. To induce stress, three common redox cyclers (menadione, PQ and plumbagin) were used. The full-length y*SCO2* was included as a positive control and functional complementation was analysed by a growth assay (see

section 2.2.2.11).

The results indicated that expression of all homologues except *K07152* and *HCC1* could rescue the *sco2* phenotype in the yeast strain Δ*sco2*Δ*sod1* (figure 13). All strains except K07152 and HCC1 showed a similar growth on menadione and plumbagin plates compared to ySCO2 but a variation in growth was observed on PQ plates. Despite the distinction between functional and non-functional homologues is clear on all plates, the slight growth difference on PQ plates among the functional strains may hint at a varying degree of functional conservation (full or partial).

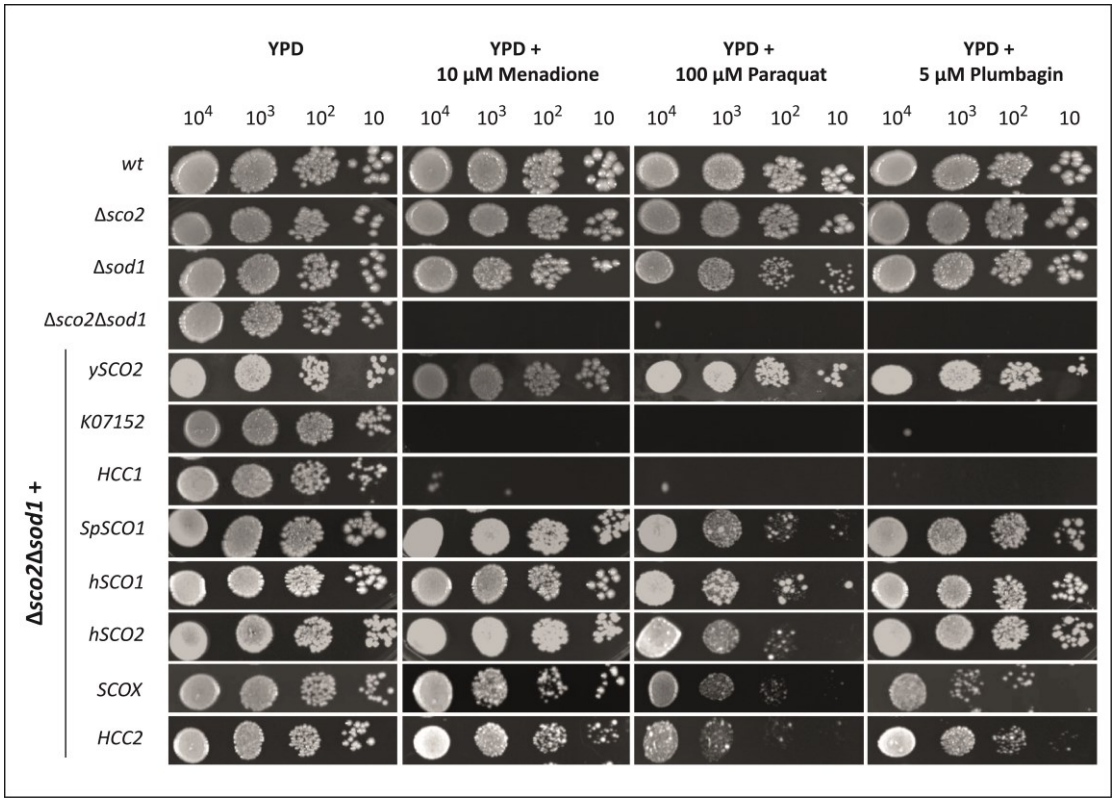

Figure 13. Complementation test with *SCO2* homologues in the presence of different oxidative stress inducers.
Yeast cells were dropped in a serial dilution on YPD plates with or without stressors. The plates were incubated for two (YPD) or three (YPD+ stress inducing reagents) days at 30 °C.

It was unexpected to find out that while the homologues with much lower similarity (hSco1, hSco2, Scox and Hcc2) could complement the putative antioxidant function of ySco2p, the homologue (K07152) with more than 50% similarity could not. Since a fused tag could disrupt the protein function owing to changes in folding and stability, a new integration cassette without HA tag was generated. This new strain K07152 (w/o HA tag) was tested by growth assay. The results of the growth assay showed that

also the expression of native protein without tag was also not able to restore the stress sensitivity (figure 14).

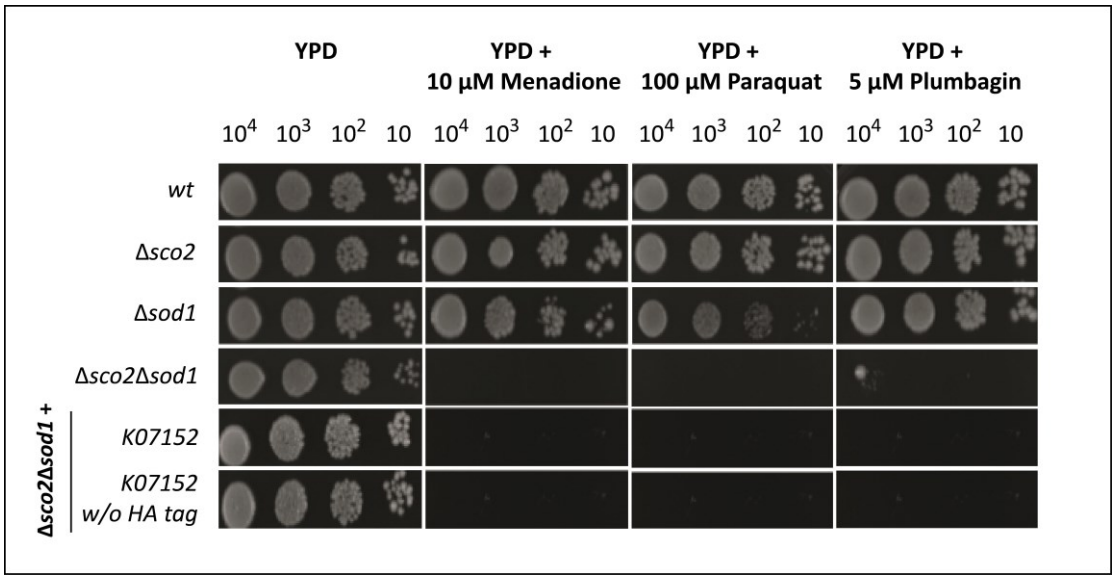

Figure 14. Complementation test with tagged and untagged *K07152* in the presence of different oxidative stress inducers.
Yeast cells were dropped in a serial dilution on YPD plates with or without stressors. The plates were incubated for two (YPD) or three (YPD+ stress inducing reagents) days at 30 °C.

3.5.2 Complementation assay in liquid media

Previous studies revealed a high consistency between the results of complementation assay in solid and liquid media [90]. As the growth differences between some strains could be more apparent in the solid media, first analyses were carried out with them. However, almost all stress-sensitive strains were unable to grow on solid media plates preventing further analyses of these strains. To address this problem, the strains were cultured in liquid media (with or without 100 µM PQ) and their growth was determined by a spectrophotometric method based on the measurement of optical density at 600 nm (OD_{600}) [91].

A similar growth trend was observed in liquid media but there are also some clear differences (figure 15). While solid media results indicated a growth difference between strains only under stress conditions, a difference was observed also at normal conditions in liquid media. The growth of strains carrying a *sod1* deletion was reduced compared to wt and Δ*sco2*. Expression of *ySCO2* can rescue the growth deficiency of Δ*sco2*Δ*sod1* strain in the presence of PQ, but not at normal conditions. Interestingly, all recombinant strains except ySCO2 exhibited a better growth at

normal conditions compared to Δ*sco2*Δ*sod1* strain. Additionally, while solid plate assays indicated a higher sensitivity towards PQ for all complementation strains (compared to ySCO2), it was not observed in liquid media (even the opposite for some strains).

Since OD measurement is an indirect method for rough estimation of cell numbers, it would be better to confirm these results by applying a more accurate method (such as plate count [92], fluorescein diacetate (FDA) staining [93]). Additionally, it should be considered that the observed differences between growth assays could result from distinct sensitivity of cells towards PQ depending on the culturing conditions (including media type).

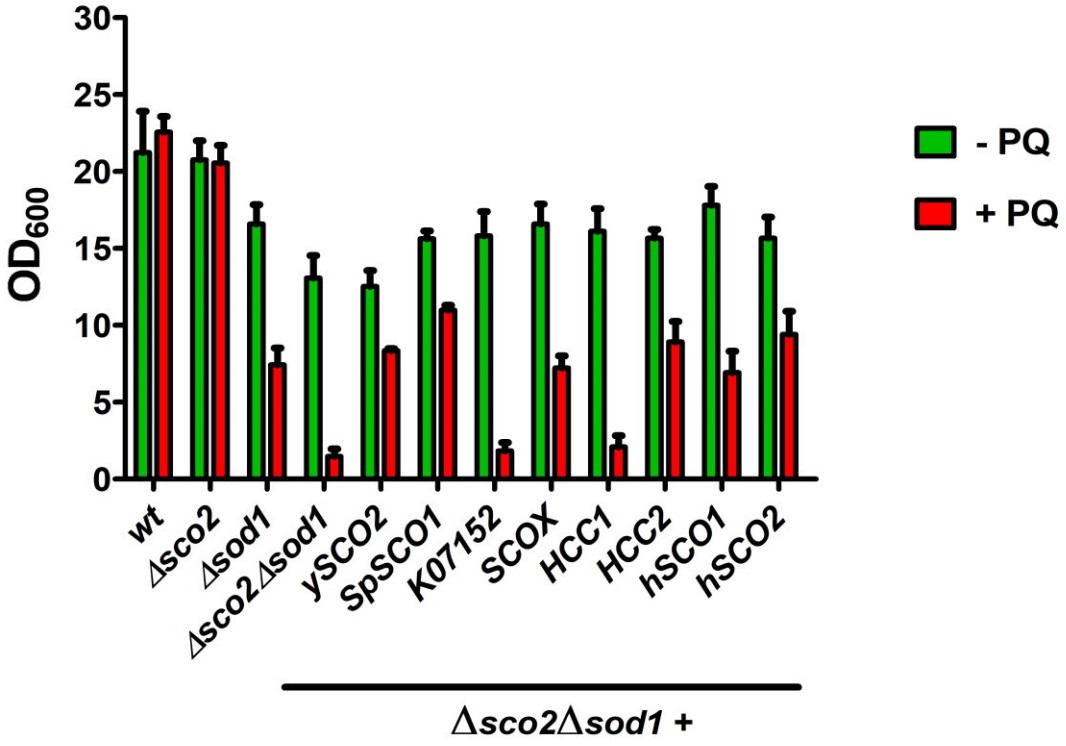

Figure 15. Determination of cell growth by OD_{600} measurement.
Yeast strains (wt, Δ*sco2*, Δ*sod1*, Δ*sco2*Δ*sod1,* ySCO2, SpSCO1, K07152, SCOX, HCC1, HCC2, hSCO1 and hSCO2) were grown in YPD (with or without 100 μM PQ). After 24 hours, OD_{600} of the samples was measured. Green and red bars represent the untreated and treated samples, respectively. The values are means + standard deviation (SD) of results from at least three independent experiments.

3.6 Determination of cell viability

The OD_{600} results indicated that the double mutant, Δ*sco2*Δ*sod1* and non-functional homologues (*K07152, HCC1*) underwent roughly only two cell divisions after PQ treatment, whereas the wt and Δ*sco2* strains divided almost 6 times. These lower OD

values could be explained by either cell death or suppressed proliferation [94].

To understand the underlying reason, methylene blue staining was performed (see section 2.2.4.1). Methylene blue is a dye that can penetrate into both living and dead cells. Only living cells can enzymatically reduce the dye hence become colorless or light blue. On the other hand, dead cells are stained in a dark blue [95].

For the analysis, four strains (wt, Δ*sco2,* Δ*sod1,* Δ*sco2*Δ*sod1*) were selected and their viability was checked either under normal (untreated) or stress (treated; 100 µM PQ for 24 h) conditions (figure 16). Despite of filtering methylene blue solution and cleaning the microscope slides, the blue-colored dirt at the background could not have been removed. As a control, wt cells treated for 30 min with 60 % ethanol were stained, and the dark blue color in dead cells was clearly observed. On the other hand, for all other strains a slight blue color was observed in cells.

The results revealed that the viability of all deletion strains is comparable to the wt in both untreated and treated cultures and hint to the fact that inhibition of cell division is likely to be reason behind the growth delay.

It is known that the cytotoxicity mode of oxidative stress could change depending on the conditions. Instead of a cell death, stress can alter the metabolic and physiological pathways including cell proliferation [96-99]. However, to support this claim, further analysis are required such as staining with resazurin [100].

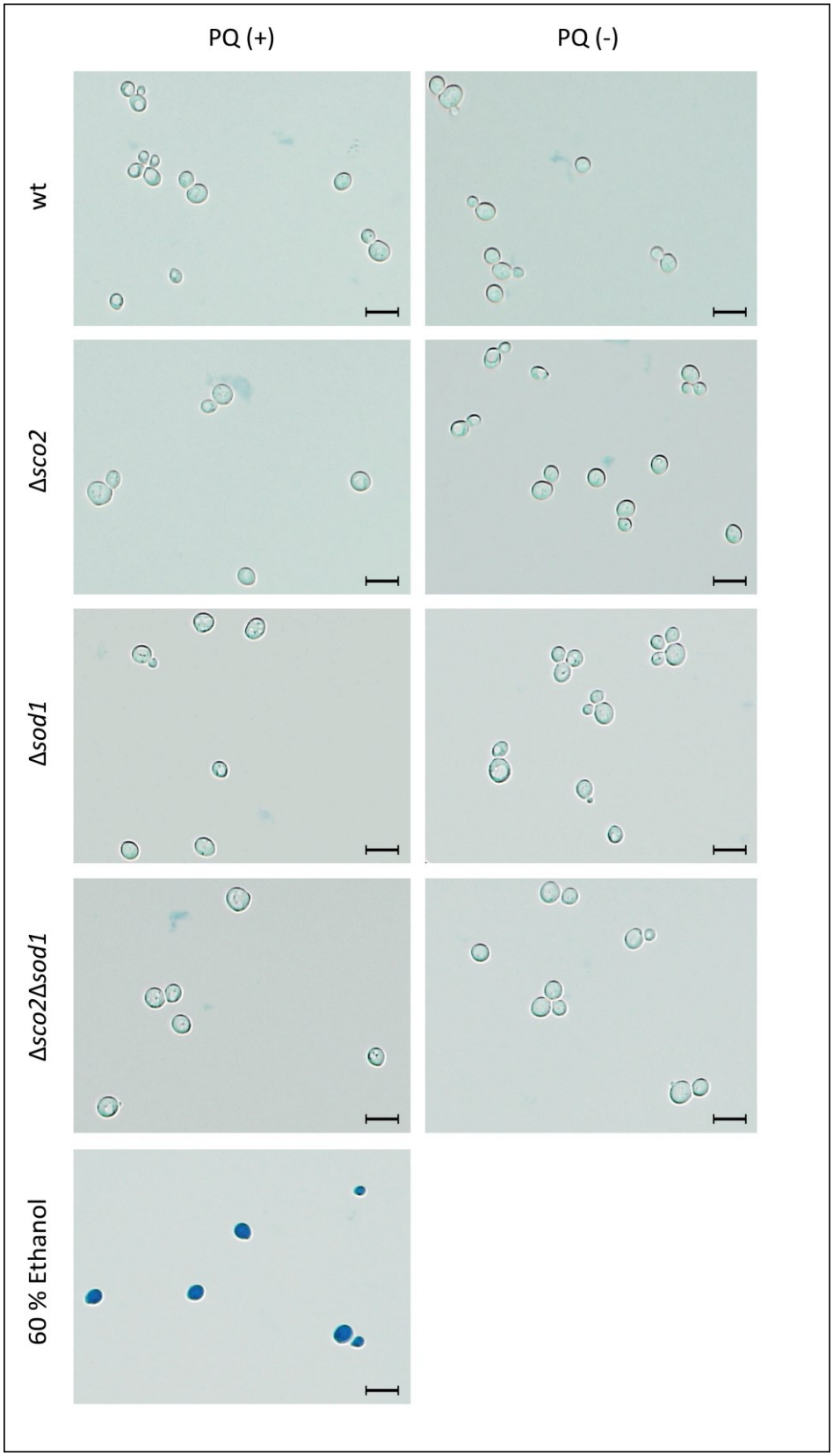

Figure 16. Methylene blue staining of selected strains (wt, Δ*sco2*, Δ*sod1*, Δ*sco2*Δ*sod1)* grown under normal or stress (100 µM PQ for 24 h) conditions.
The viability of cells was assessed by methylene blue staining (dead cells: blue color, live cells: colorless). As a control, wt cells treated with 60 % ethanol were stained and viability was examined by microscopy (40x objectives). The black scale bar corresponds to 10 µm.

3.7 Quantification of ROS

So far, the impact of oxidative stress on growth of the analysed strains has been shown. However, to strongly claim on the antioxidant role of *ySCO2* and the functional homologues, it is crucial to quantify ROS and verify the decrease in ROS levels related to the expression of these genes.

ROS levels can be quantified by direct and indirect methods [101]. Since accumulation of free radicals can damage many cellular components including nucleic acid, protein and lipid, these biomolecules can be utilized as a marker for indirect measurements [102]. In this study, oxidative stress was both assessed directly by quantifying extracellular hydrogen peroxide (H_2O_2) and indirectly by measuring lipid peroxidation levels.

3.7.1 Quantification of extracellular H_2O_2

Amplex Red (10-acetyl-3, 7-dihydroxyphenoxazine), an oxidant-sensitive probe that becomes fluorescent after a peroxidase-catalyzed reaction with H_2O_2 [103] was used. As the dye can easily be auto-oxidized at high concentrations [104], the amount was lowered to 10 μM (see section 2.2.4.2a). The probe is cell impermeable but H_2O_2 is diffusible [105] and there is an equilibrium between the inner and outer environment of cells. Therefore, the extracellular H_2O_2 level is a good indicator of produced H_2O_2 by cells.

Amplex Red results (figure 17) pointed out that there is a difference in the released H_2O_2 amount between the analysed strains at both normal and stress conditions. The variation in extracellular H_2O_2 levels between strains could not be due to only distinct stress levels but also changes in membrane permeability (owing to genetic modifications) [106]. However, the difference is more remarkable among homologues (functional vs non-functional) and deletion strains (wt, Δ*sco2*, Δ*sod1* vs Δ*sco2*Δ*sod1*) at stress conditions.

At normal conditions, a clear trend is not observed in H_2O_2 levels in strains: *e.g.* wt, hSCO1, hSCO2 Δ*sco2*Δ*sod1* have similar H_2O_2 levels but approximately 1,5- to 2-fold higher compared to SpSCO1 and Δ*sod1*. However, when stressed with PQ although all analyzed strains have significantly higher H_2O_2 levels compared to unstressed controls, this increase is more pronounced in Δ*sco2*Δ*sod1* and non-functional strains (K07152, HCC1), more than 1000-fold.

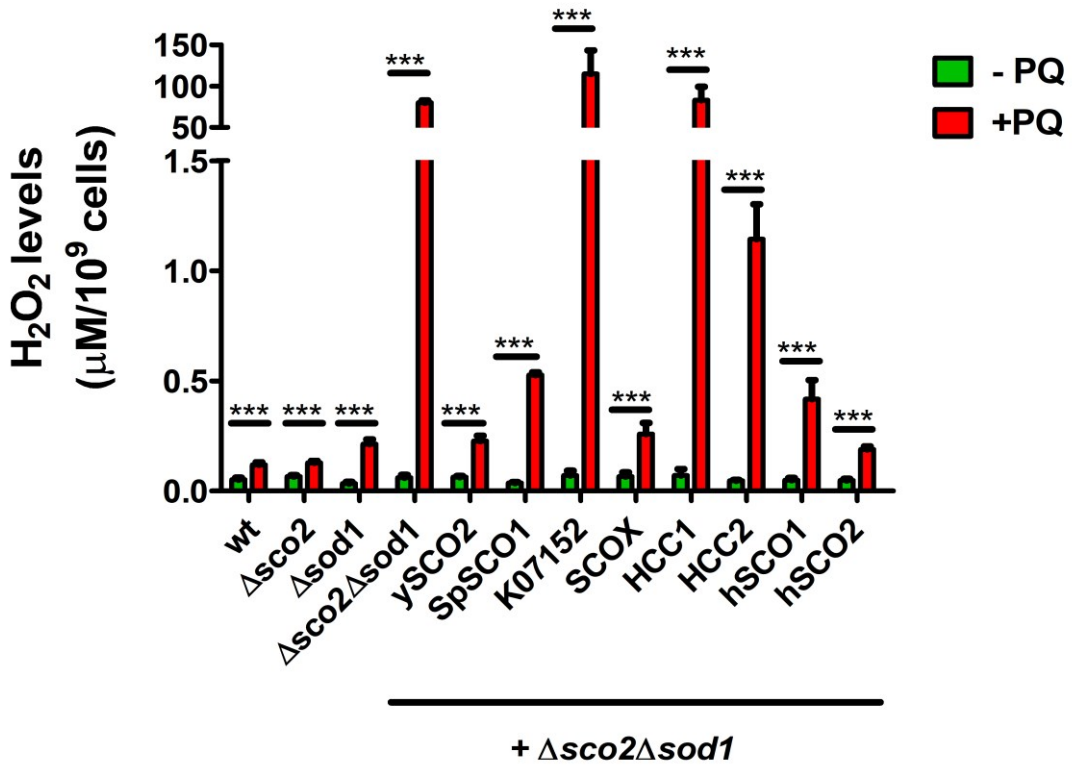

Strain	-PQ (μM $H_2O_2/ 10^9$)	+PQ (μM $H_2O_2/ 10^9$)	Fold change (+PQ / -PQ)
wt	0,052 ± 0,008	0,119 ± 0,011	2,3
Δ*sco2*	0,065 ± 0,007	0,128 ± 0,009	2
Δ*sod1*	0,034 ± 0,007	0,213 ± 0,021	6,2
Δ*sco2*Δ*sod1*	0,06 ± 0,013	80 ± 2,653	1315,3
ySCO2	0,063 ± 0,005	0,226 ± 0,025	3,6
SpSCO1	0,036 ± 0,003	0,526 ± 0,011	14,5
K07152	0,07 ± 0,022	114,828 ± 28,582	1631,8
SCOX	0,066 ± 0,020	0,258 ± 0,051	4
HCC1	0,07 ± 0,029	82,979 ± 16,388	1173
HCC2	0,046 ± 0,004	1,144 ± 0,159	24,7
hSCO1	0,049 ± 0,010	0,418 ± 0,086	8,5
hSCO2	0,047 ± 0,008	0,188 ± 0,014	4

Figure 17. Quantification of extracellular hydrogen peroxide (H_2O_2) by Amplex Red in different strains.
Yeast strains (wt, Δ*sco2*, Δ*sod1*, Δ*sco2*Δ*sod1,* ySCO2, SpSCO1, K07152, SCOX, HCC1, HCC2, hSCO1 and hSCO2) were grown in YPD (with or without 100 µM PQ). The cells were then incubated with Amplex Red and the amount of hydrogen H_2O_2 was calculated from standard curve with known concentrations. Results were shown both in graph and table with absolute numbers (below). The values are means ± SD of results from at least three independent experiments. *p < 0.05, **p < 0.01, ***p < 0.001 for significant effect of PQ treatment.

These findings indicate a direct correlation between higher stress levels and slower growth, thus consistent with growth assay results. Exemplary, even though Δ*sco2* and

wt had a comparable increase in H_2O_2 levels after PQ treatment, a dramatic increase was observed in both Δ*sod1* and Δ*sco2*Δ*sod1* when stressed (> 6 and 1000-fold, respectively). Moreover, an apparent difference was not only observed between the Δ*sod1* and Δ*sco2*Δ*sod1* but also between the functional (hSCO1, hSCO2, SCOX, SpSCO1, HCC2) and nonfunctional strains (K07152, HCC1) after PQ treatment. Furthermore, similar to growth assay results, a variation in oxidant level of functional homologues was found out.

3.7.2 Quantification of lipid peroxidation

The Bioxytech LPO-586 kit was used to determine the concentration of malondialdehyde (MDA), one of the lipid peroxidation end products [107] (see section 2.2.4.2b).

The results of the lipid peroxidation assay (figure 18) are consistent with the Amplex Red measurements and demonstrate a similar trend in analyzed strains toward PQ treatment.

A dramatic increase in MDA levels was observed in the Δ*sco2*Δ*sod1* and non-functional strains (K07152 and HCC1) when stressed with PQ. While this increase is up to 1,7-fold in functional strains, the non-functional strains have more than 10-fold higher MDA concentrations under stress.

In contrast to Amplex Red results that show a significant change in oxidant levels of all analysed strains due to PQ treatment, the MDA levels of wt, Δ*sco2* and Δ*sod1* are not significantly altered in response to elevated stress. These findings are a good indication of how oxidants are immediately eliminated by defense systems to avoid further attack on biomolecules and how existing stress products are removed by this induced protective response at mild stress conditions.

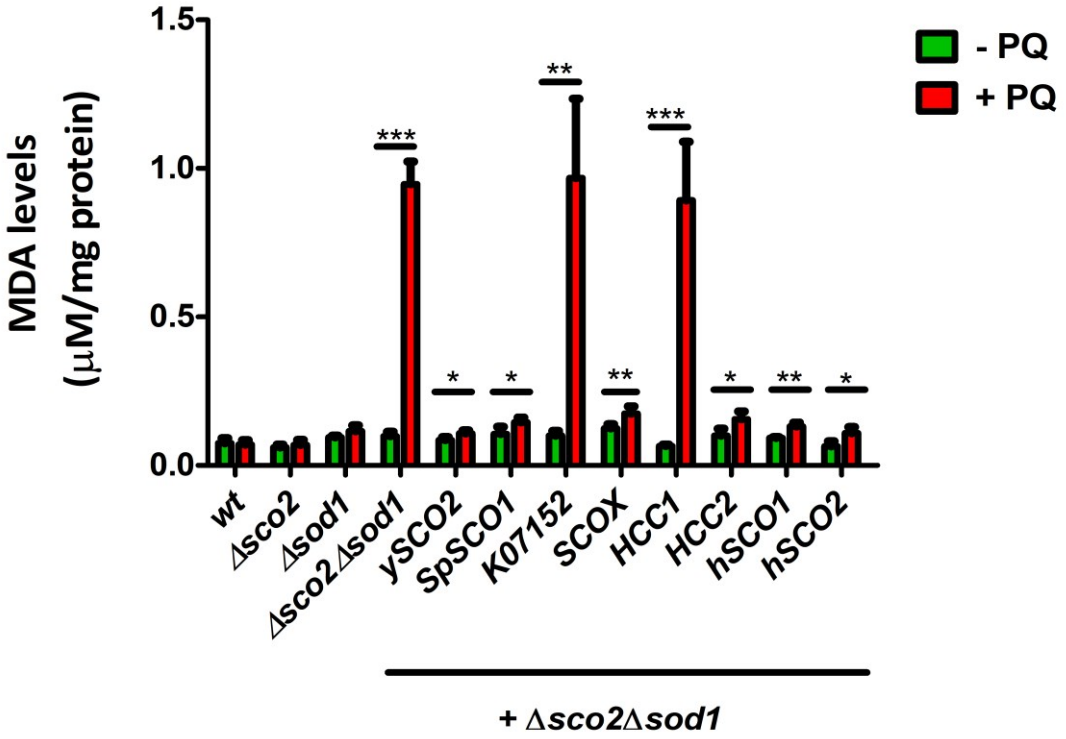

Strain	w/o PQ (μM MDA/ mg protein)	w/ PQ (μM MDA/ mg protein)	Fold change (+ PQ / - PQ)
wt	0,075 ± 0,017	0,07 ± 0,015	0,9
Δ*sco2*	0,060 ± 0,010	0,069 ± 0,017	1,1
Δ*sod1*	0,094 ± 0,006	0,115 ± 0,020	1,2
Δ*sco2*Δ*sod1*	0,099 ± 0,015	0,947 ± 0,076	9,6
ySCO2	0,085 ± 0,010	0,107 ± 0,010	1,3
SpSCO1	0,105 ± 0,025	0,145 ± 0,016	1,4
K07152	0,100 ± 0,016	1,106 ± 0,165	11
SCOX	0,124 ± 0,014	0,174 ± 0,024	1,4
HCC1	0,065 ± 0,005	0,892 ± 0,198	13,7
HCC2	0,118 ± 0,036	0,156 ± 0,026	1,3
hSCO1	0,101 ± 0,017	0,131 ± 0,013	1,3
hSCO2	0,064 ± 0,017	0,108 ± 0,021	1,7

Figure 18. Quantification of lipid peroxidation levels in different strains.
Yeast strains (wt, Δ*sco2*, Δ*sod1*, Δ*sco2*Δ*sod1,* ySCO2, SpSCO1, K07152, SCOX, HCC1, HCC2, hSCO1 and hSCO2) were grown in YPD (with or without 100 μM PQ). The malondialdehyde (MDA) concentration was assessed by the Bioxytech LPO-586 kit and normalized to the protein amount. Results were shown both in graph and table with absolute numbers (below). The values are means ± SD of results from at least three independent experiments. *p < 0.05, **p < 0.01, ***p < 0.001 for significant effect of PQ.

Both ROS measurements revealed the correlation between growth rate and oxidant levels, hence strengthen our hypothesis on the antioxidant role of *ySCO2* and its

functional homologues.

3.8 Investigation of the expression and subcellular localization of the homologues

A reason for the inability of two Sco2 homologues (*HCC1*, *K07152*) to restore the antioxidant function could be due to the lack of expression or/and mislocalization of the proteins. For Western Blot analysis, cytoplasmic and mt fractions of the strains were isolated and the expression of the proteins was detected by HA antibody. The theoretical sizes of the precursor and mature proteins (after cleavage of predicted MTS) are given in the table 14.

Table 14. Theoretical sizes of precursor and mature proteins calculated by ExPASy and MitoFates, respectively.

Protein	Precursor protein (~ kDa)	Mature protein (~ kDa)
ySco2	35	31
Hcc2	35	23
SpSco1	30	20
K07152	36	31
Hcc1	37	34
Scox	28	25
hSco1	33	26
hSco2	30	21

The fractions of the different strains were separated in a SDS-PAGE and Western blot analysis (figure 19) was performed with HA antibody and compartment-specific control antibodies against cytoplasmic phosphoglycerate kinase 1 (Pgk1p, ~ 45 kDa) and mt cytochrome *c* oxidase subunit 2 (Cox2p, ~ 29 kDa).

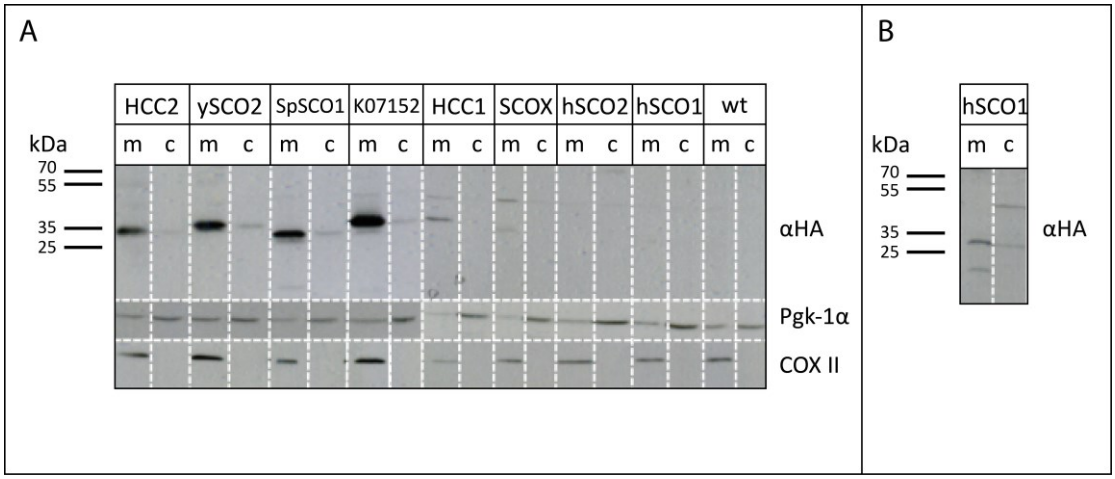

Figure 19. Western blot analysis of the strains expressing Sco2 homologues.
Total proteins extracted from the recombinant strains were subfractionated into crude mt (m) and cytoplasmic (c) fractions.
A. For analysis, 100 µg protein was loaded from each sample and Wt sample was used as a negative control. After HA detection, the membrane was stripped of bound antibodies and compartment-specific marker proteins were used to check the purity of the fractions. Pgk1p (~ 45 kDa) was used as a cytoplasmic marker and COX2p (~ 29 kDa) as a mt marker. The theoretical sizes of homologues (w/o HA tag) are shown in Table 14.
B. 400 µg protein of hSCO1 complementing strain was loaded and HA detection was repeated.

Cox2p was detected only in the mt fractions as expected, but Pgk1p was present in both fractions. This cross contamination might occur due to the crude isolation method. However, all homologues were predominantly detected in the mt fraction what points to a mt localization.

The size range of detected proteins is 30-40 kDa and this range is perfectly matching with the expected size of mature proteins (+3 kDa for HA tag) except the samples Hcc2 and SpSco1. For these samples, the observed size corresponds to the size of precursor protein but not the signal peptide-cleaved form. Estimation of the mt-targeting signals by hypothetical calculations and expression of the homologues in a non-native host could be the reason for the observed size differences.

Moreover, some other bands were present in the mt samples of K07152, HCC1, SCOX and hSCO1. In most strains, a band around 50 kDa is visible. These bands may correspond to proteins with different types of post-translational modifications. On the other hand, the band of lower molecular weight in hSCO1 could result from degradation (figure 19b).

It is apparent that the expression levels of the homologues are different. While the expression of homologues from closely related species (*S. pombe* (SpSco1) and *K. lactis* (K07152)) was higher, the proteins of distant species were hardly or not at all

detected. Such a variation in expression levels could be due to differences in codon usage preference of distinct organisms [108]. The hSco1 was only detected when the amount was increased 4-fold (400 µg, figure 19b), but the other human homologue hSco2 could not be detected in any Western blot analysis.

Since hSco2 could not be detected with the HA antibody, different antibodies either specific to hSco2 (from Aviva Biosystems and Thermo Scientific) or against another tag, c-Myc (c-Myc tagged fused to hSco2 protein) were tested. However, not any specific band corresponding to hSco2 was detected with these antibodies (not shown).

In addition to all genomic level (PCR, Southern blot) and functional (complementation assay, ROS measurements) verifications, the expression of *hSCO2* at RNA level was checked together with *hSCO1* (figure 20) by reverse transcriptase PCR (RT-PCR). Ribosomal 60S subunit protein L17A (RPL17A) used as a reference gene. In order to check possible gDNA contamination, PCR was performed on total RNA samples without reverse transcriptase (-RT) using RPL17A specific primers (gDNA: 841 bp, cDNA: 536 bp).

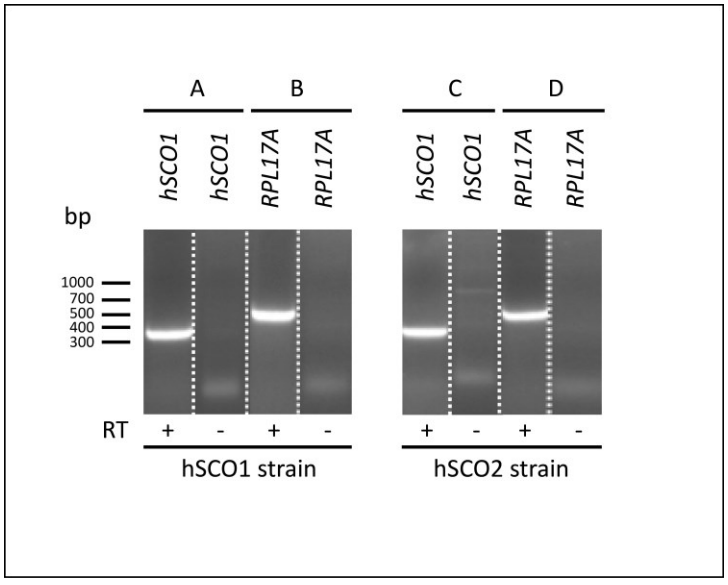

Figure 20. RT-PCR results of *hSCO1*, *hSCO2* and *RPL17A* in the complementation strains, hSCO1 & 2.
RT-PCR was performed for complementation strains with gene specific primers of *hSCO1*, *hSCO2* and *RPL17A*. The *RPL17A* served as an internal control and gDNA contamination was checked in negative samples, –RT. The expected band sizes for samples are as follows: A) 350 bp (+ & – RT); B-D) 536 bp (+RT), 841 bp (-RT); C) 352 bp (+ & – RT)

The RT-PCR results clearly showed the expression of both human homologues at RNA level. In case of contamination same-sized bands were supposed to be observed

for each human gene owing to the integration of cDNA into gDNA of the host strain, Δ*sco2*Δ*sod1*. However, no band corresponding to gDNA contamination was visualized and the upper weak bands observed in the –RT sample of (figure 20c) were nonspecific.

3.9 Investigation of the impact of pathogenic *hSCO2* mutations on its antioxidant role

The results of complementation assays showed the rescue of the *sco2* phenotype with the human homologue, *hSCO2* (figure 13). This finding paves the way to utilize *S. cerevisiae* as a model organism to gain a deeper insight into the broader effects of *hSCO2*-associated diseases. Several mutations identified in *hSCO2* led to distinct diseases including fatal infantile cardioencephalomyopathy [109], myopia 6 [110] and leigh syndrome [111]. In this study, five pathogenic missense mutations associated with fatal infantile cardioencephalomyopathy have been selected for further analysis: C133S, E140K, L151P, R171W, and S225F.

The possible effects of these mutations on the protein stability, Cu binding ability and protein-protein interactions have been investigated [109, 112-115]. Structural data showed that selected mutations mostly found in different structural units (either at connecting loops or α helices), but they all localized to the Trx domain that could be crucial for the putative redox function (figure 21).

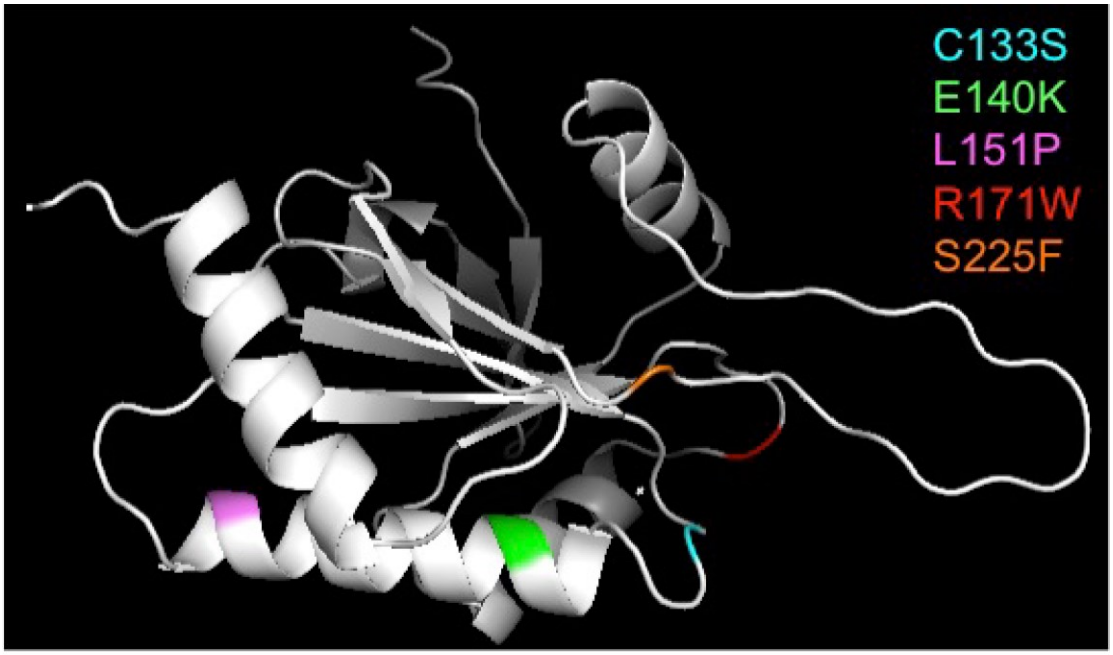

Mutation	Location on structure
C133S	Loop 3 (connecting β3 and α1)
E140K	α1
L151P	α1
R171W	Loop 5 (connecting β4 and α2)
S225F	Loop 8 (β hairpin and β6)

Figure 21. Location of the pathogenic mutations in the structure of hSco2 [61].
The characterized protein backbone of recombinant hSco2 (lacking the MTS and TM domain) is shown in grey. The sites of mutations are highlighted in different colors and their exact positions on structure are given in table (below). The figure was prepared with PyMOL by rearranging the available structure data retrieved from PDB.

Until this study, there was no clear evidence about the possible antioxidant role of *hSCO2* [61]. Thus, the effect of these pathogenic mutations on stress sensitivity has not been tested. To address this, mutant genes were generated via site directed mutagenesis (table 11) and integrated into the *SCO2* locus in Δ*sod1*Δ*sco2* strain. The growths of native and mutant hSCO2 strains were tested both under normal and stress conditions by growth assay.

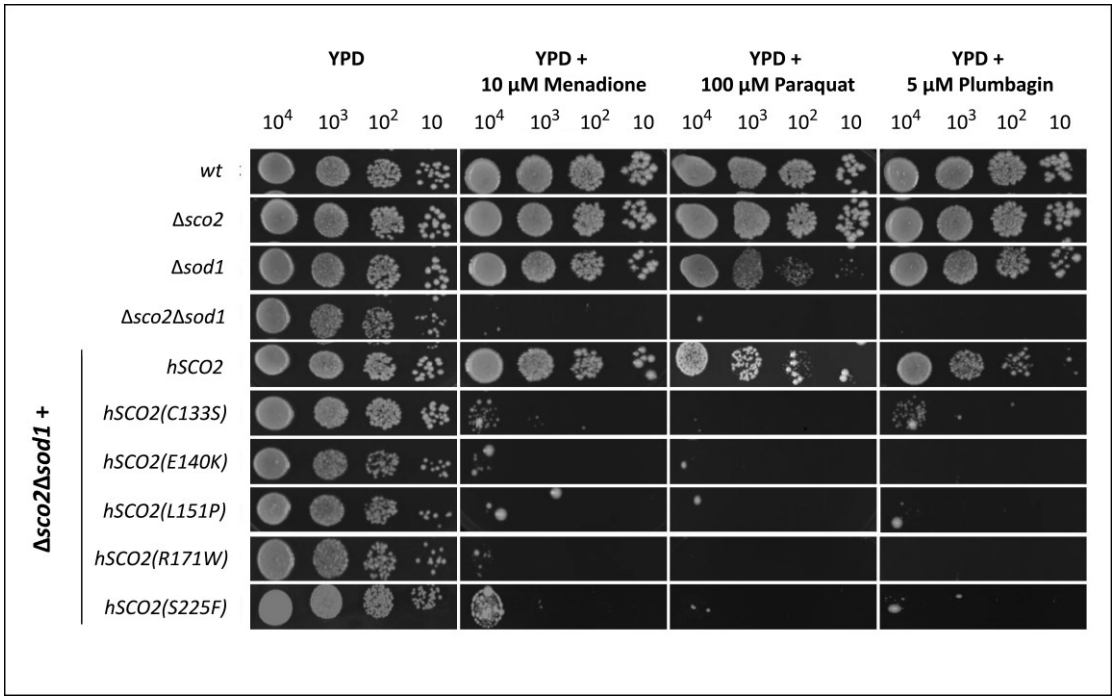

Figure 22. Complementation test with *hSCO2* and its mutant forms in the presence of different stress inducers.
Yeast cells were dropped in a serial dilution on YPD plates with or without stressors. The plates were incubated for two (YPD) or three (YPD+ stress inducing reagents) days at 30 °C.

Despite the normal growth on YPD, all mutant strains had almost no growth on stress plates (figure 22). These results indicate the loss of the defensive role against oxidative stress due to the mutations and are consistent with *in silico* analyses (SIFT, Polyphen-2, MuPro) that predict a damaging effect for all these changes [116].

3.10 Mutational analysis of *ySCO2*

So far, there are limited experimental data on the functional sites of *ySCO2*, especially associated with the antioxidant function. To extend the current knowledge whether the localization to mitochondria or the presence of the conserved cysteine(s) (of the putative Cu binding motif) are crucial for antioxidant function, mutational analyses were carried out. Mutants that either lack the N-terminal part of the gene (containing the MTS and TM) or carry a serine mutation at the conserved cysteines (of CxxxC motif) were created by site directed mutagenesis (table 11).

Complementation assay results (figure 23) showed that while the mutation of first cysteine (in the motif, CxxxC) to serine (C154S) did not affect the sensitivity to any stressor, the other two mutants (ySCO2 (w/o MTS and TM), C158S) show an increased sensitivity towards PQ, but not to the others.

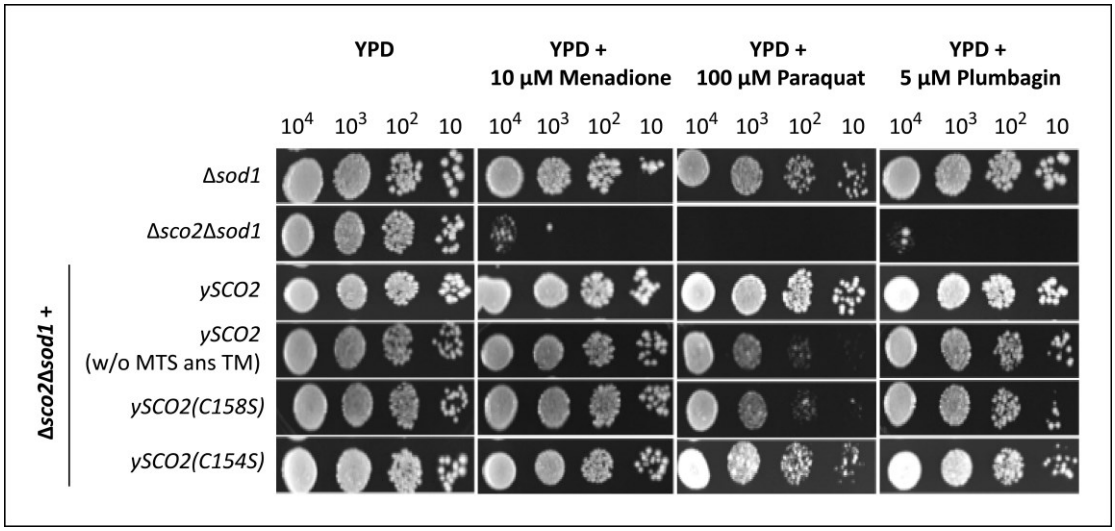

Figure 23. Complementation test with y*SCO2* homologues and derived mutant forms in the presence of oxidative stress inducers.
Yeast cells were dropped in a serial dilution on YPD plates with or without stressors. The plates were incubated for two (YPD) or three (YPD+ stress inducing reagents) days at 30 °C.

Despite the categorization of all stressors as "redox cyclers", it is apparent that they exert their cytotoxicity not only through similar but also distinct pathways. The higher sensitivity of the C158S mutant to PQ (compared to C154S) could be either due to differences in the reactivity of these cysteines (in redox reactions) or/and structural changes.

The slower growth of the mutant ySCO2 (w/o MTS and TM) points out that localization of Sco2p to mitochondria is pivotal for carrying out its antioxidant function effectively. However, this hypothesis still has to be confirmed by analysing the potential mislocalization of the mutant ySCO2 by *e.g.* Western blot analysis.

3.11 Identification of functionally important residues

The observation of the non-functional homologue from *K. lactis* (K07152) despite of the high sequence similarity to ySco2p strengthens the hypothesis on the importance of specific aa for the antioxidant function. To identify the important residue(s), analysed homologues (functional: ySco2, hSco1, hSco2, Scox, Hcc2, SpSco1 and nonfunctional: Hcc1, K07152) were aligned and the conservation was judged not only based on identity but also similarity (*e.g.* charge, hydrophobicity). The alignment identified one aa site with an opposite charge: While all homologues with antioxidant role (except SpSco1) have a negatively charged aa (located 15 aa downstream of

CxxxC motif), a positively charged lysine is found in the others (Hcc1, K07152) (figure 24).

Charged residues could be crucial for both the electrostatic potential and structural stability (salt bridge). Therefore, it can be speculated that such a change in charge at this particular site could cause the functional loss due to changes in conformation and/or protein-protein interaction(s).

Figure 24. Multiple sequence alignment of Sco2 homologues by Clustal Omega.
Within the aligned sequences (partially shown in this figure, for the full alignment refer to figure 9), the highly conserved putative copper binding site and possibly important aa for the antioxidant function are highlighted in red and green box, respectively.

To test this hypothesis, the positively charged lysine (K) was replaced by negatively charged glutamic acid (E) in the non-functional homologues (*K07152, HCC1)* and *vice versa* for selected functional homologues (*hSCO2, ySCO2*) (table 11).

To assess the effect of these mutations on the oxidative stress sensitivity of the created strain, a growth assay was performed (figure 25).

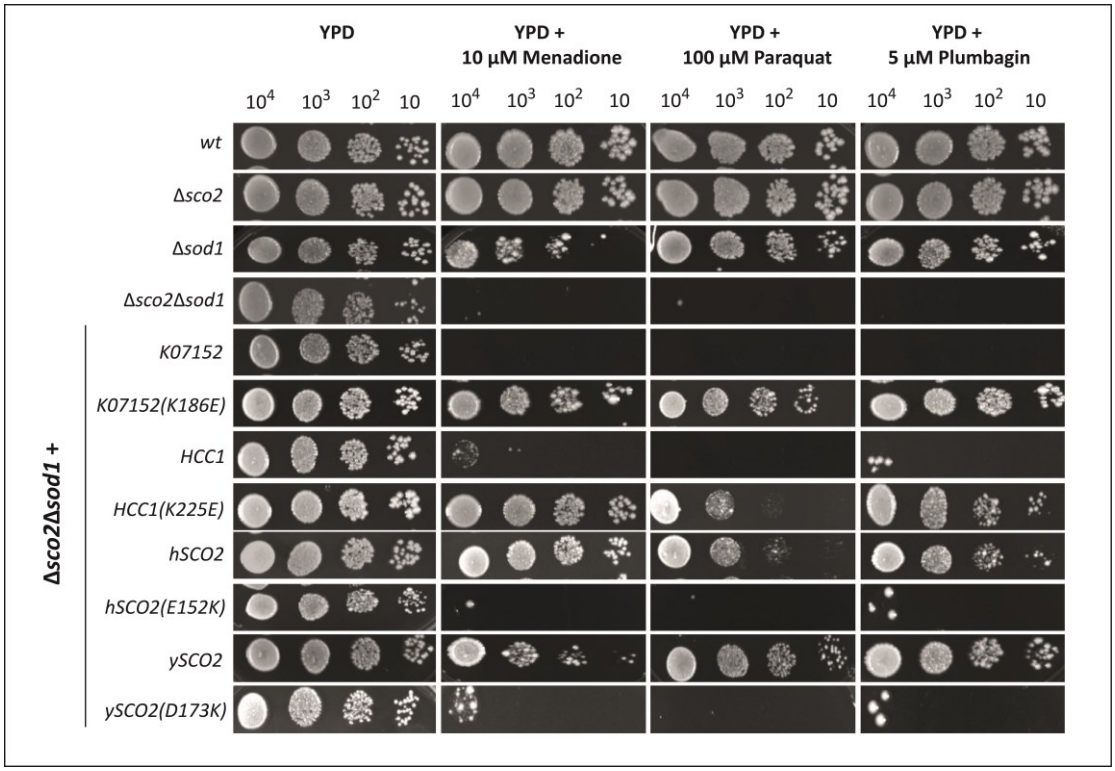

Figure 25. Complementation test with *SCO2* homologues and the derived mutant variants in the presence of different oxidative stress inducers.
Yeast cells were dropped in a serial dilution on YPD plates with or without stressors. The plates were incubated for two (YPD) or three (YPD+ stress inducing reagents) days at 30 °C.

Remarkably the mutations resulted in gain (*K07152, HCC1)* and loss of function (*hSCO2, ySCO2*), respectively. Besides growth restoration, functional gain observed in K07152 (K186E) and HCC1 (K225E) strains was also verified by lipid peroxidation assay in terms of reduced MDA levels compared to native strains (figure 26). In contrast to significantly higher MDA levels observed in native strains (K07152 and HCC1) in response to PQ, there are not a pronounced difference in MDA concentrations of mutant strains under normal and stress conditions. These results point out that the presence of a negatively charged aa at this conserved site is indeed essential for the putative antioxidant function.

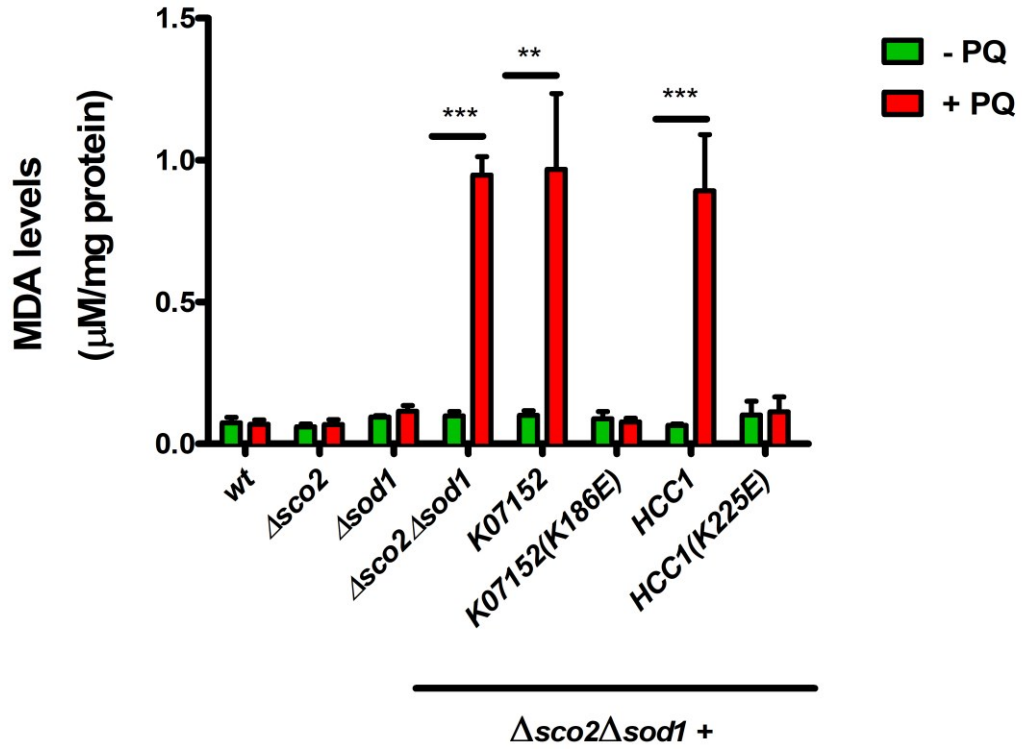

Strain	w/o PQ (μM MDA/ mg protein)	w/ PQ (μM MDA/ mg protein)	Fold change (treated / untreated)
wt	0,075 ± 0,017	0,07 ± 0,015	0,9
Δ*sco2*	0,060 ± 0,010	0,069 ± 0,017	1,1
Δ*sod1*	0,094 ± 0,006	0,115 ± 0,020	1,2
Δ*sco2*Δ*sod1*	0,099 ± 0,015	0,947 ± 0,076	9,6
K07152	0,100 ± 0,016	1,106 ± 0,165	11
K07152 (K186E)	0,088 ± 0,025	0,078 ± 0,013	0,9
HCC1	0,065 ± 0,005	0,892 ± 0,198	13,7
HCC1 (K225E)	0,102 ± 0,048	0,113 ± 0,052	1,1

Figure 26. Quantification of lipid peroxidation levels in different strains (including gain-of-function mutants).
Yeast strains (wt, Δ*sco2*, Δ*sod1*, Δ*sco2*Δ*sod1,* K07152, K07152 (K186E), HCC1, HCC1 (K225E)) were grown in YPD (with or without 100 μM PQ). The malondialdehyde (MDA) concentration was assessed by the Bioxytech LPO-586 kit and normalized to the protein amount. The values are means ± standard error of results from at least three independent experiments. **$p < 0.01$, ***$p < 0.001$ for significant effect of PQ.

However, for some mutant strains (ySCO2 (D173K), K07152 (K186E)) a clone-to-clone variation was observed. The reason for this is unclear, multiple or incorrect site integration of the cassettes could be excluded. Clone-to-clone variation is a commonly encountered problem in yeast biology (Alberti group (MPI-CBG),

personal communications). Therefore, in this study conclusions were made regarding the majority of results and 65 % was defined as a cut-off.

3.12 Prediction of salt bridges

After investigating functional changes due to mutations at conserved sites, I decided to focus on charge-related underlying reasons. It is well-known that salt bridges, formed between charged residues, could play a key role in structure stability. Thus, any alteration can lead to significant changes in protein conformations and/or protein-protein interactions [117, 118].

Therefore, it was speculated that rearrangement of salt bridge(s) could cause the functional change described above. As only hSco2 has a characterized structure among the homologues, the structure of other homologues (K07152, ySco2, Hcc1) was modeled by SWISS-PROT (see section 2.2.5) using appropriate templates (table 15).

Table 15. List of templates used for modeling by SWISS-PROT.

Protein	Template (PDB ID)
ySco2	2b7k
K07152	2rl5o
Hcc1	2gt6

A bioinformatics tool, PLIP was used to estimate possible intermolecular salt bridge(s) at the mutation sites. The programme calculates distances between atoms of positively and negatively charged aa and classifies the interaction as a salt bridge if the distance does not exceed 5.5 Å. According to the calculations of PLIP, neither Hcc1 nor the Hcc1 mutant (K225E) forms a salt bridge at the mutation site. Hence, the observed gain of function cannot be a result of such an intermolecular interaction for this homologue. On the other hand, for the other three homologues (K07152, ySco2p and hSco2), salt bridges are predicted, and pairing residues are identified (figure 27). The mutation to an opposite charged aa seems to disrupt this interaction. Thus, in those cases the conformational rearrangements could be the reason of the observed functional change.

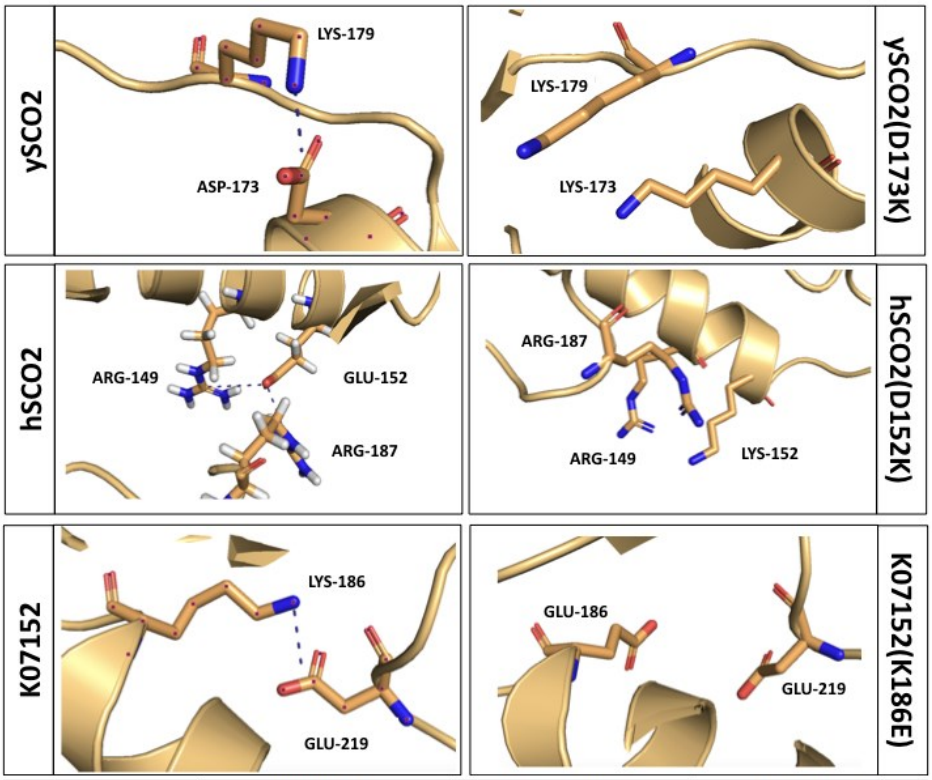

Strain	Salt bridge (Pairing residues)	Mutant Strain	Salt bridge (Pairing residues)
K07152	186-219	K07152(K186E)	N/A
HCC1	N/A	HCC1(K225E)	N/A
ySCO2	173-179	ySCO2(D173K)	N/A
hSCO2	149-152-187	hSCO2(E152K)	N/A

Figure 27. Salt bridges formed in native and mutant SCO2 homologues predicted by the PLIP programme.
Salt bridges (shown as dashed lines) and loss of this interaction are depicted on the structure of three homologues. The interactions are summarized in the table below (mutation sites are highlighted in green; pairing residues are given in blue; lack of a salt bridge is indicated as N/A).

3.13 Alanine mutagenesis

The interpretation based on the "salt bridge rearrangement" fails to explain the functional gain in the *HCC1* mutant and hints at another parameter, possibly electrostatic surface charge. It is well known that charged surfaces participate in protein-protein interactions [119, 120], but it is laborious and time-consuming to verify interactions experimentally. For this reason, I focused on generating new mutants by replacing charged residues with alanine instead of the opposite charged aa (table 11).

As alanine is a non-bulky and chemically inactive aa without any secondary structure preference, it excludes additional changes caused by charged residues [121]. Moreover, since the possible intermolecular salt bridges are disrupted also in alanine

mutants, it helps to reveal whether a functional change is due to a salt bridge or/and a local surface charge.

The data of the complementation assays show that intermolecular salt bridge formation is not crucial for the antioxidant role: While mutation to an opposite charge affected the function (figure 25), alanine mutagenesis was either well tolerated (in functional homologues, *hSCO2 and ySCO2*) or allowed functional gain (*K07152*) (figure 28).

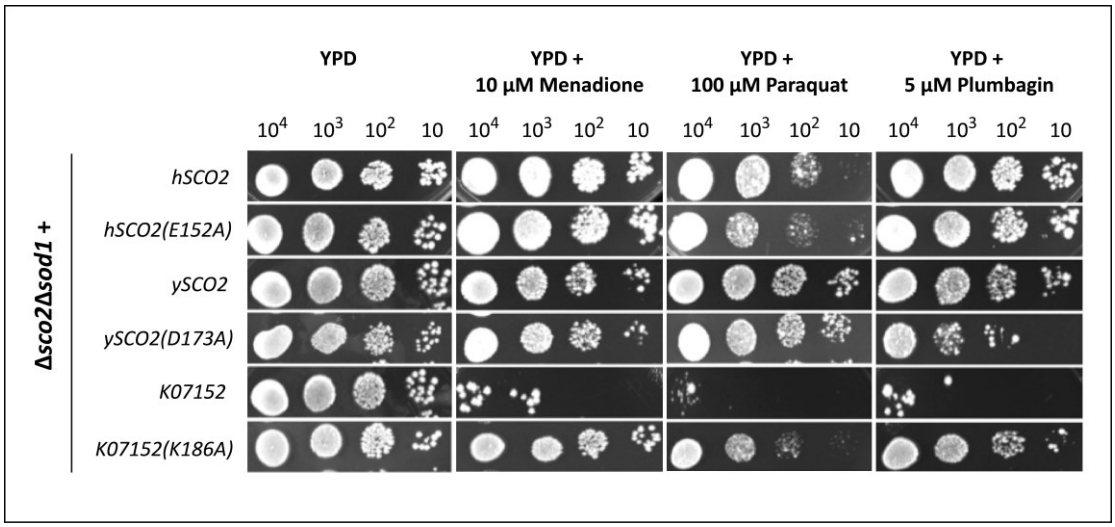

Figure 28. Complementation test with *SCO2* homologues and derived alanine mutants in the presence of oxidative stress inducers.
Yeast cells were dropped in a serial dilution on YPD plates with or without stressors. The plates were incubated for two (YPD) or three (YPD+ stress inducing reagents) days at 30 °C.

4 Discussion

The main objective of this thesis was to investigate a possible antioxidant role of Sco2 homologues from different organisms by using *S. cerevisiae* as a model organism. This putative antioxidant role of the selected homologues was tested via functional complementation studies and ROS measurements. In the light of the obtained results, functional and non-functional homologues were identified and hence an antioxidant function for these functional homologues of the complex organisms could be strongly suggested for the first time.

4.1 Functional homology between the selected homologues and *ySCO2*

The conservation of antioxidant function among *ySCO2* homologues was investigated by complementation assays under oxidative stress conditions. Functional and non-functional homologues were firstly identified based on their growth rate. Then, by ROS measurements, the correlation between slower growth rate and higher oxidant levels was revealed. A variation was clearly observed in both ROS levels and growth rate between functional and non-functional strains. Interestingly, such a variation was also seen among functional strains, possibly as a consequence of divergent degree of functional conservation.

The results point out that the high sequence similarity between homologues does not coincide with the functional conservation. While homologues with much lower similarity (hSco1, hSco2, Scox and Hcc2, around 30%) could functionally replace ySco2p, the one with the highest similarity (K07152, more than 50%) could not. This gives a hint on the importance of structural similarity and/or conserved aa for functional conservation.

4.1.1 *A. thaliana* homologues, *HCC1* & *HCC2*

The two homologues of *A. thaliana* (Hcc1, Hcc2) share the same similarity to ySco2p but behave differently towards oxidative stress. These results are not surprising when the previous knowledge about the divergent roles of these *A. thaliana* homologues [122-124] is considered.

The role of Hcc1 in COX biogenesis and Cu homeostasis has been shown, whereas the stress-related expression of *HCC2* and altered stress responsive gene expression in the *HCC2* mutant suggested a role for this homologue in redox mechanism [123, 124].

The results of this thesis further support the stress-related role of *HCC2* and strongly propose an antioxidant function for this homologue regarding the lower ROS levels (compared to Δ*sco2*Δ*sod1*) associated with its expression.

4.1.2 *H. sapiens* homologues, *hSCO1* & *hSCO2*

Interestingly, both human *SCO* genes could rescue the *sco2* phenotype. Divergent functions of these homologues are well addressed in literature. The vital role of human Sco proteins particularly in respiratory chain has connected them to ROS. While the interrelationship between hSco1 and ROS was discussed only in connection to COX [125-127], the transcriptional regulation of *SCO2* via the transcription factor, p53 broadened the scope of attention [128-131]. There are distinct studies that demonstrated the link between ROS levels to the expression of hSco2 protein. Although some studies indicated that the up-regulated expression of Sco2-induced ROS generation as a protection mechanism against cancer [130, 132], others showed that ROS levels in *SCO2* deficient cells were increased due to improper OXPHOS function (elevated oxygen toxicity at aerobic conditions) [129, 133, 134]. It seems that depending on the physiological situation of cells the impact of Sco2 on ROS production could alter.

So far, augmented ROS generation in Sco2 deficient human cell lines was reasoned by nonfunctional ETC. A possible antioxidant function of hSco2 has not been specifically addressed. As the connection between ROS and respiratory function could not be ruled out, the antioxidant role of these proteins could have been masked in human studies until now. Our studies overcame this limitation using a respiratory competent yeast strain. Since the contribution of Sco2p to COX activity could not be neglected completely [64], in all experiments untreated samples were included (as a control) together with treated (with stressors) samples, and the conclusions were drawn with regard to comparison of both samples.

Our study is the first complementation analysis in the yeast *SCO2* deletion strain with human homologues. On the other hand, the ability of human homologues to replace the respiratory deficiency in the *SCO1* deletion mutant (Δ*sco1*) was analysed and results showed that expression of neither full-length *hSCO1* nor *hSCO2* rescued the phenotype. Only the expression of a chimera with the N-terminal part of yeast and the C-terminal part (with the CxxxC domain) of human *SCO1* successfully complemented, but not any chimera of *hSCO2* [135].

When these two complementation results were taken into consideration, it is very likely that the antioxidant function of *SCO* genes is more conserved between these two distantly related species compared to the respiratory function. Additionally, despite the distinctive roles in COX assembly, human *SCO* genes might have an overlapping defensive role against oxidative stress.

4.1.3 D. melanogaster homologue, *SCOX*

Drosophila melanogaster was utilized as a model organism in earlier studies to get insight into the *in vivo* functions of Sco proteins. The COX assembly defects and consequent low energy supply was reported in *scox* mutants together with associated phenotypes including larval lethality (null mutant) and female sterility (5` UTR mutations) [136, 137].

Interestingly, prior *SCOX* overexpression studies pointed out the better performance of flies (compared to wt) on PQ-added media in terms of an increased lifespan [137]. This result is consistent with our growth assay data and proves the power of yeast-based complementation assay in revealing the functional homologues from higher organisms.

Until now, the observed stress-related consequences (ROS levels & lifespan) in this model organism have only been reasoned by respiration defects (as is the case for human homologues). However, when our data are taken into consideration, an antioxidant function could be strongly suggested for *SCOX* for the first time.

4.1.4 Yeast homologues, *K07152* & *SpSCO1*

Two different homologues from distinct yeast species were included into the complementation analyses, K07152 (*K. lactis*) and SpSco1 (*S. pombe*). The phylogenetic data pointed out that *K. lactis* is more closely related to *S. cerevisiae* compared to *S. pombe* [138, 139].

However, this close phylogenetic relationship is supported only by the higher aa identity of K07152 to ySco2p (compared to SpSco1) but not by the functional complementation assay results. The homologue of *K. lactis* could not rescue the stress sensitive phenotype of *sco2* deletion mutant whereas *SpSCO1* could. The respiratory role of *SpSCO1* was shown in previous studies [140] and our current results proposed an additional antioxidant role.

Even though the mutagenesis analysis revealed a mutation site that might be the reason of the functional loss in K07152, the mechanisms behind the relevant evolutionary processes could be more complicated. It is well known that the two yeast species; *K. lactis* and *S. cerevisiae* differ in the pathways connected to antioxidant defense mechanisms (such as respiratory mechanism and redox homeostasis) [141]. This may explain the observed functional differences of the Sco homologues in those two species.

4.2 The localization and expression pattern of homologues

MitoFates is a commonly used bioinformatics tool for prediction of MTS and cleavage sites. The high probability score calculated for presequence detection could be a reliable hint of mt localization [88]. The presequence prediction via MitoFates indicates a high mt localization probability for the Sco2 homologues. However, since they were expressed in another host organism, localization was checked experimentally in Western analyses using crude cytoplasmic and mt fractions. Despite the contamination between fractions, the homologues were predominantly detected in mt fractions and these results supported the MitoFates predictions.

It is apparent that the N-terminal part of protein is not as conserved as the C-terminal part among homologues. However, regarding the localization results it could be stated that mt targeting presequences are degenerate and most probably the positive net charge is sufficient for translocation to mitochondria. Based on our data, we could not conclude on the exact location of homologues in mt subcompartments. To reveal it, mitochondria should be isolated enzymatically, and further salt treatments should be done [142, 143].

An apparent variation in the expression levels was observed not only between the homologues of different organisms but also of the same organism such as Hcc1 and Hcc2. Extensive studies done in diverse organisms have clearly demonstrated that synonymous codons were not equally used. Moreover, such a codon bias is not observed only across organisms but also within the genome [144, 145]. It is also probable that the stability of expressed homologues is different in the host organism. Thus, both possibilities could be the reason behind the difference in the protein concentration levels of the expressed homologues.

The protein analyses clearly indicated that there is no correlation between the expression level of the proteins and their respective function. The expression level of

K07152 was the highest among all homologues but it could not complement the ySco2p. On the contrary, hardly detectable *hSCO1* (at protein level) could successfully rescue the oxidative stress phenotype of *sco2* deletion mutant.

4.3 The impact of pathogenic *hSCO2* mutations on its antioxidant role

The majority of the current knowledge on the divergent roles of *hSCO2* comes from mutation studies. To date, several *hSCO2* mutations causing distinct diseases such as fatal infantile cardioencephalomyopathy [109, 115, 146, 147], myopia 6 [110, 148] and leigh syndrome [111, 146] have been identified. The studies in patient cell lines revealed the different roles of *hSCO2* in mt Cu homeostasis [149-151] and COX biogenesis (as a thiol-disulfide oxidoreductase) [52].

In this thesis, five pathogenic mutations (C133S, E140K, L151P, R171W, and S225F) asscociated with fatal infantile cardioencephalomyopathy were selected and analysed in the yeast model. So far, all patients reported with respective mutations carry a E140K mutation in at least one allele and this rendered the analysis of the phenotypic consequences of each individual mutations (except E140K) in human [152].

Some attempts *in vitro* [112] and *in vivo* models [153, 154] predicted individual effects of E140K and S225F mutations on the physical state, Cu binding [112] and respiratory function [153]. The results of these analyses are supporting each other and consistently indicate the different impact of mutations on the respective functions. However, it should not be disregarded that while *in vitro* analyses were done with recombinant proteins (soluble part), *in vivo* analyses were based on parallel mutations (in the genes of model organisms).

In our studies, this limitation was tackled by identification of a functional complementation between *hSCO2* and *ySCO2*. As the expression of full-length *hSCO2* could successfully rescue the mutant phenotype, for the first time the effect of mutations was examined by expression of the *hSCO2* mutant genes.

Our analyses extended the current structural and experimental data (*in vitro*) that suggest overlapping but also distinct impacts for these mutations (table 16) and revealed the importance of each aa residues for resistance against oxidative stress.

Table 16. Current knowledge on the possible effects of pathogenic hSCO2 mutations [61, 112].

Mutation	Possible effect	Rescue of stress-sensitivity phenoytpe in yeast studies
C133S	• Disruption of Cu binding site	-
E140K	• Disruption of salt bridge and destabilization of side chain packing owing to replacement with an aa having a longer side chain • Changes in physical state and two-fold decrease in Cu binding capacity	-
L151P	• Destabilization of protein structure	-
R171W	• Disruption of salt bridge hence destabilization of protein structure	-
S225F	• Conformational changes due to alterations in Cu binding ability • Changes in physical state and three-fold increase in Cu binding capacity	-

As the interconnected mechanisms behind the respective antioxidant role is still unknown, it is difficult to directly support our data with Cu-associated effects at the first sight. However, the link between Cu and oxidative stress is well addressed in literature: While the increase in free Cu levels (as a consequence of Cu overload or excess exposure) might trigger stress upon generation of highly reactive hydroxyl radicals [155-157], Cu deficiency could also cause oxidative stress owing to decreased expression/activity of antioxidant enzymes including Sod1 [158-160] and catalase [161]. Thus, when the proximal locations of mutant residues to Cu binding sites are taken into consideration together with altered Cu content in patient cells [151], the possible link between Sco-regulated Cu homeostasis and antioxidant defense could not be neglected.

4.4 Mutational analysis of *ySCO2*

The knowledge on the functional sites of *ySCO2* is limited, particularly for the antioxidant role. For this purpose, mutants of possibly important cysteine residues (C154S, C158S, in the conserved CxxxC motif) were generated together with N-terminal deletion mutants (w/o the MTS and TM) and the impact of these mutations on the function were tested. The results revealed the distinct sensitivities of these three mutants (C154S, C158S & ySCO2 (w/o MTS and TM)) to PQ.

In the Sco protein family, these mutated cysteines are known to be crucial for Cu binding and trafficking [47, 50]. Although the Cu binding ability of ySco1p, hSco1 and hSco2 through these conserved cysteines and histidine were demonstrated [60-62], it has not been experimentally verified for ySco2p yet.

The experimental/structural data of its highly similar homologue, ySco1p revealed an interesting point: The coordinating cysteines could be altered related to the redox state of bound Cu ((I) or (II)). In the presence of Cu (II), the conserved cysteines (in CxxxC motif) were oxidized (unable to bind) and the Cu coordination was achieved by other cysteines [62].

As ySCO1p, ySco2p also has additional cysteines that could alternatively be involved in Cu binding. Even though there is no clear evidence about the Cu coordinating residues of ySco2p and the redox state of Cu in *S. cerevisiae* mitochondria (at normal/stress conditions), it could be still speculated that the differential sensitivity of cysteine mutants (toward oxidative stress) might be Cu-associated.

Besides the possible Cu-binding effect, the higher sensitivity of the C158S mutant towards PQ could also stem from the intrinsic differences in the reactivity of cysteines (in redox reactions) or/and structural changes. However, as it is unknown whether the antioxidant role of ySco2p is direct (participating in redox reactions with reacting cysteines) or indirect (activation of protective mechanism through protein-protein interactions and/or recycling of antioxidants), it is difficult to support any of these possibilities strongly.

Additionally, the N-terminally truncated mutant (w/o MTS and TM) also grew as slow as the C158S mutant in the presence of PQ. This data suggests a beneficial effect of mt localization for the defense aganist PQ-induced oxidative stress. On the other hand, further experiments should be performed for this (N-terminal) mutant strain to investigate the localization of the mutant ySco2 (by Western blot) and to determine the changes in ROS levels at different cellular compartments including mitochondria.

4.5 Attempts to understand the underlying reason(s) behind charge-related functional change

Identification of functional and non-functional homologues led to the question of whether there are conserved aa that are pivotal for the antioxidant function. Owing to the lack of structural data for all homologues, the conservation analysis was limited to the aa alignment but not to the position of aa residues on the structure. Regarding the

previous studies that emphasize the role of salt bridges on Sco proteins` structure and function [60, 61], the conservation of charged residues was taken into account. One specific site (15 aa downstream of CxxxC motif) with opposite charged residues (functional (+), non-functional (-)) was identified in the alignment. The observation of a functional change resulting from charge difference drew our attention to have a closer look on possible electrostatic interactions.

It is well-known that the electrostatics features of proteins are directly regulated by charged residues through the formation of salt bridges [117, 118] and distribution of global/local charges [162] that are critical for protein-protein interactions (PPI) [163-165].

Salt bridges can be formed between the residues located to either the same (intramolecular) or different subunits (intermolecular). They contribute to different aspects including stability [166], activation [167], conformation [168, 169] and interaction specificity [170, 171]. Previous studies indicated the difficulties associated with identification of intermolecular salt bridges in transient complexes [118, 172]. For this reason, intramolecular salt bridges at the (conserved) mutation site were first investigated. The bioinformatics analyses carried out with PLIP revealed these possible interactions and interacting partners. Subsequent alanine mutagenesis analyses (performed regarding the bioinformatics results) pointed out the functional gain and tolerance of neutral charge despite the lack of salt bridge formation at this mutation site. Additionally, positions of the salt-bridge partners on the structure did not influence the result. Although the predicted salt bridges are connecting the different chains of structures (hSco2 & ySco2p), their disruption did not impair the antioxidant function.

Since all estimates are either done on model or recombinant protein structures, it is impossible to make concrete conclusions about the salt bridge-structure-function relationship at this point. However, the mutagenesis data may hint at another (additional) parameter: PPI. The importance of charge-mediated interactions in the activity of different type of proteins including Cu metallochaperones, ATPases [120] and thioredoxins [173, 174] has been shown. In the light of these results, functional change due to opposite charge mutations could be a consequence of established/disrupted interactions mediated directly or indirectly (neighboring effect) by the mutated site.

The contribution of several factors including accessible surface area, geometric

complementarity, hydrogen bonds, hydrophobicity and electrostatic interactions [175-177] to PIP is well known. Thus, all these parameters should be carefully considered for further bioinformatics investigations.

Before such in-depth bioinformatics analyses, initial attempts were made to estimate both the position of mutation sites (surface exposed or buried) (figure 29) and the electrostatic potential of protein surfaces (native and mutant homologues) (figure 30).

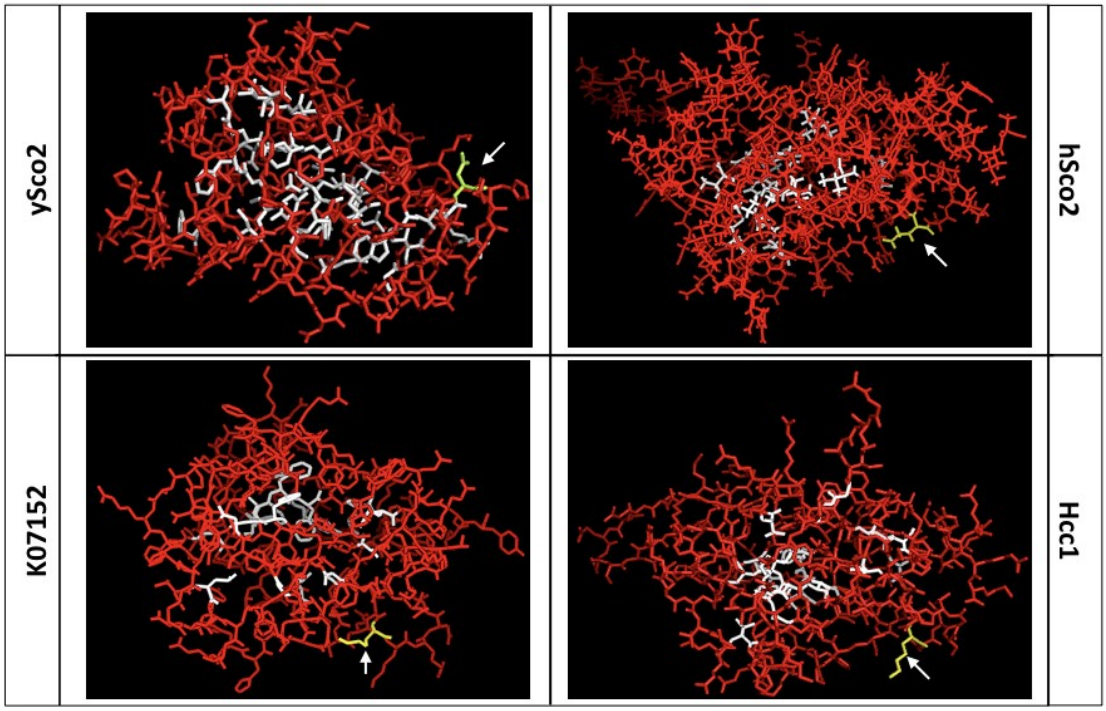

Figure 29. Model of conserved mutation sites on the protein structures of selected homologues. Protein structures are shown in sticks; red: surface exposed aa residues, white: buried aa residues. The mutation sites are shown as yellow and highlighted by white arrows. All figures were generated by PyMOL.

Surface-exposed aa residues of proteins commonly constitute the active sites that are essential for interactions with other molecules [178]. Identification of the conserved mutation sites on surface (figure 29) strengthened the claim that they might participate in PPI.

As the surface charged residues directly influence the surface potential, changes in electrostatic potential due to mutations were determined using PDB2PQR & APBS (figure 30).

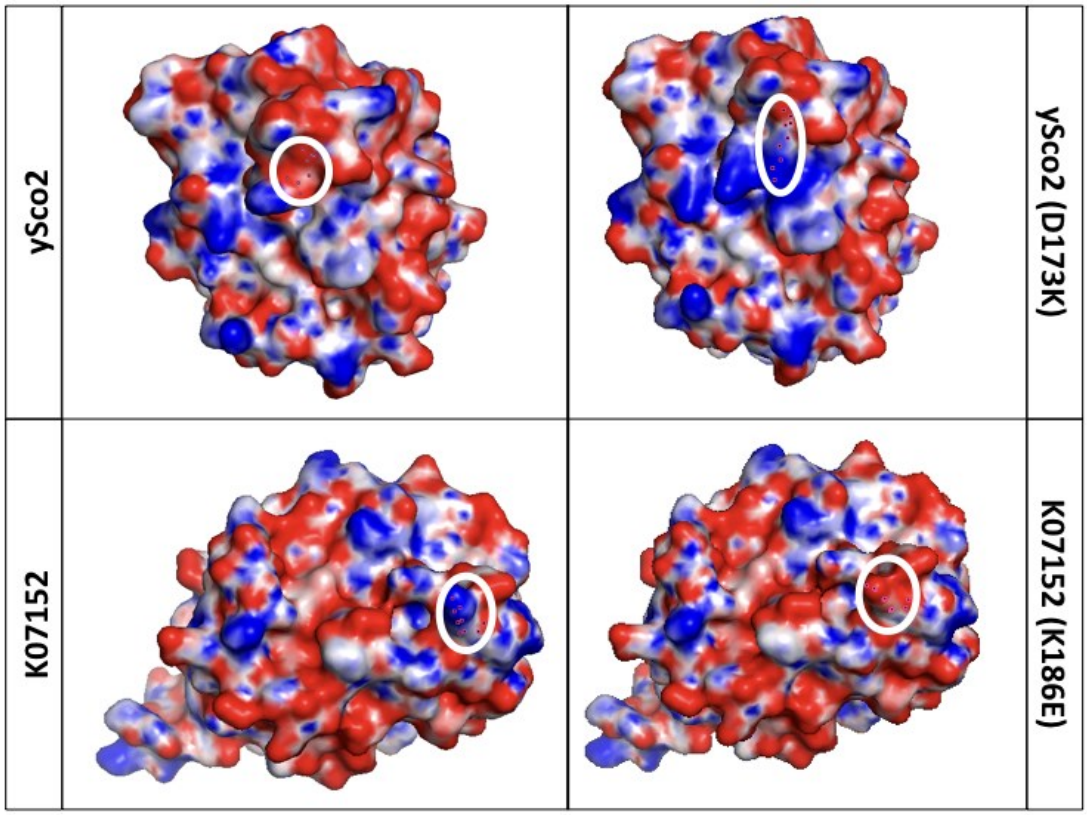

Figure 30. Electrostatic surface potential of homologues; native and mutant forms.
The surfaces are colored regarding the electrostatic potential: red 10 kT, white 0 kT, blue +10 kT using PDB2PQR & APBS (application of the linearized Poisson- Boltzmann equation). The mutation sites are highlighted in white circles.

The possible changes in electrostatic surface potential due to mutations are apparent (color change from red to blue or *vice versa*). However, further expertise is required for a detailed estimation of PPI-associated changes. Therefore, special emphasis will be put on both bioinformatics and experimental analyses. Co-immunoprecipitation experiments will be suitable to identify differences in the interaction partner(s).

So far, some physical interactions between ySco2p and different proteins have been identified. These interactors involved in distinct mechanisms including maintenance of mt structure, COX activity and respiration (Sco1p [64], Cox2p [64], Cox20p [179]), import of IMS proteins (Mic60p [180]), folding of newly synthesized polypeptides (Ssb2p [181]), transcription initiation (Kin28p [182]), degradation of mRNAs (Puf3p [183]) and regulation of pyruvate dehydrogenase activity (Ptc5p [184]) and ADP/ATP exchange (Pet9p [185]). However, it is difficult to link these interactions to possible antioxidant action directly at the first sight regarding the complexity of intertwined stress and defense pathways. Therefore, in our future co-

immunoprecipitation studies, both functional and nonfunctional (D173K) ySco2 proteins will be analysed. It is expected to gain a deeper understanding on auxiliary and overlapping pathways by comparison of Sco2 interacting partner(s) in functional and nonfunctional strains by these experimental analyses.

4.6 Potential mechanisms associated with the antioxidant action of ySco2p

This study strongly suggests an antioxidant role for ySco2p and its functional homologues, however the mechanism(s) behind this defensive function is still to be clarified.

Current knowledge in the literature about the function of ySco2p is limited to mutagenesis experiments that propose a Cu chaperone activity [66] and a role in COX assembly [65]. On the other hand, detailed studies in patient cell lines have suggested additional and cooperative roles to human Sco proteins particularly in Cu homeostasis. Based on the results of Sco2 patient cells (Cu-deficient) that have disruptions in the redox state of hSCO1, an oxidoreductase function for hSco2 has been suggested. Additionally, a regulatory role in mt signaling is proposed for hSco1 regarding the disproportionate reduction of its cysteines in several Cu-deprived patient cells. Identification of these redox-sensitive cysteines in hSco1 puts emphasis on the possibility of signal transduction mediated by a redox-sensitive interaction between hSco1 and another molecule/sensing protein [186]. According to the proposed model, alterations in the redox state of hSco1 could cause the release of an interactor, hence trigger the signaling cascade that is maintained through further interactions with other proteins localized to different compartments [186, 187].

This mechanism linked to Cu homeostasis is a good illustration of the tight connection between different pathways regulated by the divergent roles of Sco proteins: thioredoxin activity [52], redox signaling [186, 187] and Cu regulation [188]. Furthermore, it gives clues about the possible intertwined mechanisms behind the antioxidant function.

Even though the complexity of pathways varies between different organisms, our comparative studies revealed the conservation of the antioxidant function among distant species. This hints at a conservation of interconnected pathways associated with the respective function. Thus, existing information on the distinct role of human homologues could be used as evidence while taking a detailed look at the underlying mechanism(s) behind functional homologues, particularly *ySCO2*.

Based on our current results, different mechanisms might be involved in the putative antioxidant function of Sco2p (figure 31). At this point, it remains open whether the function is direct (thioredoxin-ROS scavenging function) or indirect (signaling). On the other hand, the mutagenesis analyses may suggest a signaling role to Sco proteins controlled by a charge driven protein-protein interaction. These results are important since they indicate that a suggested signaling role could not be constrained to hSco1 and Cu regulation but might also be the main driver of Sco-protein associated antioxidant defense mechanism.

The ySco2p is tethered to the inner mt membrane with the N-terminal portion facing the matrix and the C-terminal portion (including the putative Cu binding motif, CxxxC) protruding into the IMS [189]. As the globular domain with thioredoxin-like fold is localized to IMS, it is most likely that this IMS part is the locus of the action. Moreover, among a series of double deletion mutants, only the one with concomitant deletion of Sod1p (Δ*sco2*Δ*sod1*) exhibits an oxidative stress-sensitive phenotype but not others (Δ*sco2*Δ*trr2,* Δ*sco2*Δ*trx3* and Δ*sco2*Δ*sod2*) (Gehlhar, 2013). It is well-known that Sod1p is localized in the cytosol and IMS but the other antioxidant enzymes are in matrix, and this could also be an evidence for IMS-originated antioxidant response. On the other hand, it cannot be neglected that among the tested proteins Sco2p and Sod1p are the only Cu binding proteins, but others not. Thus, such a pronounced sensitivity may also be related to Cu-associated networks.

The mechanisms discussed here regarding the functional Sco2 homologues (particularly ySco2p) in oxidative stress defense are hypothetical. Since the strongest reason behind this antioxidant response is foreseen as signaling, the focus for further work will be on protein-protein interactions.

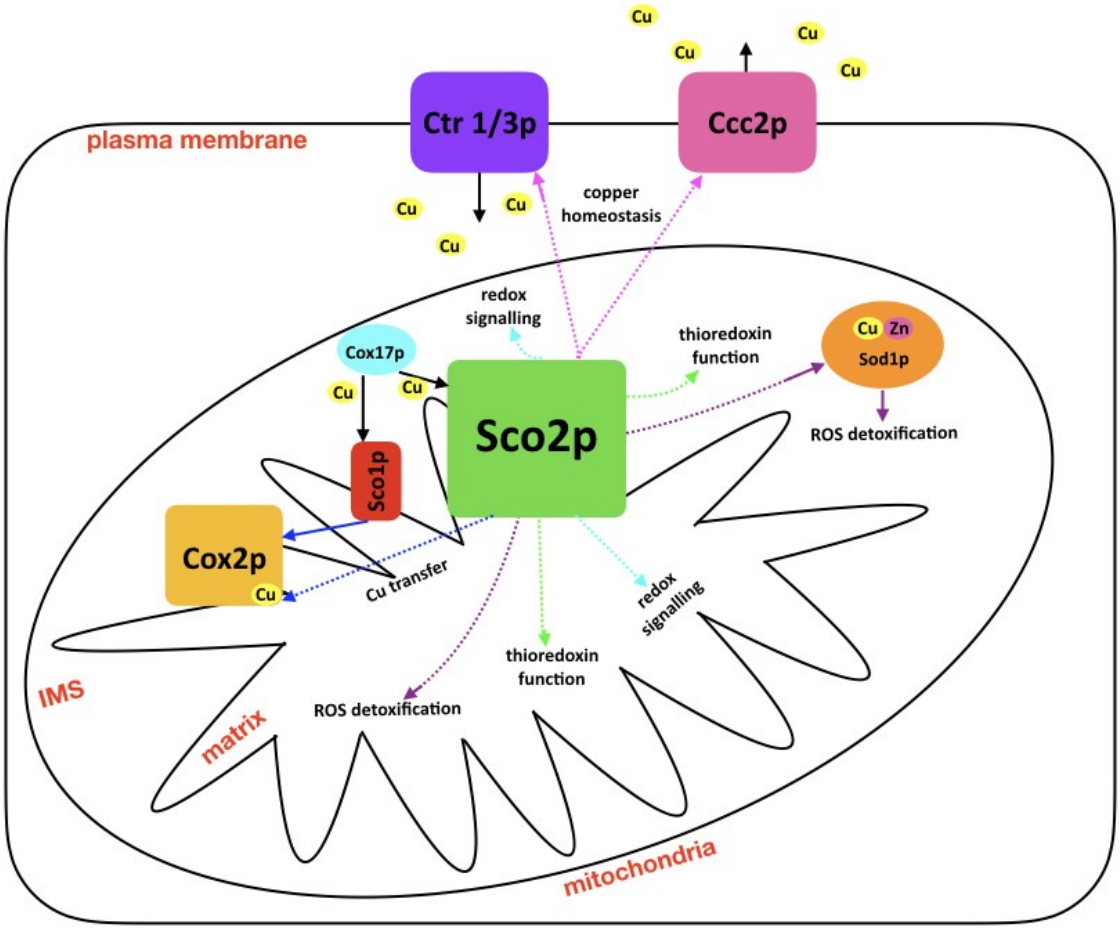

Figure 31. Model of potential mechanisms associated with the antioxidant action of ySco2p.
This is a schematic draw of a *S. cerevisiae* cell. Mitochondrial compartments (IMS and matrix) are illustrated in enlarged mitochondrial structure. The blue arrows denote the Cu transfer to Cox2p mediated by Sco proteins. While Sco1p is crucial for the Cu transfer, Sco2p might only have slight or supportive effect on that. Green and cyan arrows illustrate the thioredoxin activity and redox signaling, respectively. Possible functions of ySco2p in ROS detoxification and Cu homeostasis (by regulating Cu influx and efflux through plasma membrane-associated transporters Ctr1/3p and Ccc2p) are indicated by purple and pink arrows, respectively. While the functions suggested regarding the current knowledge on human homologues are shown by dashed lines, solid lines highlight the verified functions.

5 Summary

Sco proteins that exist in all types of organisms were firstly identified in *S. cerevisiae* as a vital gene product for the biogenesis of the cytochrome *c* oxidase (COX). However, identification of a structural similarity to antioxidant enzymes (the Trx-like fold) and investigation of several prokaryotes having *SCO* genes but not a COX [47] hint at distinct function(s) of these proteins independent of COX biogenesis. Further experimental results that demonstrated the broad roles of Sco proteins such as regulation of gene expression, defense against oxidative stress and disulfide reductase activity in prokaryotes raise the question of whether eukaryotic Sco proteins also carry out a role in the antioxidant defense.

The complexity of biological systems, particularly in higher eukaryotic organisms could complicate the identification of interconnected functions. Therefore, a simple and facultative aerobic organism, *S. cerevisiae* was chosen to investigate a conserved protective role of eukaryotic Sco proteins against ROS. Observation of a stress-sensitive phenotype for *SCO* deletion mutants of *S. cerevisiae* (Δ*sco1*Δ*sod1* and Δ*sco2*Δ*sod1*) has proposed an antioxidant role for these proteins and also gives an opportunity to perform further cross-species complementation studies in yeast.

The homologues of *ySCO2* were selected from eukaryotic organisms with different genetic complexity to assess the functional conservation across distant species*: Homo sapiens*, *Schizosaccharomyces pombe*, *Arabidopsis thaliana*, *Drosophila melanogaster* and *Kluyveromyces lactis.* The homologues were integrated into the *SCO2* locus of the Δ*sco2*Δ*sod1* strain and functional complementation was tested by both growth assays and biochemical ROS assays. Thus, complementing and non-complementing homologues were identified (table 17).

The expression and localization of all homologues were checked by Western blot analyses. All the homologues (except hSco2) were detected in mt fractions but at varying concentrations. These results clearly indicated that there is no correlation between the expression level of the proteins and their respective function.

Table 17. Summarized results of functional complementation analyses

Organism	Homologue	Functional Complementation in Δ*sco2*Δ*sod1*
Saccharomyces cerevisiae	*ySCO2*	+
Arabidopsis thaliana	*HCC1*	-
Arabidopsis thaliana	*HCC2*	+
Kluyveromyces lactis	*K07152*	-
Schizosaccharomyces pombe	*SpSCO1*	+
Drosophila melanogaster	*SCOX*	+
Homo sapiens	*hSCO1*	+
Homo sapiens	*hSCO2*	+

The complementation studies in yeast were extended to mutation analyses after identification of a functional conservation between *hSCO2* and *ySCO2*. This time, *S. cerevisiae* was utilized as a model organism to gain a deeper insight into the broader effects of *hSCO2*-associated diseases. With these studies, the current knowledge about the impact of these mutations was expanded and the importance of each aa mutation (C133S, E140K, L151P, R171W, and S225F) in patients for the postulated antioxidant role was investigated. All mutant strains exhibited almost no growth under stress conditions, indicating the loss of the defensive role against oxidative stress due to the mutations.

The observation of non-functional homologues despite of the high sequence similarity to ySco2p strengthened our hypothesis on the importance of conserved aa for the defensive role. For this purpose, selected homologues were aligned, and the conservation was judged not only based on identity but also similarity (*e.g.* charge, hydrophobicity). Alignment results indicated the presence of only one site (located 15 aa downstream of the CxxxC motif) with opposite charge: negatively charged aa in the functional homologues, but a positively charged lysine in the non-functional homologues.

The subsequent mutagenesis analyses revealed the impact of charge at this conserved site on the antioxidant function. After observation of the functional change due to the mutations, two possible underlying reasons were considered: rearrangement of intermolecular salt bridge(s) and changes in the electrostatic potential accompanied by possible alterations in protein-protein interactions. By using a bioinformatics tool (PLIP), possible intermolecular salt bridge(s) at the mutation sites were determined

but subsequent alanine mutagenesis experiments pointed out that the functional change is independent of salt bridge formation.

Since the hypothesis based on salt bridge rearrangement failed to explain the functional change, further effort will be put into the calculations of the electrostatic potential and alterations in protein-protein interactions. For this purpose, bioinformatics analyses and co-immunoprecipitations analyses will be done.

6 References

1. Commoner, B., J. Townsend, and G.E. Pake, *Free radicals in biological materials.* Nature, 1954. **174**(4432): p. 689-91.
2. Rapoport, R.M. and F. Murad, *Agonist-induced endothelium-dependent relaxation in rat thoracic aorta may be mediated through cGMP.* Circ Res, 1983. **52**(3): p. 352-7.
3. Paul, B., R. Strauss, and A.J. Sbarra, *The role of the phagocyte in host-parasite interactions. XVI. Effect of x-irradiation on H2O2 production in guinea pig exudate cells.* J Reticuloendothel Soc, 1968. **5**(6): p. 538-49.
4. Veal, E.A., A.M. Day, and B.A. Morgan, *Hydrogen peroxide sensing and signaling.* Mol Cell, 2007. **26**(1): p. 1-14.
5. Veal, E. and A. Day, *Hydrogen peroxide as a signaling molecule.* Antioxid Redox Signal, 2011. **15**(1): p. 147-51.
6. D'Autreaux, B. and M.B. Toledano, *ROS as signalling molecules: mechanisms that generate specificity in ROS homeostasis.* Nat Rev Mol Cell Biol, 2007. **8**(10): p. 813-24.
7. Lushchak, V.I., *Oxidative stress in yeast.* Biochemistry (Mosc), 2010. **75**(3): p. 281-96.
8. Rahman, T., et al., *Oxidative stress and human health.* Advances in Bioscience and Biotechnology, 2012. **Vol.03No.07**: p. 23.
9. Harman, D., *Aging: a theory based on free radical and radiation chemistry.* J Gerontol, 1956. **11**(3): p. 298-300.
10. Harman, D., *Origin and evolution of the free radical theory of aging: a brief personal history, 1954-2009.* Biogerontology, 2009. **10**(6): p. 773-81.
11. Dhawan, V., *Reactive Oxygen and Nitrogen Species: General Considerations*, in *Studies on Respiratory Disorders*, N.K. Ganguly, et al., Editors. 2014, Springer New York: New York, NY. p. 27-47.
12. Pham-Huy, L.A., H. He, and C. Pham-Huy, *Free radicals, antioxidants in disease and health.* Int J Biomed Sci, 2008. **4**(2): p. 89-96.
13. Lushchak, V.I., *Free radicals, reactive oxygen species, oxidative stress and its classification.* Chem Biol Interact, 2014. **224**: p. 164-75.
14. Turrens, J.F., *Mitochondrial formation of reactive oxygen species.* J Physiol, 2003. **552**(Pt 2): p. 335-44.
15. Farrugia, G. and R. Balzan, *Oxidative stress and programmed cell death in yeast.* Front Oncol, 2012. **2**: p. 64.
16. Wood, Z.A., L.B. Poole, and P.A. Karplus, *Peroxiredoxin evolution and the regulation of hydrogen peroxide signaling.* Science, 2003. **300**(5619): p. 650-3.
17. Davidson, J.F., et al., *Oxidative stress is involved in heat-induced cell death in Saccharomyces cerevisiae.* Proc Natl Acad Sci U S A, 1996. **93**(10): p. 5116-21.
18. Gille, G. and K. Sigler, *Oxidative stress and living cells.* Folia Microbiol (Praha), 1995. **40**(2): p. 131-52.
19. Halliwell, B. and C.E. Cross, *Oxygen-derived species: their relation to human disease and environmental stress.* Environ Health Perspect, 1994. **102 Suppl 10**: p. 5-12.

20. Avery, A.M. and S.V. Avery, *Saccharomyces cerevisiae expresses three phospholipid hydroperoxide glutathione peroxidases.* J Biol Chem, 2001. **276**(36): p. 33730-5.
21. Costa, V. and P. Moradas-Ferreira, *Oxidative stress and signal transduction in Saccharomyces cerevisiae: insights into ageing, apoptosis and diseases.* Mol Aspects Med, 2001. **22**(4-5): p. 217-46.
22. Gasch, A.P., et al., *Genomic expression programs in the response of yeast cells to environmental changes.* Mol Biol Cell, 2000. **11**(12): p. 4241-57.
23. Temple, M.D., G.G. Perrone, and I.W. Dawes, *Complex cellular responses to reactive oxygen species.* Trends Cell Biol, 2005. **15**(6): p. 319-26.
24. Lee, J., et al., *Yap1 and Skn7 control two specialized oxidative stress response regulons in yeast.* J Biol Chem, 1999. **274**(23): p. 16040-6.
25. Morgan, B.A., et al., *The Skn7 response regulator controls gene expression in the oxidative stress response of the budding yeast Saccharomyces cerevisiae.* EMBO J, 1997. **16**(5): p. 1035-44.
26. Park, J.I., et al., *The cytoplasmic Cu,Zn superoxide dismutase of saccharomyces cerevisiae is required for resistance to freeze-thaw stress. Generation of free radicals during freezing and thawing.* J Biol Chem, 1998. **273**(36): p. 22921-8.
27. Lee, J.H., et al., *Protective role of superoxide dismutases against ionizing radiation in yeast.* Biochim Biophys Acta, 2001. **1526**(2): p. 191-8.
28. Wu, C.Y., J. Steffen, and D.J. Eide, *Cytosolic superoxide dismutase (SOD1) is critical for tolerating the oxidative stress of zinc deficiency in yeast.* PLoS One, 2009. **4**(9): p. e7061.
29. Liu, X., X. Zhang, and Z. Zhang, *Cu,Zn-superoxide dismutase is required for cell wall structure and for tolerance to cell wall-perturbing agents in Saccharomyces cerevisiae.* FEBS Lett, 2010. **584**(6): p. 1245-50.
30. Jamieson, D.J., *Oxidative stress responses of the yeast Saccharomyces cerevisiae.* Yeast, 1998. **14**(16): p. 1511-27.
31. Delaunay, A., et al., *A thiol peroxidase is an H2O2 receptor and redox-transducer in gene activation.* Cell, 2002. **111**(4): p. 471-81.
32. Tachibana, T., et al., *A major peroxiredoxin-induced activation of Yap1 transcription factor is mediated by reduction-sensitive disulfide bonds and reveals a low level of transcriptional activation.* J Biol Chem, 2009. **284**(7): p. 4464-72.
33. Martin, J.L., *Thioredoxin--a fold for all reasons.* Structure, 1995. **3**(3): p. 245-50.
34. Herrero, E., et al., *Redox control and oxidative stress in yeast cells.* Biochim Biophys Acta, 2008. **1780**(11): p. 1217-35.
35. Tomanek, L., *Proteomic responses to environmentally induced oxidative stress.* J Exp Biol, 2015. **218**(Pt 12): p. 1867-79.
36. Evans, P. and B. Halliwell, *Micronutrients: oxidant/antioxidant status.* Br J Nutr, 2001. **85 Suppl 2**: p. S67-74.
37. Bronzetti, G., et al., *Protective effects of vitamins and selenium compounds in yeast.* Mutat Res, 2001. **496**(1-2): p. 105-15.
38. Raspor, P., et al., *Prevention of intracellular oxidation in yeast: the role of vitamin E analogue, Trolox (6-hydroxy-2,5,7,8-tetramethylkroman-2-carboxyl acid).* Cell Biol Int, 2005. **29**(1): p. 57-63.

39. Ito, K. and K. Inaba, *The disulfide bond formation (Dsb) system.* Curr Opin Struct Biol, 2008. **18**(4): p. 450-8.
40. Holmgren, A., et al., *Thiol redox control via thioredoxin and glutaredoxin systems.* Biochem Soc Trans, 2005. **33**(Pt 6): p. 1375-7.
41. Armstrong, R.N., *Structure, catalytic mechanism, and evolution of the glutathione transferases.* Chem Res Toxicol, 1997. **10**(1): p. 2-18.
42. Atkinson, H.J. and P.C. Babbitt, *An atlas of the thioredoxin fold class reveals the complexity of function-enabling adaptations.* PLoS Comput Biol, 2009. **5**(10): p. e1000541.
43. Schulze, M. and G. Rodel, *SCO1, a yeast nuclear gene essential for accumulation of mitochondrial cytochrome c oxidase subunit II.* Mol Gen Genet, 1988. **211**(3): p. 492-8.
44. Pereira, M.M., M. Santana, and M. Teixeira, *A novel scenario for the evolution of haem-copper oxygen reductases.* Biochim Biophys Acta, 2001. **1505**(2-3): p. 185-208.
45. Khalimonchuk, O. and G. Rödel, *Biogenesis of cytochrome c oxidase.* Mitochondrion, 2005. **5**(6): p. 363-88.
46. Poyton, R.O. and J.E. McEwen, *Crosstalk between nuclear and mitochondrial genomes.* Annu Rev Biochem, 1996. **65**: p. 563-607.
47. Banci, L., et al., *The functions of Sco proteins from genome-based analysis.* J Proteome Res, 2007. **6**(4): p. 1568-79.
48. Wang, X., et al., *Comparative study of human mitochondrial proteome reveals extensive protein subcellular relocalization after gene duplications.* BMC Evolutionary Biology, 2009. **9**(1): p. 275.
49. Glerum, D.M., A. Shtanko, and A. Tzagoloff, *SCO1 and SCO2 act as high copy suppressors of a mitochondrial copper recruitment defect in Saccharomyces cerevisiae.* J Biol Chem, 1996. **271**(34): p. 20531-5.
50. Banci, L., et al., *Seeking the determinants of the elusive functions of Sco proteins.* FEBS J, 2011. **278**(13): p. 2244-62.
51. Bertini, I. and G. Cavallaro, *Metals in the "omics" world: copper homeostasis and cytochrome c oxidase assembly in a new light.* J Biol Inorg Chem, 2008. **13**(1): p. 3-14.
52. Leary, S.C., et al., *Human SCO2 is required for the synthesis of CO II and as a thiol-disulphide oxidoreductase for SCO1.* Hum Mol Genet, 2009. **18**(12): p. 2230-40.
53. Abriata, L.A., et al., *Mechanism of Cu(A) assembly.* Nat Chem Biol, 2008. **4**(10): p. 599-601.
54. Eraso, J.M. and S. Kaplan, *From redox flow to gene regulation: role of the PrrC protein of Rhodobacter sphaeroides 2.4.1.* Biochemistry, 2000. **39**(8): p. 2052-62.
55. Badrick, A.C., et al., *PrrC, a Sco homologue from Rhodobacter sphaeroides, possesses thiol-disulfide oxidoreductase activity.* FEBS Lett, 2007. **581**(24): p. 4663-7.
56. Saenkham, P., P. Vattanaviboon, and S. Mongkolsuk, *Mutation in sco affects cytochrome c assembly and alters oxidative stress resistance in Agrobacterium tumefaciens.* FEMS Microbiol Lett, 2009. **293**(1): p. 122-9.
57. Seib, K.L., M.P. Jennings, and A.G. McEwan, *A Sco homologue plays a role in defence against oxidative stress in pathogenic Neisseria.* FEBS Lett, 2003. **546**(2-3): p. 411-5.

58. Chinenov, Y.V., *Cytochrome c oxidase assembly factors with a thioredoxin fold are conserved among prokaryotes and eukaryotes.* J Mol Med (Berl), 2000. **78**(5): p. 239-42.
59. Ye, Q., et al., *Identification of a disulfide switch in BsSco, a member of the Sco family of cytochrome c oxidase assembly proteins.* Biochemistry, 2005. **44**(8): p. 2934-42.
60. Banci, L., et al., *A hint for the function of human Sco1 from different structures.* Proc Natl Acad Sci U S A, 2006. **103**(23): p. 8595-600.
61. Banci, L., et al., *A structural characterization of human SCO2.* Structure, 2007. **15**(9): p. 1132-40.
62. Abajian, C. and A.C. Rosenzweig, *Crystal structure of yeast Sco1.* J Biol Inorg Chem, 2006. **11**(4): p. 459-66.
63. Williams, J.C., et al., *Crystal structure of human SCO1: implications for redox signaling by a mitochondrial cytochrome c oxidase "assembly" protein.* J Biol Chem, 2005. **280**(15): p. 15202-11.
64. Lode, A., C. Paret, and G. Rödel, *Molecular characterization of Saccharomyces cerevisiae Sco2p reveals a high degree of redundancy with Sco1p.* Yeast, 2002. **19**(11): p. 909-22.
65. Ghosh, A., et al., *Mitochondrial disease genes COA6, COX6B and SCO2 have overlapping roles in COX2 biogenesis.* Hum Mol Genet, 2016. **25**(4): p. 660-71.
66. Glerum, D.M., A. Shtanko, and A. Tzagoloff, *SCO1 and SCO2 Act as High Copy Suppressors of a Mitochondrial Copper Recruitment Defect in Saccharomyces cerevisiae.* Journal of Biological Chemistry, 1996. **271**(34): p. 20531-20535.
67. Balatri, E., et al., *Solution structure of Sco1: a thioredoxin-like protein Involved in cytochrome c oxidase assembly.* Structure, 2003. **11**(11): p. 1431-43.
68. Khalimonchuk, O., A. Bird, and D.R. Winge, *Evidence for a pro-oxidant intermediate in the assembly of cytochrome oxidase.* J Biol Chem, 2007. **282**(24): p. 17442-9.
69. Jamieson, D.J., S.L. Rivers, and D.W. Stephen, *Analysis of Saccharomyces cerevisiae proteins induced by peroxide and superoxide stress.* Microbiology, 1994. **140 (Pt 12)**: p. 3277-83.
70. Cocheme, H.M. and M.P. Murphy, *Complex I is the major site of mitochondrial superoxide production by paraquat.* J Biol Chem, 2008. **283**(4): p. 1786-98.
71. Thornalley, P.J., et al., *The formation of active oxygen species following activation of 1-naphthol, 1,2- and 1,4-naphthoquinone by rat liver microsomes.* Chem Biol Interact, 1984. **48**(2): p. 195-206.
72. Dunham, M.J. and D.M. Fowler, *Contemporary, yeast-based approaches to understanding human genetic variation.* Curr Opin Genet Dev, 2013. **23**(6): p. 658-64.
73. Hamza, A., et al., *Complementation of Yeast Genes with Human Genes as an Experimental Platform for Functional Testing of Human Genetic Variants.* Genetics, 2015. **201**(3): p. 1263-74.
74. Osborn, M.J. and J.R. Miller, *Rescuing yeast mutants with human genes.* Brief Funct Genomic Proteomic, 2007. **6**(2): p. 104-11.

75. Marini, N.J., P.D. Thomas, and J. Rine, *The use of orthologous sequences to predict the impact of amino acid substitutions on protein function.* PLoS Genet, 2010. **6**(5): p. e1000968.
76. Barrientos, A., *Yeast models of human mitochondrial diseases.* IUBMB Life, 2003. **55**(2): p. 83-95.
77. Winzeler, E.A., et al., *Functional characterization of the S. cerevisiae genome by gene deletion and parallel analysis.* Science, 1999. **285**(5429): p. 901-6.
78. Steinmetz, L.M., et al., *Systematic screen for human disease genes in yeast.* Nat Genet, 2002. **31**(4): p. 400-4.
79. Barrientos, A., et al., *Cytochrome oxidase in health and disease.* Gene, 2002. **286**(1): p. 53-63.
80. Gietz, R.D. and R.A. Woods, *Transformation of yeast by lithium acetate/single-stranded carrier DNA/polyethylene glycol method.* Methods Enzymol, 2002. **350**: p. 87-96.
81. Neuhoff, V., et al., *Improved staining of proteins in polyacrylamide gels including isoelectric focusing gels with clear background at nanogram sensitivity using Coomassie Brilliant Blue G-250 and R-250.* Electrophoresis, 1988. **9**(6): p. 255-62.
82. Salentin, S., et al., *PLIP: fully automated protein-ligand interaction profiler.* Nucleic Acids Res, 2015. **43**(W1): p. W443-7.
83. L DeLano, W., *The PyMOL Molecular Graphics System (2002) DeLano Scientific, Palo Alto, CA, USA.* http://www.pymol.org. 2002.
84. Baker, N.A., et al., *Electrostatics of nanosystems: application to microtubules and the ribosome.* Proc Natl Acad Sci U S A, 2001. **98**(18): p. 10037-41.
85. Dolinsky, T.J., et al., *PDB2PQR: an automated pipeline for the setup of Poisson-Boltzmann electrostatics calculations.* Nucleic Acids Res, 2004. **32**(Web Server issue): p. W665-7.
86. Guex, N., M.C. Peitsch, and T. Schwede, *Automated comparative protein structure modeling with SWISS-MODEL and Swiss-PdbViewer: a historical perspective.* Electrophoresis, 2009. **30 Suppl 1**: p. S162-73.
87. Haas, J., et al., *The Protein Model Portal--a comprehensive resource for protein structure and model information.* Database (Oxford), 2013. **2013**: p. bat031.
88. Fukasawa, Y., et al., *MitoFates: Improved Prediction of Mitochondrial Targeting Sequences and Their Cleavage Sites.* Molecular & Cellular Proteomics : MCP, 2015. **14**(4): p. 1113-1126.
89. Gray, M. and S.M. Honigberg, *Effect of chromosomal locus, GC content and length of homology on PCR-mediated targeted gene replacement in Saccharomyces.* Nucleic Acids Res, 2001. **29**(24): p. 5156-62.
90. Sun, S., et al., *An extended set of yeast-based functional assays accurately identifies human disease mutations.* Genome Res, 2016. **26**(5): p. 670-80.
91. Sherman, F., *Getting started with yeast.* Methods Enzymol, 2002. **350**: p. 3-41.
92. Trevors, J.T., et al., *A comparison of methods for assessing yeast viability.* Biotechnology Letters, 1983. **5**(2): p. 131-134.
93. Breeuwer, P., et al., *Characterization of uptake and hydrolysis of fluorescein diacetate and carboxyfluorescein diacetate by intracellular esterases in*

Saccharomyces cerevisiae, which result in accumulation of fluorescent product. Applied and Environmental Microbiology, 1995. **61**(4): p. 1614-1619.
94. Kwolek-Mirek, M. and R. Zadrag-Tecza, *Comparison of methods used for assessing the viability and vitality of yeast cells.* FEMS Yeast Res, 2014. **14**(7): p. 1068-79.
95. Painting, K. and B. Kirsop, *A quick method for estimating the percentage of viable cells in a yeast population, using methylene blue staining.* World J Microbiol Biotechnol, 1990. **6**(3): p. 346-7.
96. Kwolek-Mirek, M., G. Bartosz, and C.M. Spickett, *Sensitivity of antioxidant-deficient yeast to hypochlorite and chlorite.* Yeast, 2011. **28**(8): p. 595-609.
97. Kwolek-Mirek, M., et al., *Acrolein toxicity involves oxidative stress caused by glutathione depletion in the yeast Saccharomyces cerevisiae.* Cell Biol Toxicol, 2009. **25**(4): p. 363-78.
98. Kwolek-Mirek, M., R. Zadrag-Tecza, and G. Bartosz, *Ascorbate and thiol antioxidants abolish sensitivity of yeast Saccharomyces cerevisiae to disulfiram.* Cell Biol Toxicol, 2012. **28**(1): p. 1-9.
99. Kwolek-Mirek, M., et al., *Yeast Saccharomyces cerevisiae devoid of Cu,Zn-superoxide dismutase as a cellular model to study acrylamide toxicity.* Toxicol In Vitro, 2011. **25**(2): p. 573-9.
100. Czekanska, E.M., *Assessment of cell proliferation with resazurin-based fluorescent dye.* Methods Mol Biol, 2011. **740**: p. 27-32.
101. Sharma, R., et al., *Methods to Measure Reactive Oxygen Species (ROS) and Total Antioxidant Capacity (TAC) in the Reproductive System.* 2017: p. 17-46.
102. Durackova, Z., *Some current insights into oxidative stress.* Physiol Res, 2010. **59**(4): p. 459-69.
103. Mishin, V., et al., *Application of the Amplex red/horseradish peroxidase assay to measure hydrogen peroxide generation by recombinant microsomal enzymes.* Free Radic Biol Med, 2010. **48**(11): p. 1485-91.
104. Dikalov, S.I. and D.G. Harrison, *Methods for detection of mitochondrial and cellular reactive oxygen species.* Antioxid Redox Signal, 2014. **20**(2): p. 372-82.
105. Sousa-Lopes, A., et al., *Decreased cellular permeability to H2O2 protects Saccharomyces cerevisiae cells in stationary phase against oxidative stress.* FEBS Lett, 2004. **578**(1-2): p. 152-6.
106. Bienert, G.P., J.K. Schjoerring, and T.P. Jahn, *Membrane transport of hydrogen peroxide.* Biochim Biophys Acta, 2006. **1758**(8): p. 994-1003.
107. Grotto, D., et al., *Importance of the lipid peroxidation biomarkers and methodological aspects FOR malondialdehyde quantification.* Química Nova, 2009. **32**: p. 169-174.
108. Quax, T.E., et al., *Codon Bias as a Means to Fine-Tune Gene Expression.* Mol Cell, 2015. **59**(2): p. 149-61.
109. Papadopoulou, L.C., et al., *Fatal infantile cardioencephalomyopathy with COX deficiency and mutations in SCO2, a COX assembly gene.* Nat Genet, 1999. **23**(3): p. 333-7.
110. Tran-Viet, K.N., et al., *Mutations in SCO2 are associated with autosomal-dominant high-grade myopia.* Am J Hum Genet, 2013. **92**(5): p. 820-6.

111. Kohda, M., et al., *A Comprehensive Genomic Analysis Reveals the Genetic Landscape of Mitochondrial Respiratory Chain Complex Deficiencies.* PLoS Genet, 2016. **12**(1): p. e1005679.
112. Foltopoulou, P.F., et al., *Human recombinant mutated forms of the mitochondrial COX assembly Sco2 protein differ from wild-type in physical state and copper binding capacity.* Mol Genet Metab, 2004. **81**(3): p. 225-36.
113. Sacconi, S., et al., *Mutation screening in patients with isolated cytochrome c oxidase deficiency.* Pediatr Res, 2003. **53**(2): p. 224-30.
114. Salviati, L., et al., *Cytochrome c oxidase deficiency due to a novel SCO2 mutation mimics Werdnig-Hoffmann disease.* Arch Neurol, 2002. **59**(5): p. 862-5.
115. Jaksch, M., et al., *Mutations in SCO2 are associated with a distinct form of hypertrophic cardiomyopathy and cytochrome c oxidase deficiency.* Hum Mol Genet, 2000. **9**(5): p. 795-801.
116. Chadha, R., R. Shah, and S. Mani, *Analysis of reported SCO2 gene mutations affecting cytochrome c oxidase activity in various diseases.* Bioinformation, 2014. **10**(6): p. 329-33.
117. Karshikoff, A. and I. Jelesarov, *Salt Bridges and Conformational Flexibility: Effect on Protein Stability.* Biotechnology & Biotechnological Equipment, 2008. **22**(1): p. 606-611.
118. Xu, D., C.J. Tsai, and R. Nussinov, *Hydrogen bonds and salt bridges across protein-protein interfaces.* Protein Eng, 1997. **10**(9): p. 999-1012.
119. Hu, Z., et al., *Conservation of polar residues as hot spots at protein interfaces.* Proteins, 2000. **39**(4): p. 331-42.
120. Rosenzweig, A.C., *Copper delivery by metallochaperone proteins.* Acc Chem Res, 2001. **34**(2): p. 119-28.
121. Gibbs, C.S. and M.J. Zoller, *Identification of functional residues in proteins by charged-to-alanine scanning mutagenesis.* Methods, 1991. **3**(3): p. 165-173.
122. Steinebrunner, I., et al., *HCC1, the Arabidopsis homologue of the yeast mitochondrial copper chaperone SCO1, is essential for embryonic development.* J Exp Bot, 2011. **62**(1): p. 319-30.
123. Steinebrunner, I., et al., *Divergent functions of the Arabidopsis mitochondrial SCO proteins: HCC1 is essential for COX activity while HCC2 is involved in the UV-B stress response.* Front Plant Sci, 2014. **5**: p. 87.
124. Attallah, C.V., et al., *Plants contain two SCO proteins that are differentially involved in cytochrome c oxidase function and copper and redox homeostasis.* J Exp Bot, 2011. **62**(12): p. 4281-94.
125. Jayanthi, S., B.D. Lewis, and J.L. Cadet, *Fas-induced apoptosis of glioma cells is associated with down-regulation of the hSCO1 protein, a subunit of complex IV.* Brain Res Mol Brain Res, 2001. **91**(1-2): p. 131-6.
126. Ji, X., et al., *Potential hepatic toxicity of buprofezin at sublethal concentrations: ROS-mediated conversion of energy metabolism.* J Hazard Mater, 2016. **320**: p. 176-186.
127. Mitsunaga, S., et al., *Aggregation of rare/low-frequency variants of the mitochondria respiratory chain-related proteins in rheumatoid arthritis patients.* J Hum Genet, 2015. **60**(8): p. 449-54.

128. Matoba, S., et al., *p53 regulates mitochondrial respiration.* Science, 2006. **312**(5780): p. 1650-3.
129. Wanka, C., et al., *Synthesis of cytochrome C oxidase 2: a p53-dependent metabolic regulator that promotes respiratory function and protects glioma and colon cancer cells from hypoxia-induced cell death.* Oncogene, 2012. **31**(33): p. 3764-76.
130. Madan, E., et al., *SCO2 induces p53-mediated apoptosis by Thr845 phosphorylation of ASK-1 and dissociation of the ASK-1-Trx complex.* Mol Cell Biol, 2013. **33**(7): p. 1285-302.
131. Sinthupibulyakit, C., et al., *p53 Protects lung cancer cells against metabolic stress.* Int J Oncol, 2010. **37**(6): p. 1575-81.
132. Li, J., et al., *Alpha particle-induced bystander effect is mediated by ROS via a p53-dependent SCO2 pathway in hepatoma cells.* Int J Radiat Biol, 2013. **89**(12): p. 1028-34.
133. Sung, H.J., et al., *Mitochondrial respiration protects against oxygen-associated DNA damage.* Nat Commun, 2010. **1**: p. 5.
134. Zhdanov, A.V., et al., *Cellular ROS imaging with hydro-Cy3 dye is strongly influenced by mitochondrial membrane potential.* Biochim Biophys Acta, 2017. **1861**(2): p. 198-204.
135. Paret, C., et al., *Human members of the SCO1 gene family: complementation analysis in yeast and intracellular localization.* FEBS Lett, 1999. **447**(1): p. 65-70.
136. Porcelli, D., et al., *Genetic, functional and evolutionary characterization of scox, the Drosophila melanogaster ortholog of the human SCO1 gene.* Mitochondrion, 2010. **10**(5): p. 433-48.
137. Nguyen, T.B., et al., *Role of SCOX in determination of Drosophila melanogaster lifespan.* Am J Cancer Res, 2014. **4**(4): p. 325-36.
138. Scannell, D.R., G. Butler, and K.H. Wolfe, *Yeast genome evolution--the origin of the species.* Yeast, 2007. **24**(11): p. 929-42.
139. Kurtzman, C.P., *Use of gene sequence analyses and genome comparisons for yeast systematics.* Int J Syst Evol Microbiol, 2014. **64**(Pt 2): p. 325-32.
140. Takeda, K., et al., *The critical glucose concentration for respiration-independent proliferation of fission yeast, Schizosaccharomyces pombe.* Mitochondrion, 2015. **22**: p. 91-5.
141. Gonzalez-Siso, M.I., et al., *Sugar metabolism, redox balance and oxidative stress response in the respiratory yeast Kluyveromyces lactis.* Microb Cell Fact, 2009. **8**: p. 46.
142. Meisinger, C., T. Sommer, and N. Pfanner, *Purification of Saccharomcyes cerevisiae mitochondria devoid of microsomal and cytosolic contaminations.* Anal Biochem, 2000. **287**(2): p. 339-42.
143. Gey, U., et al., *Proteomic analysis reveals a novel function of the kinase Sat4p in Saccharomyces cerevisiae mitochondria.* PLoS One, 2014. **9**(8): p. e103956.
144. Angellotti, M.C., et al., *CodonO: codon usage bias analysis within and across genomes.* Nucleic Acids Res, 2007. **35**(Web Server issue): p. W132-6.
145. Salim, H.M.W. and A.R.O. Cavalcanti, *Factors influencing codon usage bias in genomes.* Journal of the Brazilian Chemical Society, 2008. **19**: p. 257-262.

146. Mobley, B.C., et al., *A novel homozygous SCO2 mutation, p.G193S, causing fatal infantile cardioencephalomyopathy.* Clin Neuropathol, 2009. **28**(2): p. 143-9.
147. Tarnopolsky, M.A., et al., *Novel SCO2 mutation (G1521A) presenting as a spinal muscular atrophy type I phenotype.* Am J Med Genet A, 2004. **125a**(3): p. 310-4.
148. Jiang, D., et al., *Detection of mutations in LRPAP1, CTSH, LEPREL1, ZNF644, SLC39A5, and SCO2 in 298 families with early-onset high myopia by exome sequencing.* Invest Ophthalmol Vis Sci, 2014. **56**(1): p. 339-45.
149. Leary, S.C., et al., *Human SCO1 and SCO2 have independent, cooperative functions in copper delivery to cytochrome c oxidase.* Hum Mol Genet, 2004. **13**(17): p. 1839-48.
150. Leary, S.C., et al., *COX19 mediates the transduction of a mitochondrial redox signal from SCO1 that regulates ATP7A-mediated cellular copper efflux.* Mol Biol Cell, 2013. **24**(6): p. 683-91.
151. Leary, S.C., et al., *The human cytochrome c oxidase assembly factors SCO1 and SCO2 have regulatory roles in the maintenance of cellular copper homeostasis.* Cell Metab, 2007. **5**(1): p. 9-20.
152. Jaksch, M., et al., *Homozygosity (E140K) in SCO2 causes delayed infantile onset of cardiomyopathy and neuropathy.* Neurology, 2001. **57**(8): p. 1440-6.
153. Dickinson, E.K., et al., *A human SCO2 mutation helps define the role of Sco1p in the cytochrome oxidase assembly pathway.* J Biol Chem, 2000. **275**(35): p. 26780-5.
154. Yang, H., et al., *Analysis of mouse models of cytochrome c oxidase deficiency owing to mutations in Sco2.* Hum Mol Genet, 2010. **19**(1): p. 170-80.
155. Cheeseman, K.H. and T.F. Slater, *An introduction to free radical biochemistry.* Br Med Bull, 1993. **49**(3): p. 481-93.
156. Aust, S.D., L.A. Morehouse, and C.E. Thomas, *Role of metals in oxygen radical reactions.* J Free Radic Biol Med, 1985. **1**(1): p. 3-25.
157. Gaetke, L.M. and C.K. Chow, *Copper toxicity, oxidative stress, and antioxidant nutrients.* Toxicology, 2003. **189**(1-2): p. 147-63.
158. Sukalski, K.A., T.P. LaBerge, and W.T. Johnson, *In Vivo Oxidative Modification of Erythrocyte Membrane Proteins in Copper Deficiency.* Free Radical Biology and Medicine, 1997. **22**(5): p. 835-842.
159. Dong, K., et al., *The Yeast Copper Response Is Regulated by DNA Damage.* Molecular and Cellular Biology, 2013. **33**(20): p. 4041-4050.
160. Harris, E.D., *Copper as a cofactor and regulator of copper,zinc superoxide dismutase.* J Nutr, 1992. **122**(3 Suppl): p. 636-40.
161. Lai, C.C., et al., *Antioxidant enzyme gene transcription in copper-deficient rat liver.* Free Radic Biol Med, 1996. **21**(2): p. 233-40.
162. Sinha, N. and S.J. Smith-Gill, *Electrostatics in protein binding and function.* Curr Protein Pept Sci, 2002. **3**(6): p. 601-14.
163. Zhao, N., et al., *Charged residues at protein interaction interfaces: unexpected conservation and orchestrated divergence.* Protein Sci, 2011. **20**(7): p. 1275-84.
164. Jones, S. and J.M. Thornton, *Principles of protein-protein interactions.* Proc Natl Acad Sci U S A, 1996. **93**(1): p. 13-20.

165. McCoy, A.J., V. Chandana Epa, and P.M. Colman, *Electrostatic complementarity at protein/protein interfaces.* J Mol Biol, 1997. **268**(2): p. 570-84.
166. Li, J., et al., *Glutathione-coordinated [2Fe-2S] cluster is stabilized by intramolecular salt bridges.* J Biol Inorg Chem, 2015. **20**(8): p. 1221-7.
167. Dey, M., et al., *Conserved intermolecular salt bridge required for activation of protein kinases PKR, GCN2, and PERK.* J Biol Chem, 2007. **282**(9): p. 6653-60.
168. Morin-Leisk, J., et al., *An intramolecular salt bridge drives the soluble domain of GTP-bound atlastin into the postfusion conformation.* J Cell Biol, 2011. **195**(4): p. 605-15.
169. Brown, L.R., et al., *The influence of a single salt bridge on static and dynamic features of the globular solution conformation of the basic pancreatic trypsin inhibitor. 1H and 13C nuclear-magnetic-resonance studies of the native and the transaminated inhibitor.* Eur J Biochem, 1978. **88**(1): p. 87-95.
170. Blees, A., et al., *Assembly of the MHC I peptide-loading complex determined by a conserved ionic lock-switch.* Sci Rep, 2015. **5**: p. 17341.
171. Fersht, A.R., *Basis of biological specificity.* Trends in Biochemical Sciences, 1984. **9**(4): p. 145-147.
172. Lo Conte, L., C. Chothia, and J. Janin, *The atomic structure of protein-protein recognition sites.* J Mol Biol, 1999. **285**(5): p. 2177-98.
173. Capitani, G., et al., *Crystal structures of two functionally different thioredoxins in spinach chloroplasts.* J Mol Biol, 2000. **302**(1): p. 135-54.
174. Mora-Garcia, S., R. Rodriguez-Suarez, and R.A. Wolosiuk, *Role of electrostatic interactions on the affinity of thioredoxin for target proteins. Recognition of chloroplast fructose-1, 6-bisphosphatase by mutant Escherichia coli thioredoxins.* J Biol Chem, 1998. **273**(26): p. 16273-80.
175. Zahiri, J., J.H. Bozorgmehr, and A. Masoudi-Nejad, *Computational Prediction of Protein–Protein Interaction Networks: Algo-rithms and Resources.* Current Genomics, 2013. **14**(6): p. 397-414.
176. Jones, S. and J.M. Thornton, *Analysis of protein-protein interaction sites using surface patches11Edited by G.Von Heijne.* Journal of Molecular Biology, 1997. **272**(1): p. 121-132.
177. Erijman, A., E. Rosenthal, and J.M. Shifman, *How Structure Defines Affinity in Protein-Protein Interactions.* PLoS ONE, 2014. **9**(10): p. e110085.
178. Lins, L., A. Thomas, and R. Brasseur, *Analysis of accessible surface of residues in proteins.* Protein Sci, 2003. **12**(7): p. 1406-17.
179. Lorenzi, I., et al., *The ribosome-associated Mba1 escorts Cox2 from insertion machinery to maturing assembly intermediates.* Mol Cell Biol, 2016.
180. von der Malsburg, K., et al., *Dual role of mitofilin in mitochondrial membrane organization and protein biogenesis.* Dev Cell, 2011. **21**(4): p. 694-707.
181. Willmund, F., et al., *The cotranslational function of ribosome-associated Hsp70 in eukaryotic protein homeostasis.* Cell, 2013. **152**(1-2): p. 196-209.
182. Ptacek, J., et al., *Global analysis of protein phosphorylation in yeast.* Nature, 2005. **438**(7068): p. 679-84.

183. Kershaw, C.J., et al., *Integrated multi-omics analyses reveal the pleiotropic nature of the control of gene expression by Puf3p.* Sci Rep, 2015. **5**: p. 15518.
184. Guo, X., et al., *Integrative proteomics and biochemical analyses define Ptc6p as the Saccharomyces cerevisiae pyruvate dehydrogenase phosphatase.* J Biol Chem, 2017. **292**(28): p. 11751-11759.
185. Claypool, S.M., et al., *Cardiolipin defines the interactome of the major ADP/ATP carrier protein of the mitochondrial inner membrane.* J Cell Biol, 2008. **182**(5): p. 937-50.
186. Leary, S.C., D.R. Winge, and P.A. Cobine, *"Pulling the plug" on cellular copper: the role of mitochondria in copper export.* Biochim Biophys Acta, 2009. **1793**(1): p. 146-53.
187. Leary, S.C., *Redox regulation of SCO protein function: controlling copper at a mitochondrial crossroad.* Antioxid Redox Signal, 2010. **13**(9): p. 1403-16.
188. Baker, Z.N., P.A. Cobine, and S.C. Leary, *The mitochondrion: a central architect of copper homeostasis.* Metallomics, 2017. **9**(11): p. 1501-1512.
189. Khalimonchuk, O. and D.R. Winge, *Function and redox state of mitochondrial localized cysteine-rich proteins important in the assembly of cytochrome c oxidase.* Biochim Biophys Acta, 2008. **1783**(4): p. 618-28.